

GEORGIA INSTITUTE OF TECHNOLOGY
OFFICE OF RESEARCH ADMINISTRATION

RESEARCH PROJECT INITIATION

Date: September 16, 1974

Project Title: An Investigation of the Flow Disturbances Created by
Sub-Total Vascular Stenosis

Project No. E-16-654

Principal Investigator: Dr. Don P. Giddens/Dr. Robert F. Mabon

Sponsor: National Science Foundation

Agreement Period: From 9/1/74 Until 2/29/76

Type Agreement: Grant No. ENG74-21986

Amount: \$43,100 NSF
5,940 GIT(E-16-347)
\$49,040 Total

Reports Required:

Annual Letter (if renewal is granted)
Final Report

Sponsor Contact Person (s):

Technical
Fluid Mechanics Program
Dr. George K. Lea
Program Director
National Science Foundation
Washington, D. C. 20550

Administrative
Thru ORA
Mr. Wilbur W. Bolton, Jr.
Grants Officer
National Science Foundation
Washington, D. C. 20550

Assigned to: Aerospace Engineering

COPIES TO:

<input type="checkbox"/> Principal Investigator	<input type="checkbox"/> Library
<input type="checkbox"/> School Director	<input type="checkbox"/> Rich Electronic Computer Center
<input type="checkbox"/> Dean of the College	<input type="checkbox"/> Photographic Laboratory
<input type="checkbox"/> Director, Research Administration	<input type="checkbox"/> Project File
<input type="checkbox"/> Director, Financial Affairs (2)	
<input type="checkbox"/> Security Reports Property Office	
<input type="checkbox"/> Patent Coordinator	Other _____



GEORGIA INSTITUTE OF TECHNOLOGY
OFFICE OF CONTRACT ADMINISTRATION

SPONSORED PROJECT TERMINATION

Date: July 13, 1977

Posted
add
OK

Title: An Investigation of the Flow Disturbances Created by Sub-Total Vascular Stenosis.

No: E-16-654

Director: Dr. D. P. Giddens, Dr. R. F. Mabon

r: National Science Foundation

ve Termination Date: 3/31/77

ice of Accounting Charges: 3/31/77

Contract Closeout Actions Remaining:

- ☐ Final Invoice and Closing Documents
- ☒ Final Fiscal Report
- ☒ Final Report of Inventions
- ☐ Govt. Property Inventory & Related Certificate
- ☐ Classified Material Certificate
- ☐ Other _____

Assigned to: Aerospace Engineering (School/Laboratory)

COPIES TO:

Project Director
Division Chief (EES)
School/Laboratory Director
Dean/Director—EES
Accounting Office
Procurement Office
Security Coordinator (OCA) ✓
Reports Coordinator (OCA) ✓

Library, Technical Reports Section
Office of Computing Services
Director, Physical Plant
EES Information Office
Project File (OCA)
Project Code (GTRI)
Other _____

NSF Grant No. ENG74-21986

AN INVESTIGATION OF THE FLOW DISTURBANCES
CREATED BY SUB-TOTAL VASCULAR STENOSIS

A. Report of Present Year's Activity

The progress of the first year of this proposal has adhered rather closely to the projected schedule. A very satisfactory assemblage of data has been obtained in the warm-blooded animals studied. A considerable amount of information relative to turbulence and energy spectra engendered by extravascular occlusion has been collected and stored on tape. Additional analysis of this accumulated data is currently being accomplished. There are several methods of utilizing this information. We have gained considerable experience in analysis of complete velocity waveforms and are presently extending this effort to the examination of energy spectra correlated with specific events in the electro-cardiographic tracings which were recorded concurrently during these studies.

Extensive in vitro studies with modelled stenoses, employing both steady and pulsatile flows, have been completed. These have provided an understanding of detailed flow phenomena accompanying circumferential constrictions in tubes. Comparison of this information with the in vivo data is in progress.

Attached are abstracts of papers presented at several meetings, which incorporate some of the major results and conclusions. Two manuscripts, one on the animal studies and the other encompassing

in vitro findings, are under preparation.

Fortunately, there have been only two problems of consequence encountered to date in this project. These are the unavoidable invasive nature and reliability of the hot film probe. It has been our experience that blood flow probes furnished by DISA have been much more reliable than those manufactured by Thermo-Systems (TSI). We have also had the experience of finding that a certain probe will work beautifully with little drifting of the calibration, performing faithfully in several successive experiments. Again one may encounter probe after probe which will function either poorly or fail suddenly in the middle of an experiment, which can be heart-rending. The hot-film probes mounted on catheters by DISA have also proved quite dependable in comparison with those of other manufacturers.

During the second week of July, 1975, Francis McLeod of Colorado State University, Fort Collins, Colorado, will be in our laboratory. He has considerable expertise employing the pulsed ultrasonic Doppler velocimeter. As a matter of fact, he was one of the original developers of this instrument. We plan to collaborate with him in our study of turbulence and to determine whether or not this instrument has the capability of critically measuring this aspect of disordered flow. He has constructed a single channel device for our research program. Using this as a prototype, we plan to expand our capability and familiarity with this instrument, and to construct a multi-channel unit. This development is

of the utmost importance, since it will permit using a non-invasive instrument to measure mean velocity and velocity profiles at various stations without penetrating the vessel under study. A real effort should be made to determine the feasibility of using Doppler ultrasound techniques to analyze disordered flow patterns because of the tremendous flexibility of this instrument. We intend to determine if this device can be employed to explore the micro-regions of disordered flow.

It is our hope that small budgetary modifications will be possible to incorporate this added instrumentation into the second year of our project (See Proposed Budget).

B. Participating Students and Status

R. A. Cassanova - (1/4 time support)

Mr. Cassanova is a research engineer in the School of Aerospace Engineering who is concurrently working on the Ph.D. Degree. He utilized some of the in vitro experiments under this grant as his dissertation. His degree is to be awarded in September, 1975.

M. Deshpande

Mr. Deshpande is a Ph.D. student supported by matching Georgia Tech funds for this grant. He is presently working on a theoretical analysis of turbulent flow through stenoses as his dissertation topic.

V. J. Saxena

Mr. Saxena was supported under this grant for his first year of graduate school. He will complete the M.S.A.E. degree in September, 1975.

C. Alterations to Proposed Research

We anticipate no major alterations to the proposed research plan as originally outlined. However, in view of the exciting potential of employing the noninvasive Doppler ultrasound velocimeter for investigating disordered and turbulent blood flows, we are most anxious to incorporate an effort directed toward this purpose. We are therefore requesting a slight addition to the proposed budget to cover anticipated supplies and consultations. We also wish to expend some of the allotted personal services time to develop techniques for the non-invasive description of turbulent flows.

D. Budget Projection to Anniversary Date

We anticipate that all awarded first-year funds will be spent prior to the end of the initial year of the grant, September 1, 1975.

Don P. Giddens, Ph.D.

Robert F. Mabon, M.D.

REVISED RESEARCH GRANT PROPOSAL BUDGET

(Second Year) Beginning September 1, 1975

Budget Category	NSF Cal	Funded Acad	Man-Months Sum	Proposed Amount
A. SALARIES AND WAGES				
1. Senior Personnel				
a. Don Giddens, Ph.D. Co-Principal Investigator 27% time at \$28,000/yr	0.3	2.25	0.75	\$ 7,500
b. Robert F. Mabon, M.D. Co-Principal Investigator 15% time at \$45,000/yr	1.8	1.35	0.45	6,750
2. Other Personnel				
a. Robert A. Cassanova, Ph.D. Research Engineer 27% time at \$17,600/yr	0.3	2.25	0.75	\$ 4,750
b. John T. Godwin, M.D.	0.5 month total			2,000
c. Graduate Research Assistant	0.4	3.0	1.0	4,000
Total Salaries and Wages				\$25,000
B. STAFF BENEFITS				
15% of applicable Salaries and Wages				\$ 1,838
C. TOTAL SALARIES, WAGES AND STAFF BENEFITS				\$26,838
D. PERMANENT EQUIPMENT - none				

E. SUPPLIES

Hot film anemometer probes	\$ 1,000
Miscellaneous supplies (strip chart paper, FM tape, plexiglas tubing, etc.	750
Material for slide preparation for histological studies in long term animal experiments	1,000
Supplies for multichannel Doppler ultrasound instrumentation	1,500
Consulting fees for F. D. McLeod, Colorado State University	1,000

Total Supplies	<u>\$ 5,250</u>
----------------	-----------------

F. TRAVEL

Domestic travel for investigators to attend technical conference	\$ 750
--	--------

G. PUBLICATION COSTS

	\$ 250
--	--------

H. COMPUTER COSTS

CDC CYBER-74, grantee owned	\$ 1,000
-----------------------------	----------

I. OTHER COSTS

Animal experiments, 10 long term studies necessitating sterile techniques (\$100/procedure)	\$ 1,000
Board for animal recuperation at veterinarian	\$ 750

Total Other Costs	<u>\$ 1,750</u>
-------------------	-----------------

J. TOTAL DIRECT COSTS

	\$35,838
--	----------

K. INDIRECT COSTS

	\$14,260
--	----------

On campus, 62 percent of direct salaries and wages for Georgia Tech personnel (.62 x 23,000)

TOTAL SECOND YEAR COSTS	\$50,098
-------------------------	----------

TURBULENCE MEASURED DISTAL TO SUBTOTAL
VASCULAR STENOSSES - IN VIVO

by

D. P. Giddens, R. F. Mabon and R. A. Cassanova
School of Aerospace Engineering
Georgia Institute of Technology
Atlanta, Georgia

Vascular stenosis may create a turbulent velocity field distal to the obstruction. Such a turbulent flow may contribute to intimal injury [1] or to poststenotic dilatation [2]. Although the extent of its occurrence in the normal vasculature is unknown, the production of turbulence distal to obstructions in the larger arteries is a natural supposition of the fluid dynamicist. Direct in vivo verification has recently been provided by preliminary studies in the canine aorta [3]. In the present investigation we have systematically examined the velocity field distal to partial occlusions of varying degrees positioned on the descending thoracic aortas of mongrel dogs and have concentrated upon the spectral analysis of the velocity waveforms generated.

Under general anesthesia, the aortas were surgically exposed by means of a left thoracotomy. Velocity measurements within the vessel were obtained with a hot film probe sensor mounted on the conical tip of a one millimeter diameter right angle needle, and employing a DISA anemometer (55D01) and linearizer (55D10). The probe was inserted through the aortic wall, bleeding being controlled using a purse string suture. Volume flow rate was monitored with an electromagnetic flowmeter (Carolina Medical Electronics) stationed several centimeters distal to the velocity sensor. An ECG signal was also utilized to register events in the cardiac cycle. These data were recorded on FM tape for subsequent analysis.

Energy spectra were obtained by subjecting the entire velocity waveform to Fourier analysis with a Hewlett-Packard Model 5452B Fourier Analyzer. Frequency bandwidth resolution for the data reported here is one Hertz and 50 samples, each comprised of 1024 digitized data points, of the velocity signal were analyzed.

The partial occlusions were created with a mechanical device applied externally to the vessel and could be adjusted to yield varying degrees of blockage. Application of this device to a pressurized, excised segment of canine aorta demonstrated that the resulting stenoses were reasonably circular and axisymmetric.

The occurrence of disturbances in the velocity waveforms recorded distally to the stenoses is readily noticeable. Figure 1 illustrates this for one of the experiments. The waveform for no occlusion is relatively undisturbed. However, distinct variations appear when even relatively small stenoses are present. For severe occlusions the pulsatile nature of the flow is greatly suppressed and the distal flow resembles a confined turbulent jet.

These trends are reflected in the energy spectra of the waveforms (Figure 2). The spectra obtained with no occlusion present are comprised primarily of harmonics of the fundamental heart rate. When partial occlusions are used, the spectral shift is to larger energy in the higher frequencies.

We have examined the possibility of relating similarity parameters to the energy spectra and degree of stenosis. Although no general conclusions have been drawn, we have found regions of the distal flow for which a semi-local form of the Strouhal number appears valid. This form is fd/U_L , where f is the frequency, d is the diameter of the occlusion, and U_L is the peak velocity at the site of measurement. The correlation provided is illustrated for one case in Figure 3. The spectra for no occlusion is clearly separated from the occlusion spectra since little discernible turbulence was present. However, all the remaining spectra are closely correlated.

REFERENCES

- 1 Fry, D. L., "Responses of the Arterial Wall to Certain Physical Factors," in Atherogenesis: Initiating Factors, A Ciba Foundation Symposium 12 (New Series), pp. 93-125, Elsevier. Excerpta Medica. North Holland, Amsterdam, 1973.
2. Roach, M. R., "Poststenotic Dilatation in Arteries," in Cardiovascular Fluid Dynamics, Vol. 2, edited by D. Bergel, Academic Press, London, 1972.
- 3 Giddens, D. P, Mabon, R. F., Cassanova, R. A. , Menon, R. K. and Chandler, J., "The Velocity Field Distal to Partial Occlusions in Arteries," paper presented at 10th Anniversary Meeting of the Society of Engineering Science, North Carolina State University, Raleigh, N. C., November 1973. (To be published in the Proceedings).

ACKNOWLEDGEMENTS

This work was supported by the National Heart and Lung Institute under Grant Number HL 15519 and by the National Science Foundation under Grant Number ENG74-21986.

FIGURE 1. VELOCITY WAVEFORMS

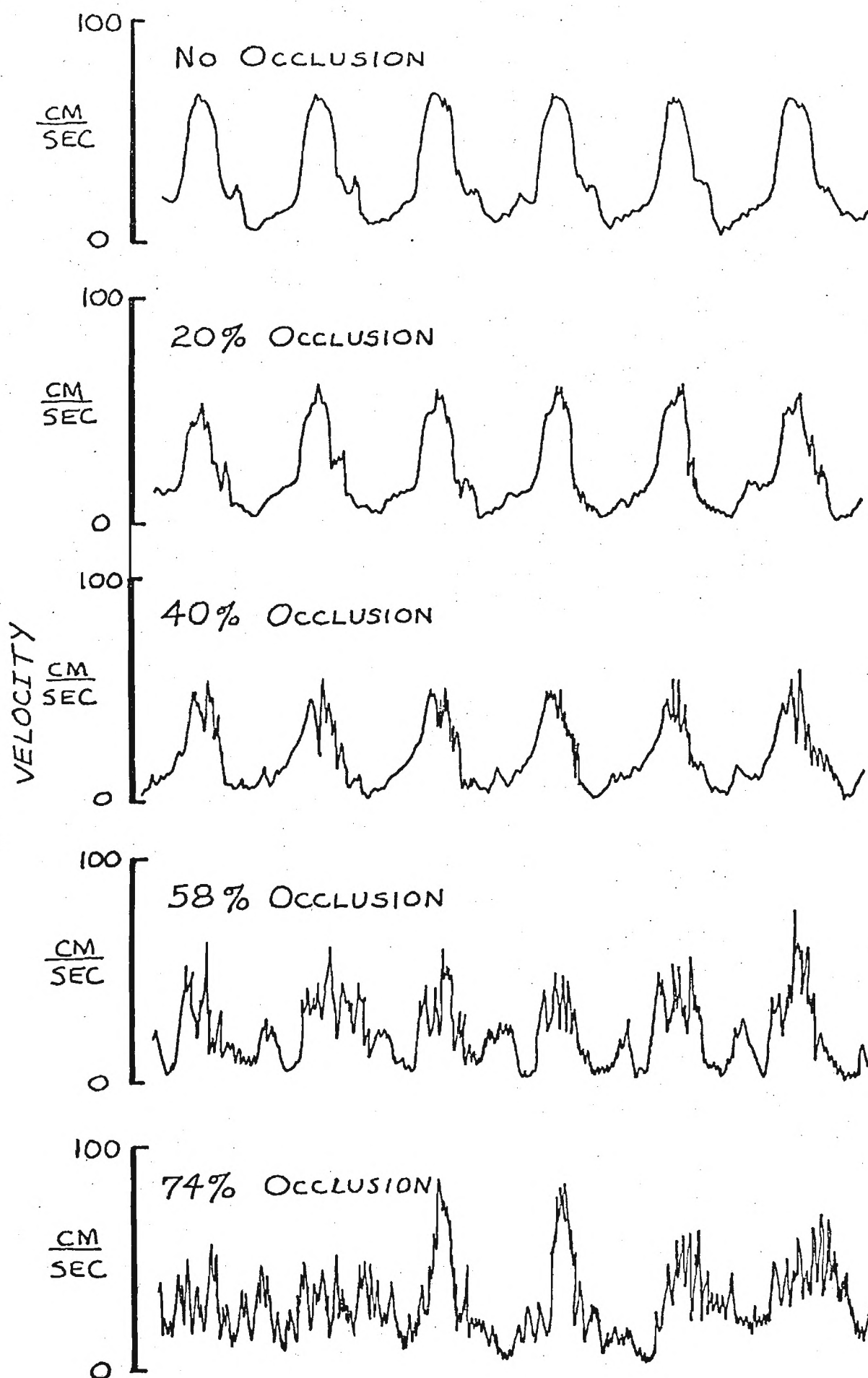


FIGURE 2. ENERGY SPECTRA

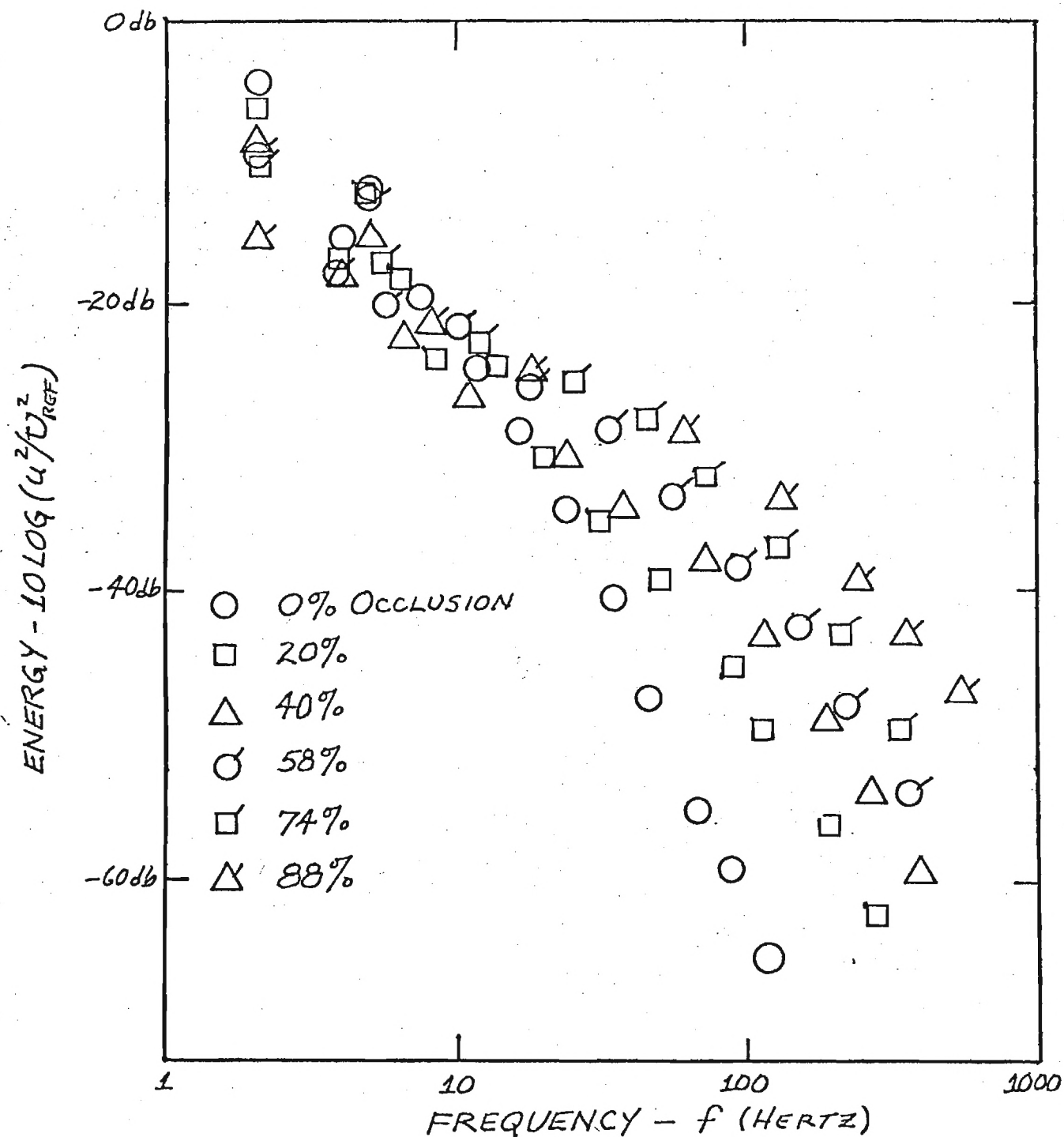
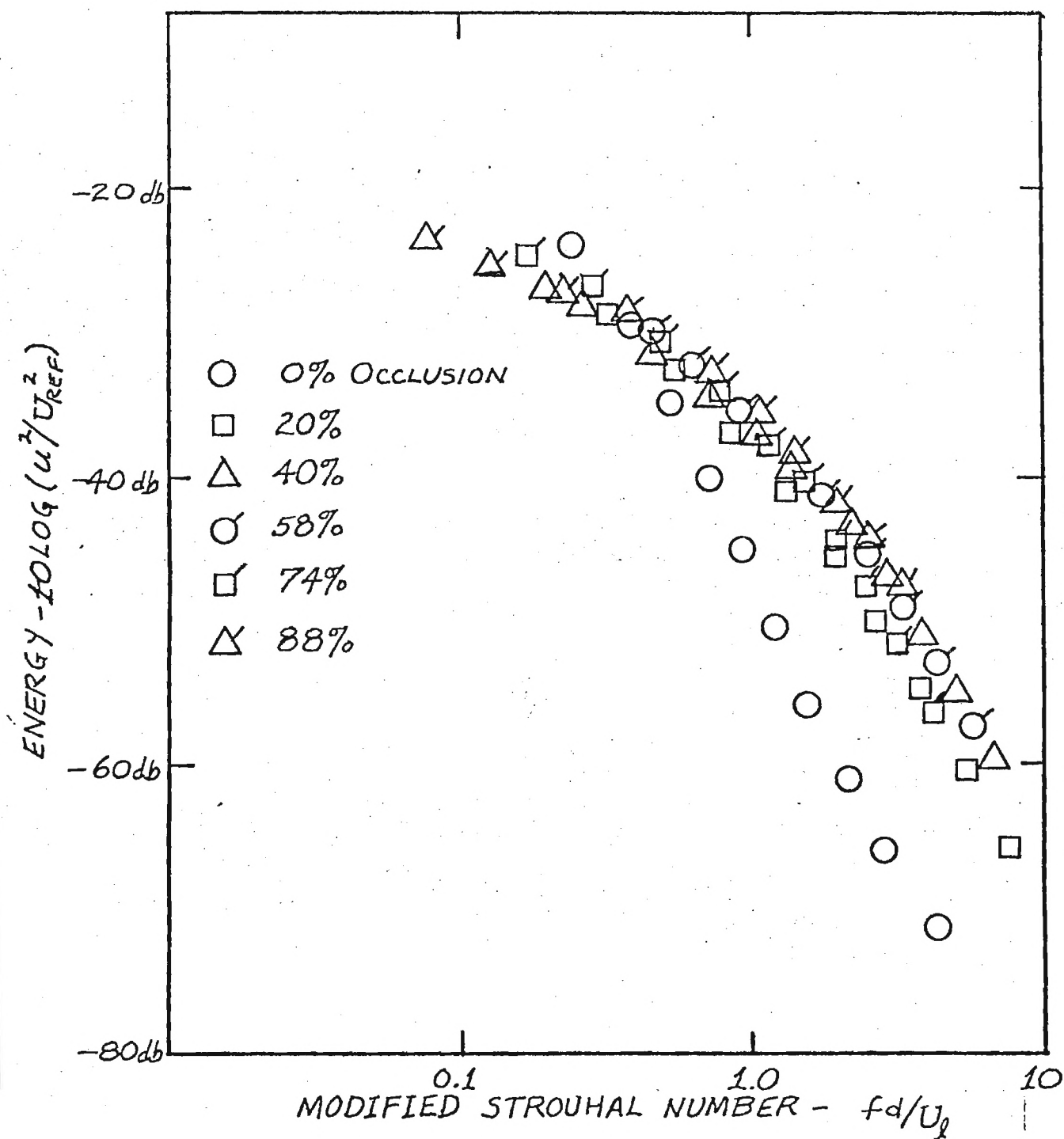


FIGURE 3. CORRELATION OF ENERGY SPECTRA



STEADY, LAMINAR FLOW THROUGH PARTIAL STENOSES

by

M. D. Deshpande, D. P. Giddens and R. F. Mabon, M.D.

School of Aerospace Engineering

Georgia Institute of Technology

Atlanta, Georgia

Hydrodynamic phenomena have been found to be associated with the occurrence of atherosclerosis. For this reason, the flow characteristics in the region of partial vascular stenoses are of interest in the etiology and proliferation of this arterial disease. Previous studies have considered this flow problem from both theoretical and experimental viewpoints. Lee and Fung (Ref. 1) obtained numerical solutions for steady, laminar flows through rigid, constricted tubes for Reynolds numbers up to 25. Experimental data on pressure drop across a stenosis and on separation and reattachment points have been presented by Young and Tsai (Ref. 2).

In the present paper numerical solutions are obtained for steady, Newtonian, incompressible flows through rigid, axisymmetric tubes with different degrees of axisymmetric stenoses. The form of the stenosis is a cosine curve

$$\frac{R_o}{a_o} = 1 - \frac{\alpha}{2} \left[1 + \cos \left(\frac{\pi Z}{Z_o} \right) \right]$$

where Z is the axial coordinate, a_o is the unobstructed tube radius, Z_o is the length of the constriction, and α may be adjusted to vary the degree of occlusion. The steady state Navier-Stokes equations are solved for stream function and vorticity using the numerical scheme of Ref. 3 extended to curved boundary shapes. Poiseuille flow is assumed far upstream and downstream of the occlusion. Solutions were obtained for four stenoses:

Model	α	$\frac{Z_o}{a_o}$	Area Reduction	Reynolds Number
M0	0.25	1	75%	0 - 300
M1	0.333	4	56%	0 - 2000
M2	0.667	4	89%	0 - 200
M3	0.667	2	89%	0 - 100

M1, M2 and M3 are the same as those used in the experiments of Ref. 2.

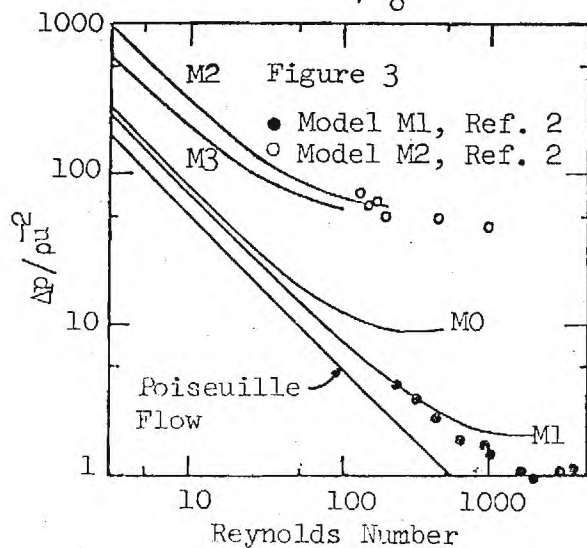
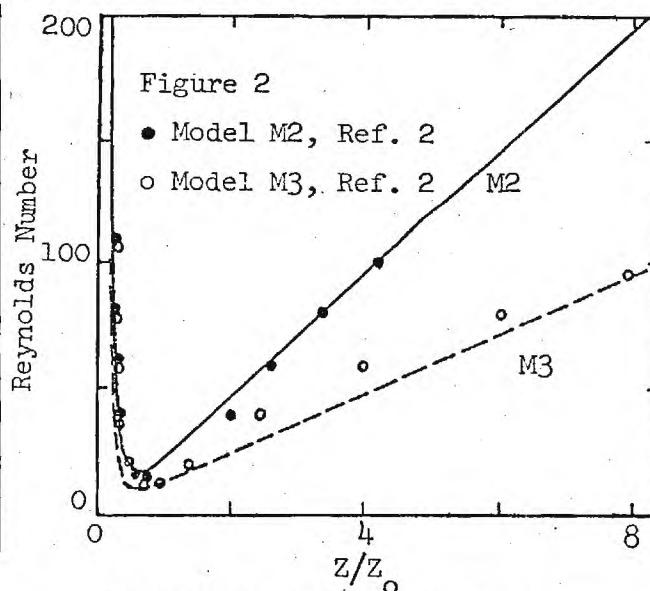
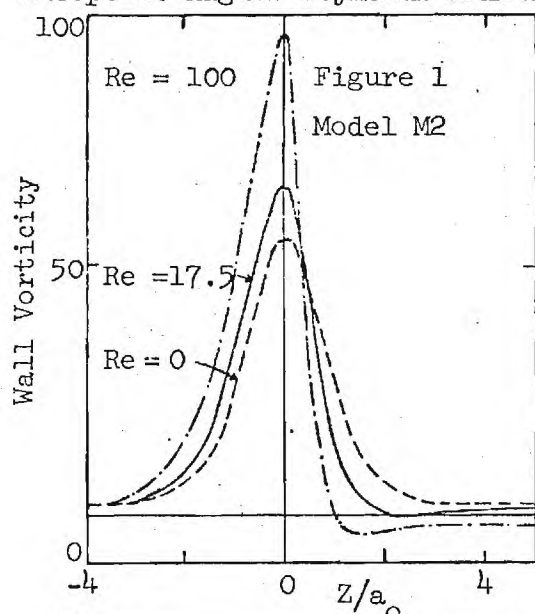
Figure 1 shows typical results for wall vorticity distributions, which are proportional to shear stresses. Peak shear stresses occur slightly upstream of the minimum area for Reynolds numbers > 0 (the Reynolds number is based on unoccluded diameter and mean velocity). The negative values of shear stress indicate regions of separated flow.

Figure 2 compares separation and reattachment points with the data from Ref. 2. The Reynolds numbers at which separation first occurs are in good agreement with the experimental data for models M1 and M3 (195 and 8.75, respectively, from computation compared with 190 and 10 determined from the data presented in Ref. 2). However, a significant difference between theory and experiment was found for model M2. The

calculated separation Reynolds number was 17, whereas the value reported by Young and Tsai is approximately 10. The reason for this deviation is not clear. A calculation for model M0, which very closely approximates the shape used by Lee and Fung, gave a separation Reynolds number of 10.1 which agrees quite well with their reported value of 9.9.

The calculated and measured separation points are generally compatible. However, the reattachment points do not agree as well. This is thought to be caused by two factors; the reattachment point is difficult to locate experimentally, and the assumption of laminar flow is not accurate at the higher Reynolds numbers. In Ref. 2 transitional flow was detected locally for Reynolds numbers of 300 ± 20 , 300 ± 20 and 185 ± 25 for models M1, M2 and M3, respectively.

Figure 3 compares the calculated pressure drop across the stenoses with the data from Ref. 2. Again very good correspondence is found except at higher Reynolds numbers where the flow is no longer laminar.



Acknowledgment: This work was partially supported under Grant number HL15519 of the National Heart and Lung Institute.

References

1. Lee, J. S. and Fung, Y. C., J. Appl. Mech., March 1970, p. 9.
2. Young, D. F. and Tsai, F. Y., J. Biomechanics, 1973, Vol. 6, p. 395.
3. Gosman, A. D., et al., Heat and Mass Transfer in Recirculating Flows, Academic Press, 1969.

A COMPARISON OF STENOTIC FLUID DYNAMICS IN STEADY AND PULSATILE FLOW

by

R. A. Cassanova, D. P. Giddens and R. F. Mabon
School of Aerospace Engineering
Georgia Institute of Technology
Atlanta, Georgia

The turbulence produced distal to a stenosis has been implicated as one of the factors in the development of poststenotic dilation and arterial wall damage (Ref. 1). Experimental studies of stenotic fluid dynamics (i.e., Refs. 2,3,4) have for the most part employed steady mean flow through the constrictions, although some aspects of pulsatile flow were considered in Refs. 3 and 4. This approach has the advantage of simplifying related mathematical computations in any theoretical treatment and of providing a less complicated flow for experimentally investigating vortex shedding and the development of turbulence. However, direct carryover of these steady flow experimental results to a more physiologically realistic pulsatile flow case must be considered cautiously. This paper reports on one aspect of a series of experiments which were conducted with both steady and pulsatile flows through simulated stenoses and were designed to compare the salient features of the turbulence generated by the two flows.

Measurements of the turbulent energy spectra were made with a conical hot film probe distal to a simulated axisymmetric partial occlusion in a 2.54 cm I.D. rigid tube. The minimum area of the occlusion was 25% of the unoccluded area and had a smoothly contoured shape both proximal and distal to the minimum constriction. The experiments were conducted with water. For steady flow, the Reynolds number was 1270 based on conditions proximal to the stenosis. The pulsatile flow upstream of the occlusion had a sinusoidal-shaped waveform with a pulse rate of 0.2 Hz, a frequency parameter of 15, a peak Reynolds number of 2540, and a mean Reynolds number of 1270. The energy spectra of the linearized hot film anemometer output was obtained with an HP Fourier Analyzer. For the pulsatile flow case the entire waveform was analyzed.

Figure 1 shows the centerline pulsatile waveform at several axial positions distal to the minimum area. The development of a turbulent signal during the higher velocity portion of the pulse can be seen. For the most part, this turbulence is dissipated during the lower velocity phase of the pulse.

Figures 2a and 2b show a comparison of the radial variation of the steady and pulsatile flow energy spectra obtained at $x = 2.125D$ ($D =$ unoccluded diameter). The steady flow spectra show a distinct peak at $r = 0$ characteristic of the shedding of vortex rings distal to axisymmetric constrictions and a more broadly dispersed spectra closer to the wall ($r = \frac{1}{2}D$) indicating the breakup of these rings by interaction with the tube wall. The pulsatile results, however, show a more radially homogeneous energy spectra with only a slight spectral peak for $r = 0$.

Figures 3a and 3b illustrate a comparison of the axial variation of the energy spectra for the steady and pulsatile flows. In steady flow, the initial shedding of vortices at $x = 1.5D$ and the development of a random turbulence at more distal positions ($x = 3.125D$, $x = 6.125D$) are characteristic. For the pulsatile case, the spectra did not show a concentration of energy in a narrow frequency band at $x = 1.5D$ as did the steady flow data.

The results of these experiments demonstrate that both the steady and pulsatile stenotic flow can produce turbulent frequencies in the range associated with arterial wall damage (Ref. 1). However, the shedding of vortices in steady flow produces centerline energy spectra with distinct peaks immediately distal to the stenosis.

Flow visualization conducted in the same apparatus indicates that while the steady flow through the stenosis produces a relatively large, low energy recirculation region distal to the stenosis, the pulsatile flow causes a large low frequency vortex to swirl into this same region during the initial phase

of the velocity pulse. Therefore, the pulsatile flow case is characterized by the lack of continuous and distinct recirculation zone and reattachment point.

REFERENCES

- 1 Roach, M. R., "Poststenotic Dilatation in Arteries," in Cardiovascular Fluid Dynamics, Vol. 2, edited by D. H. Bergel, Academic Press, 1972.
- 2 Yellin, E. L., "Hydraulic Noise in Submerged and Bounded Liquid Jets," in Biomedical Fluid Mechanics Symposium, Denver, 1966, pp. 209-221.
- 3 Kim, B. M. and Corcoran, W. H., "Experimental Measurements of Turbulence Spectra Distal to Stenosis," J. Biomechanics, Vol. 7, 1974, pp. 335-342.
- 4 Young, D. F. and Tsai, F. Y., "Flow Characteristics in Models of Arterial Stenosis - I. Steady Flow," J. Biomechanics, Vol. 6, 1973, pp. 395-410. Also, "Flow Characteristics in Models of Arterial Stenosis - II. Unsteady Flow," J. Biomechanics, Vol. 6, 1973, pp. 547-559.

ACKNOWLEDGEMENT

This work was supported by the National Heart and Lung Institute, Grant Number HL15519 and the National Science Foundation, Grant Number ENG74-21986.

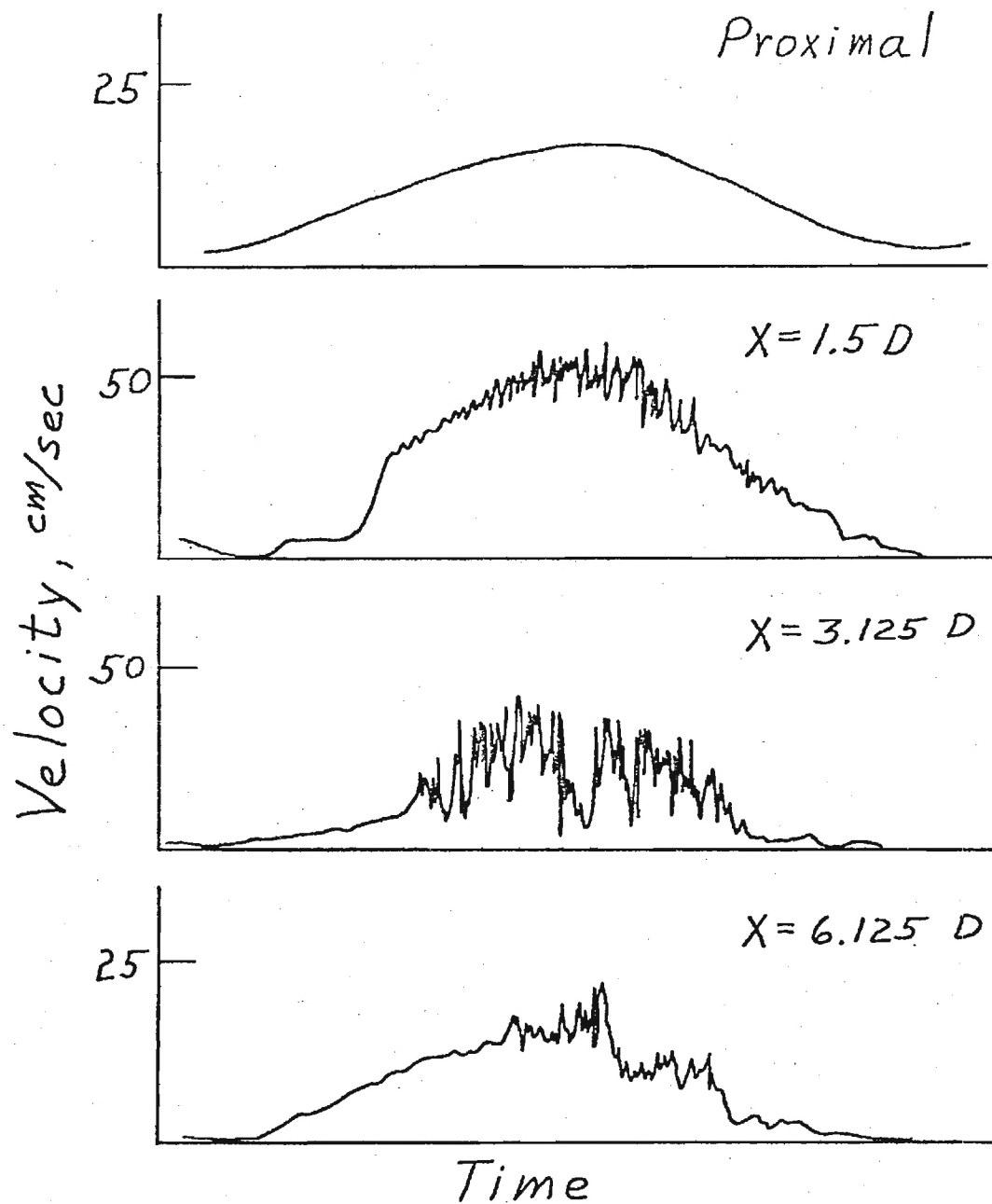


Figure 1. Velocity Waveform in Pulsatile Stenotic Flow

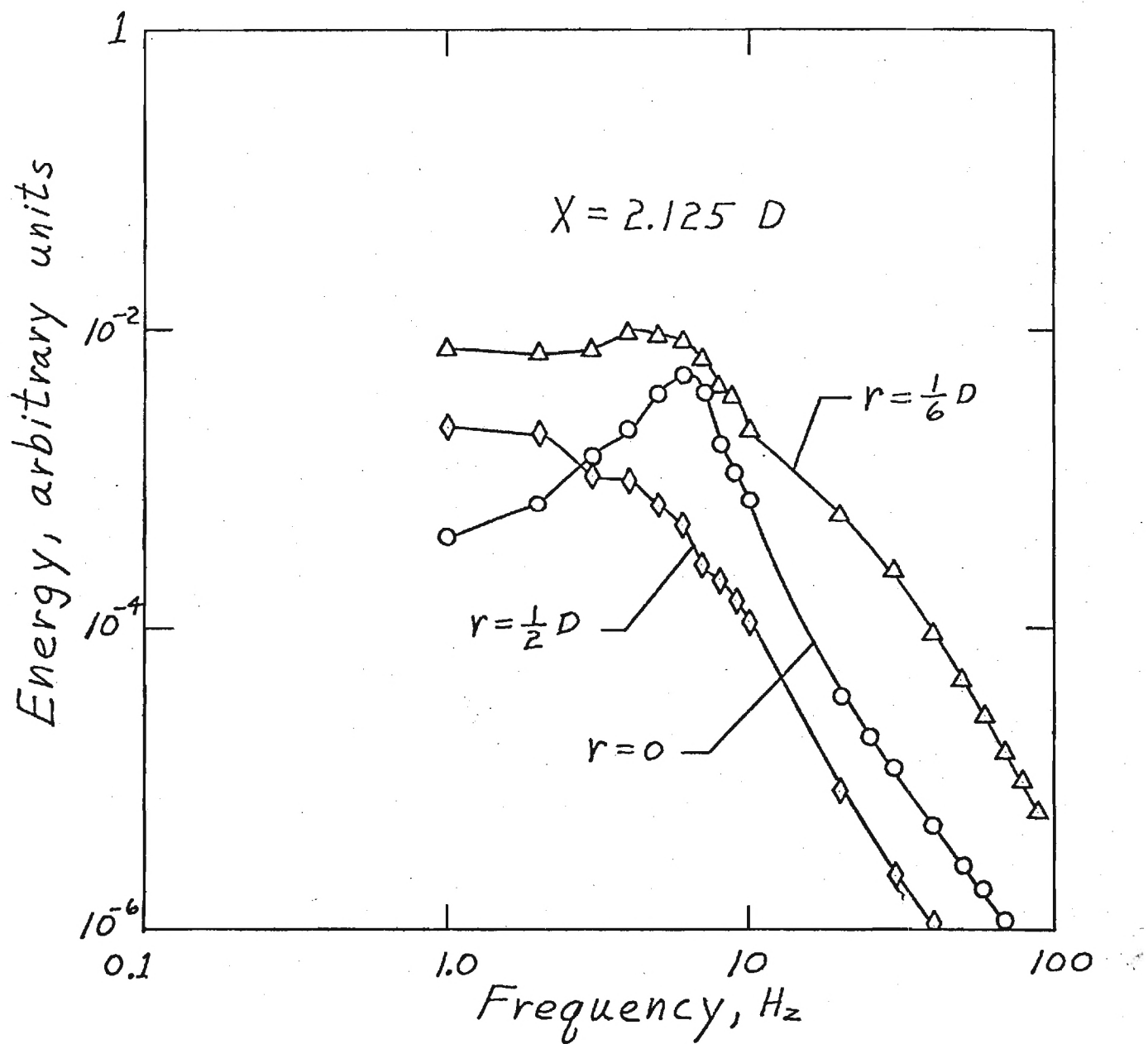


Figure 2a. Radial Variation of Energy Spectra - Steady Flow

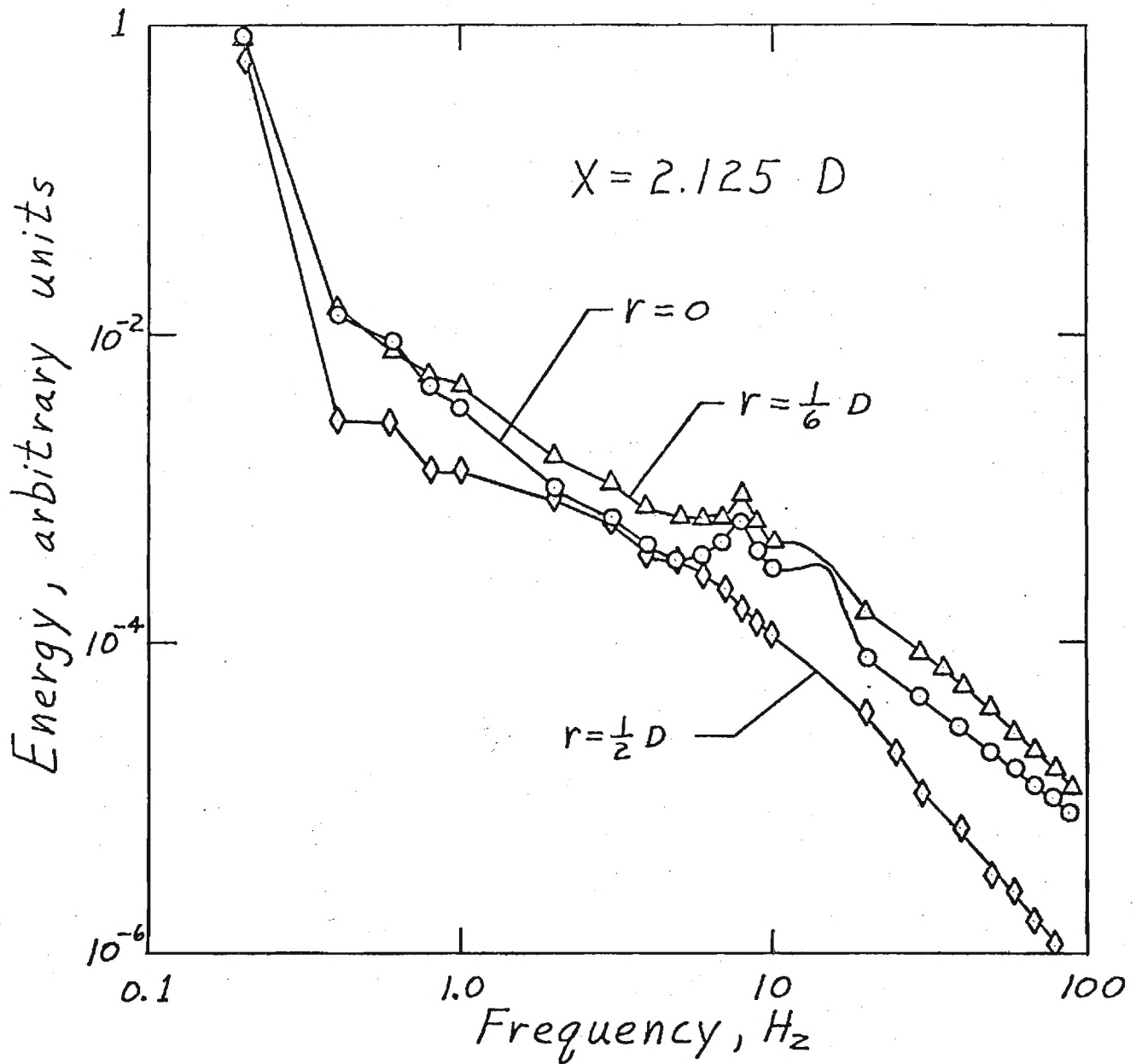


Figure 2b. Radial Variation of Energy Spectra - Pulsatile Flow

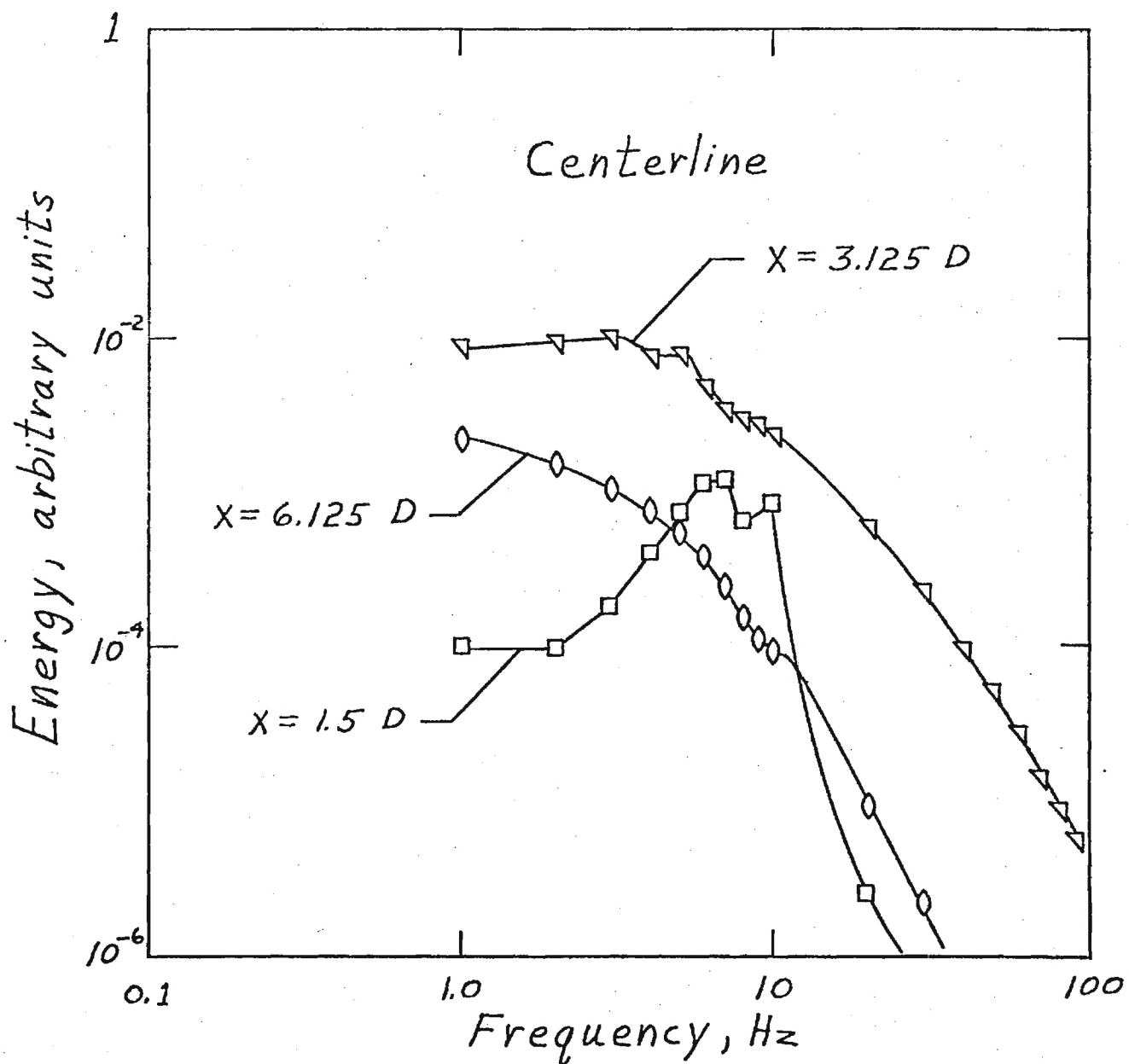


Figure 3a.- Axial Variation of Energy Spectra - Steady Flow

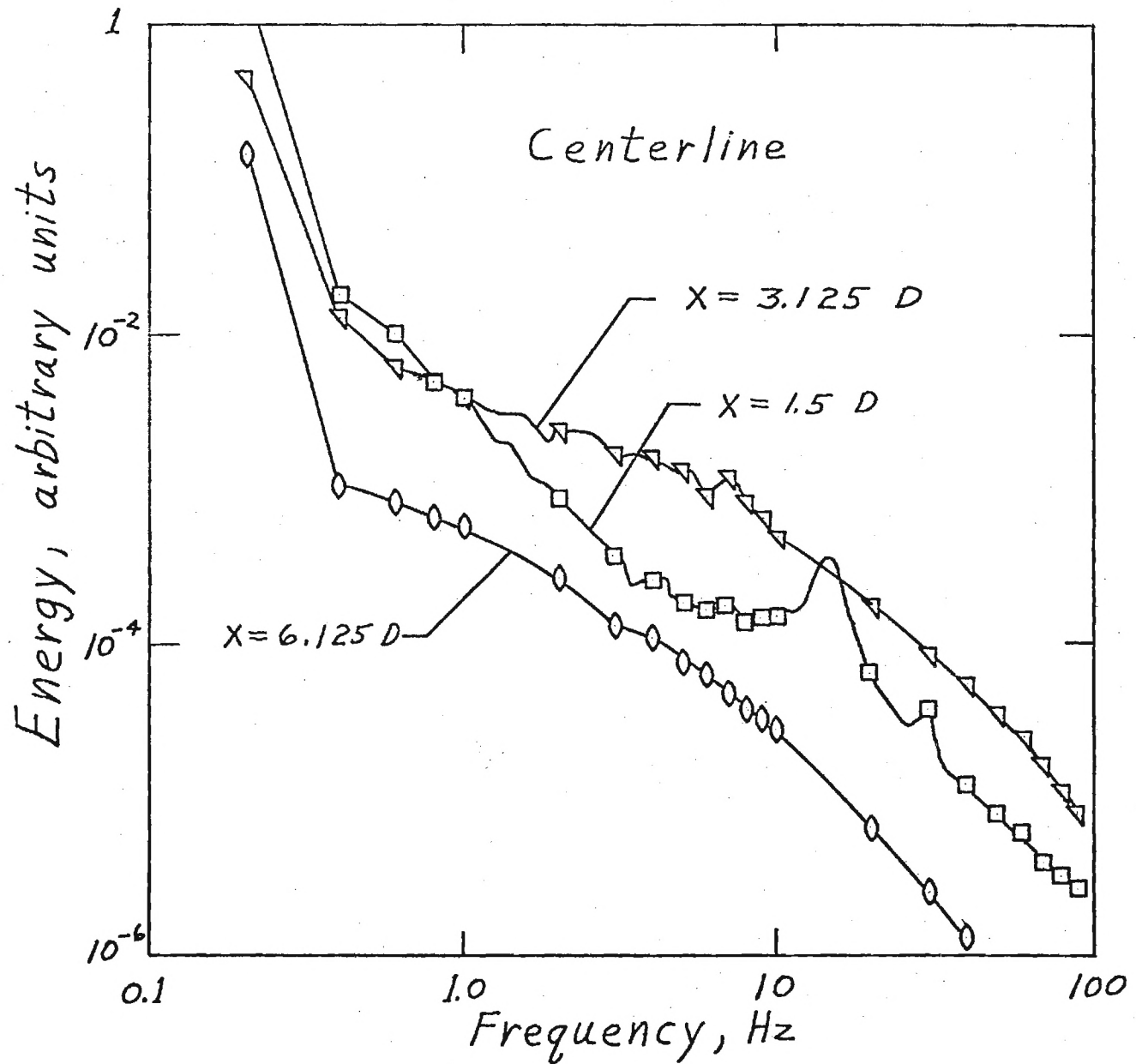


Figure 3b. Axial Variation of Energy Spectra - Pulsatile Flow


Please read instructions on reverse carefully before completing this form.

1. INSTITUTION AND ADDRESS School of Aerospace Engineering Georgia Institute of Technology Atlanta, Georgia 30332		2. NSF PROGRAM National Science Foundation Washington, D. C. 20550	3. GRANT PERIOD 9/1/74-3/31/77 from to
4. GRANT NUMBER ENG74-21986	5. BUDGET DUR. (MO) 30	6. PRINCIPAL INVESTIGATOR(S) D. P. Giddens, R. F. Mabon	7. GRANTEE ACCOUNT NUMBER E-16-654
8. SUMMARY (Attach list of publications to form) R. A. Cassanova, M. D. Deshpande			

Extensive theoretical and experimental investigations into flows through subtotal stenoses have been completed under NSF Grant ENG74-21986. A detailed Final Report is provided which reports the findings obtained during these studies. A brief summary of results follows here.

1. Computer programs were developed for finite difference solutions to the steady Navier-Stokes equations for laminar flow and the $k-\epsilon$ model equations for turbulent flow through contoured constrictions in rigid tubes. These provide theoretical models for stenotic flow fields over a wide range of Reynolds numbers.
2. Our calculations demonstrate that damagingly high wall shear stresses can occur at the site of maximum constriction. These high stresses could lead to the dislodgement of ulcerous material from an atherosclerotic plaque, causing emboli which obstruct distal vessels.
3. Experiments indicate that mild stenoses create marked disorder in distal velocity waveforms for both in vivo and in vitro environments. For example, flow visualization studies in pulsatile flow (frequency parameter = 15, peak upstream Reynolds number = 2540) indicate the formation of a large vortex-like swirl near the distal wall of a constriction, occurring during the initial acceleration portion of each velocity pulse. This vortex breaks away from the wall during the deceleration phase of the cycle and migrates to the center region of the tube, breaking up as it travels.

(continued on attached pages...)

SIGNATURE OF PRINCIPAL INVESTIGATOR/ PROJECT DIRECTOR 	TYPED OR PRINTED NAME D. P. Giddens	DATE 6/28/77
--	--	-----------------

Thus, even for a 25 percent stenosis, significant turbulent disturbances are seen for a pulsatile flow, whereas the corresponding steady flow case exhibited no turbulence. In vivo measurements consistently showed distinct flow disorder for 20-25 percent stenoses.

4. Discrete vortex shedding was observed for 50, 75, and 90 percent stenoses over a wide range of Reynolds numbers studied in vitro for steady flow.
5. Sharp-edge occlusions produced flow instabilities at lower Reynolds numbers in steady flow than did the contoured occlusions. Also, more intense velocity fluctuations were produced by the sharp-edged constrictions.
6. The maximum turbulence energy at the centerline occurred between two and three unoccluded diameters for all occlusions in pulsatile flow.
7. For mild stenoses in vivo the decay of flow disorder is sufficiently rapid that there is no carryover of disturbances from one cycle to the next; but for moderate to severe obstructions, flow disorder persists throughout the cycle.
8. Time ensemble average waveforms in vivo show "split systolic peaks" for moderate stenoses and may offer an early detection technique for moderate arterial obstruction. The mechanism creating these peaks was not isolated.
9. Comparison of energy spectra for acceleration vs. deceleration phases of the velocity waveform is a sensitive method for detecting mild stenoses.

10. Correlation of energy spectra by similarity parameters exists over a limited region distal to stenoses for the in vivo experiments.
11. The pulsed Doppler with phaselock loop capture of the audio signal has been shown to give good high frequency response (up to 500 Hz) in a turbulent pipe flow at a Reynolds number of 23,000. This offers potential for noninvasive measurements of flow disorder if the technique can be applied to pulsatile flows at lower Reynolds numbers.

Publications:

a. In Print

1. "Steady Flow Through Modelled Vascular Stenoses," by M. D. Deshpande, D. P. Giddens, and R. F. Mabon; Journal of Biomechanics, Vol. 9, pp. 165-174, 1976.
2. "Measurements of Disordered Flows Distal to Subtotal Vascular Stenoses in the Thoracic Aortas of Dogs," by D. P. Giddens, R. F. Mabon, and R. A. Cassanova; Circulation Research, Vol. 39, No. 1, pp. 112-119, 1976.

b. Accepted for Publication

1. "Direct Solution of Two Linear Systems of Equations Forming Coupled Tridiagonal - Type Matrices," by M. D. Deshpande and D. P. Giddens; International Journal for Numerical Methods in Engineering.

c. Under Review

1. "Characterization of Flow Disorder Distal to Modeled Stenoses in Steady and Pulsatile Flow," by R. A. Cassanova and D. P. Giddens; submitted to Journal of Biomechanics.
2. "Computations of Turbulent Entrance Flow using a Two-Equation Model," by M. D. Deshpande and D. P. Giddens; submitted to Physics of Fluids, as a Research Note.
3. "Analysis of Disorder in Pulsatile Flows with Application to Poststenotic Blood Velocity Measurement in Dogs," by A. M. A. Khalifa and D. P. Giddens; submitted to Journal of Biomechanics.

d. Under Preparation

A paper is being prepared on results of calculations and measurements of turbulent flow through stenosis models. This is from material in a Ph.D. thesis by M. D. Deshpande.

Theses:

1. "An Experimental Investigation of Steady and Pulsatile Flow Through Partial Occlusion in a Rigid Tube," by R. A. Cassanova; Ph.D. Thesis, Georgia Institute of Technology, 1975.
2. "Steady Laminar and Turbulent Flow Through Vascular Stenosis Models," by M. D. Deshpande; Ph.D. Thesis, Georgia Institute of Technology, 1977.

Inventions: None

Scientific Collaborators:

1. F. D. McLeod, Research Associate, Colorado State University.
2. J. T. Godwin, M. D., Chief of Pathology, St. Joseph's Infirmary, Atlanta, Georgia.
3. R. A. Cassanova, Ph.D., Research Engineer, School of Aerospace Engineering, Georgia Institute of Technology, Atlanta, Georgia.
4. M. D. Deshpande, Ph.D., graduate student at Georgia Tech and presently postdoctoral Fellow, Civil Engineering, Catholic University, Washington, D.C.
5. A.M.A. Khalifa, graduate student at Georgia Institute of Technology.

Comments:

Although we believe that much has been accomplished by this research, it is clear that several important problems remain. One of these is the separation of biological disorder from flow disturbances. The physiologically normal flow in the region of a bifurcation, the prevalent geometry for development of atherosclerotic plaque, may contain a degree of disorder due to the highly three-dimensional nature of the

flow field. This must be established before stenosis-induced flow disorder can be recognized at an early stage of disease development.

A second problem is that of nonstationarity of the disorder for mild to moderate stenoses. The disturbance velocity $u'(t)$ is found to be a nonstationary random variable; and thus the usual concepts of energy spectra, correlation functions, and rms disturbances must be modified. A rigorous treatment of this problem has not been put forth, but our present research efforts are progressing in this area.

The separate and synergistic effects of the flow and the compliant vessel wall have not been isolated. Within the scope of our studies we did not examine whether the split systolic peaks in the time varying ensemble average waveforms were due to vessel elasticity or to a flow phenomenon such as vortex shedding. Likewise, the effects of the flow environment on the vessel wall were not studied.

Finally, the eventual application of characterizing flow disorder for diagnostic purposes in vascular disease will not be possible unless noninvasive methods of making the required measurements are developed. For this reason and from the standpoint of attempting to achieve basic advances in Doppler ultrasound, we have recently devoted considerable effort in studies which are directed at using a pulsed ultrasonic Doppler technique to measure turbulent velocities.

In our follow-on grant, ENG76-23876, we shall be pursuing several of these objectives.

Don P. Giddens, Ph.D.
Associate Professor
School of Aerospace Engineering
Georgia Institute of Technology

E-16-654

GEORGIA INSTITUTE OF TECHNOLOGY
ATLANTA, GEORGIA 30332

OFFICE OF
THE DIRECTOR OF
FINANCIAL AFFAIRS

September 22, 1977

Division of Grants and Contracts
National Science Foundation
Washington, D. C. 20550

Gentlemen:

Enclosed in triplicate is the final fiscal report for Grant
Number ENG74-21986 A02.

If you have any questions or desire additional information,
please let us know.

Sincerely yours,

Evan Crosby
Associate Director of
Financial Affairs

EC/bs
enclosures:

cc: Dr. D. P. Giddens
Dr. R. F. Mabon
Dr. A. L. Ducoffe
Mr. E. E. Renfro
Mr. A. H. Becker ✓
File E-16-654, E-16-347

RESEARCH GRANT
BUDGET & FISCAL REPORT

Form Approved
Budget Bureau No. 99-R0013

Please read instructions on reverse side carefully before completing this form.

INSTITUTION AND ADDRESS Georgia Institute of Technology Atlanta, Georgia		NSF PROGRAM Fluid Mechanics		GRANT PERIOD from 9/1/74 to 3/31/77	
GRANT NUMBER ENG74-21986 A02		BUDGET DUR. (MOS.) 12		REPORTING PERIOD from 9/1/74 to 9/13/77 *	
PRINCIPAL INVESTIGATOR(S) Giddens and Mabon		GRANTEE ACCOUNT NUMBER E-16-654			

	NSF Funded Man Months			NSF AWARD BUDGET	CUMULATIVE GRANT EXPENDITURES <i>Do Not Round</i>
	Cal.	Acad.	Summ.		
A. SALARIES AND WAGES					
1. Senior Personnel					
a. 2 (Co)Principal Investigator(s)		4	1	\$ 14,250	
b. Faculty Associates					
Sub-Total				\$ 14,250	\$ 27,721.00
2. Other Personnel (Non-Faculty)					
a. Research Associates—Postdoctoral					
b. 1 Non-Faculty Professionals		2	1	4,750	
c. 1 Graduate Students				4,000	
d. Pre-Baccalaureate Students					
e. Secretarial—Clerical					
f. Technical, Shop, and Other					
TOTAL SALARIES AND WAGES				\$ 23,000	\$ 48,058.00
B. STAFF BENEFITS IF CHARGED AS DIRECT COST				1,838	2,284.20
C. TOTAL SALARIES, WAGES, AND STAFF BENEFITS (A + B)				\$ 24,838	\$ 50,342.20
D. PERMANENT EQUIPMENT					
E. EXPENDABLE EQUIPMENT AND SUPPLIES				4,200	3,533.65
F. TRAVEL 1. DOMESTIC (INCLUDING CANADA) 2. FOREIGN				750	1,301.40
G. PUBLICATION COSTS				200	352.03
H. COMPUTER COSTS IF CHARGED AS DIRECT COST				1,000	1,801.20
I. OTHER DIRECT COSTS Animal Experiments \$1,750 Consultants - J. T. Godwin \$2,000 F. D. McLeod \$1,000				4,750	3,200.00
J. TOTAL DIRECT COSTS (C through I)				\$ 35,738	\$ 60,530.48
K. INDIRECT COSTS 62% of salaries and wages				14,260	32,170.73 **
L. TOTAL COSTS (J plus K)				\$ 49,998	\$ 92,701.21
M. AMOUNT OF THIS AWARD (ROUNDED)				\$ 50,000	
N. CUMULATIVE GRANT AMOUNT				\$ 93,100	
O. UNEXPENDED BALANCE (N. BUDGET MINUS L. EXPENDITURE)					\$ 398.79

REMARKS: Use extra sheet if necessary * No obligations were incurred outside the grant period of 9/1/74 through 3/31/77.	**65% of \$16,957.00=\$11,022.05	FOR NSF USE ONLY Final Fiscal Report Accepted Grant Closed _____ Remains Open _____ By _____ Date _____ Grants Administration Section, Area _____
	68% of \$31,101.00=\$21,148.68	
	\$48,058.00 \$32,170.73	

SIGNATURE OF PRINCIPAL INVESTIGATOR <i>Don P. Giddens</i>	TYPED OR PRINTED NAME Don P. Giddens/Robert F. Mabon	DATE 9/15/77
I CERTIFY THAT ALL EXPENDITURES REPORTED ARE FOR APPROPRIATE PURPOSES AND IN ACCORDANCE WITH THE AGREEMENTS SET FORTH IN THE APPLICATION AND AWARD DOCUMENTS		
SIGNATURE OF AUTHORIZED OFFICIAL <i>Evan Crosby</i>	TYPED OR PRINTED NAME & TITLE Evan Crosby, Associate Director of Financial Affairs	DATE 9/22/77

FOR NSF USE ONLY

Organ. Code	F.Y.	Fund	Prog. Code	Ob. Class	O/Dres.	Award No.	Amd.	Inst. Code	Unexpended Balance	Trans.	Lot
									\$		

E-16-654

GEORGIA INSTITUTE OF TECHNOLOGY
ATLANTA, GEORGIA 30332

OFFICE OF
THE DIRECTOR OF
FINANCIAL AFFAIRS

October 19, 1977

Division of Grants and Contracts
National Science Foundation
Washington, D. C. 20550

Gentlemen:

Enclosed in triplicate is the revised final fiscal report for Grant
Number ENG74-21986 A02.

If you have any questions or desire additional information,
please let us know.

Sincerely yours,

for Evan Crosby
Associate Director of
Financial Affairs

EC/bs
Enclosures as stated
cc: Dr. D. P. Giddens
Dr. R. F. Mabon
Dr. A. L. Ducoffe
Mr. E. E. Renfro
Mr. A. H. Becker ✓
File E-16-654, E-16-347

RESEARCH GRANT BUDGET & FISCAL REPORT

Please read instructions on reverse side carefully before completing this form.

INSTITUTION AND ADDRESS Georgia Institute of Technology Atlanta, Georgia		NSF PROGRAM Fluid Mechanics		GRANT PERIOD from 9/1/74 to 3/31/77	
GRANT NUMBER ENG74-21986 A02		BUDGET DUR. (MOS.) 12		REPORTING PERIOD from 9/1/74 to 9/13/77*	
PRINCIPAL INVESTIGATOR(S) Giddens and Mabon		GRANTEE ACCOUNT NUMBER E-16-654			

A. SALARIES AND WAGES	NSF Funded Man Months			NSF AWARD BUDGET	CUMULATIVE GRANT EXPENDITURES Do Not Round
	Cal.	Acad.	Summ.		
1. Senior Personnel					
a. 2 (Co)Principal Investigator(s)		4	1	\$ 14,250	
b. Faculty Associates					
Sub-Total				\$ 14,250	\$ 27,721.00
2. Other Personnel (Non-Faculty)					
a. Research Associates—Postdoctoral					
b. 1 Non-Faculty Professionals		2	1	4,750	
c. 1 Graduate Students				4,000	
d. Pre-Baccalaureate Students					
e. Secretarial—Clerical					
f. Technical, Shop, and Other					
TOTAL SALARIES AND WAGES				\$ 23,000	\$ 48,058.00
B. STAFF BENEFITS IF CHARGED AS DIRECT COST				1,838	2,284.20
C. TOTAL SALARIES, WAGES, AND STAFF BENEFITS (A + B)				\$ 24,838	\$ 50,342.20
D. PERMANENT EQUIPMENT					
E. EXPENDABLE EQUIPMENT AND SUPPLIES				4,200	3,533.65
F. TRAVEL 1. DOMESTIC (INCLUDING CANADA)				750	1,501.40
2. FOREIGN					
G. PUBLICATION COSTS				200	352.03
H. COMPUTER COSTS IF CHARGED AS DIRECT COST				1,000	1,801.20
I. OTHER DIRECT COSTS Animal Experiments \$1,750					
Consultants - J. T. Godwin \$2,000					
F. D. McLeod \$1,000				4,750	3,200.00
J. TOTAL DIRECT COSTS (C through I)				\$ 35,738	\$ 60,730.48
K. INDIRECT COSTS					
62% of salaries and wages				14,260	32,170.73
L. TOTAL COSTS (J plus K)				\$ 49,998	\$ 92,901.21
M. AMOUNT OF THIS AWARD (ROUNDED)				\$ 50,000	
N. CUMULATIVE GRANT AMOUNT				\$ 93,100	
O. UNEXPENDED BALANCE (N. BUDGET MINUS L. EXPENDITURE)					\$ 198.79

REMARKS: Use extra sheet if necessary *No obligations were incurred outside the grant period of 9/1/74 through 3/31/77.	65% of \$16,957.00 = \$11,022.05	FOR NSF USE ONLY Final Fiscal Report Accepted Grant Closed _____ Remains Open _____ By _____ Date _____ Grants Administration Section, Area _____
	68% of 31,101.00 = 21,148.68	
	\$48,058.00 \$32,170.73	

SIGNATURE OF PRINCIPAL INVESTIGATOR <i>[Signature]</i>	TYPED OR PRINTED NAME Don P. Giddens/Robert F. Mabon	DATE 10/14/77
I CERTIFY THAT ALL EXPENDITURES REPORTED ARE FOR APPROPRIATE PURPOSES AND IN ACCORDANCE WITH THE AGREEMENTS SET FORTH IN THE APPLICATION AND AWARD DOCUMENTS		
SIGNATURE OF AUTHORIZED OFFICIAL <i>[Signature]</i>	TYPED OR PRINTED NAME & TITLE Evan Crosby, Associate Director of Financial Affairs	DATE 10/19/77

FOR NSF USE ONLY

Organ. Code	F.Y.	Fund ID	Prog. Code	Ob. Class	O/Dres.	Award No.	Amd.	Inst. Code	Unexpended Balance	Trans.	Lot

E-16-654

FINAL REPORT

AN INVESTIGATION OF THE FLOW DISTURBANCES
CREATED BY SUBTOTAL VASCULAR STENOSIS

by

D. P. Giddens, R. F. Mabon
R. A. Cassanova and M. D. Deshpande
School of Aerospace Engineering
Georgia Institute of Technology

for

National Science Foundation Grant ENG74-21986

June 1977

FINAL REPORT

AN INVESTIGATION OF THE FLOW DISTURBANCES
CREATED BY SUBTOTAL VASCULAR STENOSIS

by

D. P. Giddens, R. F. Mabon
R. A. Cassanova and M. D. Deshpande

School of Aerospace Engineering
Georgia Institute of Technology

for

National Science Foundation Grant ENG74-21986

June 1977

TABLE OF CONTENTS

	Page
SUMMARY	ii
I. INTRODUCTION	1
II. STEADY LAMINAR FLOW THROUGH STENOSES	8
III. STEADY TURBULENT FLOW THROUGH STENOSES	41
IV. DISORDER IN PULSATILE FLOWS	90
V. TURBULENCE MEASUREMENTS WITH DOPPLER ULTRASOUND	144
VI. DISCUSSION AND DIRECTIONS FOR FUTURE RESEARCH	147
REFERENCES	151

SUMMARY

Extensive theoretical and experimental research into the fluid mechanics of flow through subtotal stenoses in vessels and models has been carried out under NSF Grant ENG74-21986. This report gives some of the results obtained under the program. Efforts were concentrated on detailed flow field descriptions including velocity profiles, turbulence quantities, and energy spectra. A primary result is that flow disorder occurs during parts of the cardiac cycle when relatively mild vascular constrictions exist.

I. INTRODUCTION

Disturbances in blood flow may occur both naturally and in certain pathologic conditions. In man the fourth component of the first heart sound is usually attributed to turbulence created by blood rapidly entering the ascending aorta and pulmonary artery¹. Turbulence has been detected in the descending aorta of dogs^{2,3}. The conditions under which it occurs suggest a dependence upon Reynolds number and frequency parameter⁴. Flow visualization studies in glass tubing models of branches and bifurcations indicate regions of separated flow and recirculation⁵. The possibility of high frequency fluctuations occurring in these inherently unstable regions should not be overlooked. Sites which may experience this phenomenon are the ramification of the common iliac vessels and the carotid arterial complex. These same areas exhibit a predilection for the deposition of cholesterol-laden plaques within the arterial wall. An erratic flow field is usually present in aortic stenosis and other cardiac valvular disorders¹. Atherosclerosis is responsible for more disabilities and deaths than any other disease. It is characterized by the occurrence of localized plaques in arterial walls, forming constrictions in the vessel lumen which may either reduce blood supply to distal regions or originate emboli that are transported downstream to occlude smaller vessels. Such incomplete vascular stenoses may initiate turbulent velocity fluctuations⁶⁻¹⁰.

Understanding the role of disorder in poststenotic blood flow is important from at least two standpoints: (i) the early detection and diagnosis of occlusive arterial disease and (ii) the pathogenesis and proliferation of atherosclerosis. There is widespread interest in

these areas because of the clinical problems of arterial disease and the inability to explain its origins or to detect its presence in the initial stages.

Physicians have employed the stethoscope since it was introduced by Laennec in 1819 to interpret audible cardiac sounds. It is a very useful tool, but obviously has severe limitations. Verified tape recorded heart sounds have been played for qualified physicians, and the correct identification of the sounds varied from 50 to 75 percent in accuracy¹¹. The difficulty in this method of identification is the determination of the site of origin and the power spectra of the audible frequencies. Currently, there is no available noninvasive technique to quantitatively analyze the location and source of cardiac sounds transmitted through the chest wall to the body surface.

There are two groups of investigators who have recorded sounds generated by turbulent flows distal to vessel obstructions and attempted to relate these to the degree of blockage. Tobin et al¹² have reported on sound measurements taken downstream of brass stenoses placed in a Latex rubber tube. All stenoses were rather severe (75 - 95 percent); and although recognition of this type of lesion is most urgent from a clinical standpoint, it is highly desirable to develop techniques which may be used in earlier stages of plaque development as well.

The work of Lees and Dewey⁷, Fredberg¹³, and Duncan et al¹⁴ goes much further in developing a description of sounds produced at the arterial wall and the distortion of spectra occurring when these sounds are monitored at the surface of the skin. The spectral correlation developed by these investigators to describe the power spectral density

of measured sounds is not the same as that proposed in Ref. 12.

Duncan et al¹⁴ have applied the results of Refs. 7 and 13 in a clinical setting with some degree of success. Estimates of stenosis diameters were made on carotid arteries and compared to angiograms. It appears that these sound measurement techniques are limited in application to lesions which are in an advanced stage of development.

The research results in the present report were obtained by taking the approach that the behavior of the velocity field is the fundamental phenomenon to be studied since the velocity fluctuations comprise the mechanism for creating sounds. Experiments^{9,10} have indicated that disturbances to the velocity are a much more sensitive indicator of mild to moderate stenoses. Furthermore, the velocity field may have profound effects upon both the vessel intima and the transport of material to and from the wall.

Hemodynamic factors have long been suspected culprits in the initiation of arterial disease. These suspicions were aroused by the clinical observation that there is a predilection for atherosclerotic plaques to form at particular sites in the vascular tree, notably regions of vessel branching and bifurcation. The complexity of the problem of pathogenesis is well illustrated by a review of the various fluid dynamic hypotheses proposed as explanations, not to mention the varied biochemical postulates. In the past several years continuing investigations into blood flow patterns have contributed important data which may help in clarifying the puzzling initiation of atherosclerosis, but at the present time an adequate comprehension of causative mechanisms is far from available.

Of particular interest is the work of Fry et al at the National Institutes of Health¹⁵⁻²¹. Among other things their studies have shown that a moderate unidirectional wall shear stress created by the flowing blood tends to orient the endothelial cells and subjacent connective tissue in the direction of the applied stress, whereas unstable stress patterns tend to yield disoriented endothelial cells and collagen and increased quantities of smooth muscle and connective tissue, leading to a greater permeability to proteins²¹.

These and other experimental observations indicate that normal endothelial lining interposes a significant barrier to the transport of albumin and probably lipoproteins as well. This evidence is in general agreement with the hypothesis that most lipids penetrate the arterial wall as lipoproteins²² and that such entry is via the interstices between endothelial cells. However, it has been shown that cholesterol, for example, also enters the vessel structure from the adventitial surface^{23,23}.

Not only are the endothelial cells influenced by local flow patterns, but the underlying collagen, smooth muscle, and connective tissue are affected as well¹⁶. The mechanisms of stimulation are not completely understood, however. Some vessels appear to respond to the flow environment by reacting protectively while others become oriented pathologically.

In another line of approach, several investigators have studied the wall uptake of tagged cholesterol or albumin under varying hemodynamic conditions²⁵⁻²⁷. These experiments were performed to determine if the vessel uptake of lipoproteins is controlled by boundary layer diffusion, surface phenomena, or transport of the material within the wall. Under the conditions imposed it appeared that the diffusion coefficients

necessary to insure that the measured uptake was diffusion controlled were several orders of magnitude less than expected coefficients of the proteins or lipoproteins. The accumulation, however, exhibited a weak but perceptible shear dependence. These authors have therefore concluded that movement of labelled cholesterol from serum to artery wall is not controlled by the diffusion boundary layer²⁶. Caro²⁶ has further suggested that wall shear stress may affect the properties of the arterial interface, perhaps by altering the endothelial surface.

There has been much progress recently in the theoretical description of blood flow. Several treatments of laminar flows have been given for various geometrical configurations. For example, pulsatile flow in distensible and tapered arteries has been studied by Ling and Atabek^{28,29}. Very low Reynolds number flow through partially occluded tubes has been calculated for both steady³⁰ and pulsatile³¹ models. Zones of separation and recirculation are predicted under certain conditions. Recirculating flows have also been computed in the region near a modelled stenotic valve by Hung³². Morgan and Young³³ have developed an integral method of solution for calculating laminar flows through contoured stenoses, and Imbert et al³⁴ have presented finite difference computations of the Navier-Stokes equations for a similar geometry. Deshpande et al³⁵ have provided a very comprehensive treatment of laminar stenotic flows which shall be discussed in Chapter II.

These are but a few examples of calculations of laminar blood flow. However, turbulent flows in the arterial system have not received such attention. Menon³⁶ has studied the turbulent field created in certain angiographic injections using the boundary layer equations and the

k-W model³⁷ of turbulence. In a related line, calculations by Runchal have been reported in Ref. 38 for the flow downstream of a sudden pipe enlargement using this particular turbulence model. The geometry is similar to that of a partial occlusion; and results indicate relatively high values for turbulent intensity in the region where the flow reattaches to the wall, distal to the recirculation region. We have not found any other turbulent blood flow studies in which flow field calculations were made.

A related area of analysis is that of describing disorder in a pulsatile flow. Since the disorder occurring in cardiovascular flows is often such that it exists only over a segment of the cardiac cycle, the fluid dynamics description requires examination of a nonstationary random variable, the disturbance velocity, superimposed on a rather complex velocity waveform. Although several investigators have dealt with the development of turbulence during a pulsatile flow (i.e. Pawel³⁹, Parker⁴⁰, Hussain⁴¹, and Giddens et al¹⁰), there has yet to be presented a rigorous or comprehensive treatment of this problem.

At the beginning of this grant period the state-of-the-art of stenotic flow fields was such that only very low Reynolds number laminar flows had been treated theoretically or experimentally, and virtually nothing was known of the velocity field over a wide range of experimental conditions. Disordered flow analyses were limited to a few measurements of energy spectra of the total velocity waveform and no characterizations of disturbance velocities for conditions found in major arterial flows were available.

The research conducted at the Georgia Institute of Technology for the National Science Foundation has contributed significantly to expanding knowledge of stenotic flows and in the analysis of disorder in pulsatile flows. The following chapters give some of the results obtained under this research program.

II. STEADY LAMINAR FLOW THROUGH STENOSES

The theoretical investigation presented here is one portion of an overall study of flows in regions of subtotal vascular stenoses. The analysis is restricted to steady, laminar flow of a Newtonian fluid through a rigid tube which has a localized axisymmetric constriction. Clearly, such restrictions prevent a direct application of the results to the in vivo situation. The primary effort is to provide a comprehensive treatment of a realistically shaped occlusion contour by obtaining flow field solutions at Reynolds numbers sufficiently large to insure that the full range of laminar flow is covered -- and to compare the results directly with available experimental data.

A. Equations and Boundary Conditions

The continuity and Navier-Stokes equations in cylindrical polar coordinates are taken as the governing relations for the problem. These are

$$\frac{\partial v_r}{\partial r} + \frac{v_r}{r} + \frac{\partial v_z}{\partial z} = 0 \quad (1a)$$

$$v_r \frac{\partial v_r}{\partial r} + v_z \frac{\partial v_r}{\partial z} = -\frac{1}{\rho} \frac{\partial p}{\partial r} + \nu \left[\frac{\partial^2 v_r}{\partial r^2} + \frac{1}{r} \frac{\partial v_r}{\partial r} - \frac{v_r}{r^2} + \frac{\partial^2 v_r}{\partial z^2} \right] \quad (1b)$$

$$v_r \frac{\partial v_z}{\partial r} + v_z \frac{\partial v_z}{\partial z} = -\frac{1}{\rho} \frac{\partial p}{\partial z} + \nu \left[\frac{\partial^2 v_z}{\partial r^2} + \frac{1}{r} \frac{\partial v_z}{\partial r} + \frac{\partial^2 v_z}{\partial z^2} \right] \quad (1c)$$

where r and z are the physical coordinates with the z -axis located along the axis of symmetry of the tube. A sketch of the geometry and coordinate system is shown in Figure 1. No secondary or swirling flows have been allowed so that the total velocity is defined by v_r and v_z , the radial and axial components. The pressure, density and kinematic viscosity are denoted by p , ρ , and ν .

The boundary conditions on velocity at the wall are the usual no slip requirements

$$v_r = v_z = 0 \quad \text{at} \quad r = r_o(z) \quad (2)$$

where $r_o(z)$ describes the local wall radius as a function of z . For the calculations reported here the conditions at a considerable distance upstream and downstream of the stenosis are assumed to correspond to Hagen-Poiseuille flow through a long circular tube of constant cross-section;

$$v_z = U \left(1 - \frac{r^2}{a_o^2} \right) \quad z \rightarrow \pm \infty \quad (3)$$

$$v_r = 0$$

Here, U is the maximum velocity of the parabolic profile and a_o is the radius of the tube in the unoccluded portion.

Nondimensional variables are defined as

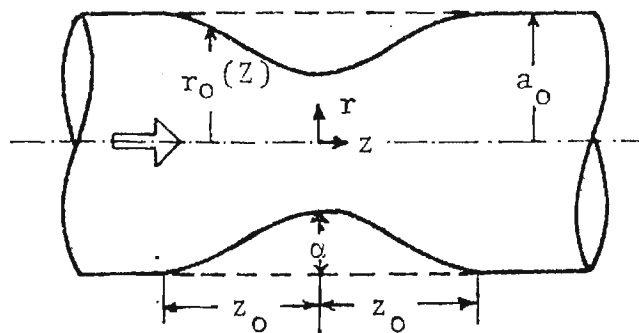


Figure 1. Geometry of Model Stenoses

$$R = \frac{r}{a_o} \quad ; \quad Z = \frac{z}{a_o} \quad ; \quad R_o(Z) = \frac{r_o(z/a_o)}{a_o}$$

$$V_R = \frac{v_r}{U} \quad ; \quad V_Z = \frac{v_z}{U} \quad ; \quad P = \frac{pa_o}{\rho v U}$$

$$Re = \frac{Ua_o}{v} \text{ (Reynolds number).}$$

The stream function Ψ and vorticity ω are introduced by

$$V_Z = \frac{1}{R} \frac{\partial \Psi}{\partial R} \quad ; \quad V_R = - \frac{1}{R} \frac{\partial \Psi}{\partial Z} \quad (4)$$

and

$$\omega = \frac{\partial V_R}{\partial Z} - \frac{\partial V_Z}{\partial R}$$

Using Equations (4) the vorticity and stream functions are related by

$$\omega = - \frac{1}{R} \left(\frac{\partial^2 \Psi}{\partial R^2} + \frac{\partial^2 \Psi}{\partial Z^2} \right) + \frac{1}{R^2} \frac{\partial \Psi}{\partial R} \quad (5)$$

The nondimensional total head is

$$H = P + \frac{Re}{2} \left(V_R^2 + V_Z^2 \right) \quad (6)$$

Equations (1b, 1c) can next be written in terms of Ψ , ω , and H , and then H may be eliminated in the usual manner of cross-differentiation. After additional manipulation one obtains

$$R^2 \left[\frac{\partial}{\partial Z} \left(\frac{\omega}{R} \frac{\partial \Psi}{\partial R} \right) - \frac{\partial}{\partial R} \left(\frac{\omega}{R} \frac{\partial \Psi}{\partial Z} \right) - \frac{1}{Re} \frac{\partial}{\partial Z} \left[R^3 \frac{\partial}{\partial Z} \left(\frac{\omega}{R} \right) \right] \right. \\ \left. - \frac{1}{Re} \frac{\partial}{\partial R} \left[R^3 \frac{\partial}{\partial R} \left(\frac{\omega}{R} \right) \right] \right] = 0 \quad (7)$$

Equations (5) and (7) now provide the governing equations for the problem.

Application of the boundary conditions at $Z = \pm \infty$ causes some difficulty. It is somewhat unsatisfactory to simply impose these at "large" finite values of $|Z|$ since, with increasing Reynolds number, the disturbances created by the stenoses are sizable even far downstream. A suitable transformation may be introduced to map the infinite region of interest into a finite one. This allows a precise application of the boundary conditions. Further, it enables one to space numerical grid points uniformly (in the transformed variable) and yet economically.

The transformation used here is

$$\eta = \tanh(KZ) \quad (8)$$

where K is a constant which can be chosen to group the grid points in an efficient manner. For cases reported here K was taken to be between 0.04 and 0.3 depending upon stenosis geometry. Equations (5) and (7) are written in the new coordinate system as

$$\begin{aligned}
& R^2 \left\{ K(1-\eta^2) \frac{\partial}{\partial \eta} \left(\frac{\omega}{R} \frac{\partial \Psi}{\partial R} \right) - \frac{\partial}{\partial R} \left[\frac{\omega}{R} K(1-\eta^2) \frac{\partial \Psi}{\partial \eta} \right] \right\} \\
& - \frac{K(1-\eta^2)}{Re} \frac{\partial}{\partial \eta} \left[R^3 K(1-\eta^2) \frac{\partial}{\partial \eta} \left(\frac{\omega}{R} \right) \right] - \frac{1}{Re} \frac{\partial}{\partial R} \left[R^3 \frac{\partial}{\partial R} \left(\frac{\omega}{R} \right) \right] = 0 \quad (9)
\end{aligned}$$

$$\frac{\partial}{\partial \eta} \left[\frac{K(1-\eta^2)}{R} \frac{\partial \Psi}{\partial \eta} \right] + \frac{\partial}{\partial R} \left[\frac{1}{K(1-\eta^2)R} \frac{\partial \Psi}{\partial R} \right] + \frac{\omega}{K(1-\eta^2)} = 0 \quad (10)$$

The boundary conditions, in terms of Ψ and ω , become

$$\left. \begin{aligned} \Psi &= \frac{1}{2} R^2 - \frac{1}{4} R^4 \\ \frac{\omega}{R} &= 2 \end{aligned} \right\} \quad \text{at } \eta = \pm 1 \quad (11)$$

$$\left. \begin{aligned} \Psi &= \frac{1}{4} \\ \frac{\partial \Psi}{\partial R} &= \frac{\partial \Psi}{\partial \eta} = 0 \end{aligned} \right\} \quad \text{at } R = R_o(Z) \quad (12)$$

Symmetry at the axis imposes the requirements that

$$\Psi = \omega = 0 \quad \text{at} \quad R = 0 \quad (13)$$

The boundary condition on ω/R along the wall is much more difficult to express and must be treated in an approximate fashion. This is discussed in Ref. 42 since the derivation is not brief.

B. Numerical Solution

Equations (9) and (10) may be recast into the general form:

$$\begin{aligned} a \left[\frac{\partial}{\partial \eta} \left(\Phi \frac{\partial \Psi}{\partial R} \right) - \frac{\partial}{\partial R} \left(\Phi \frac{\partial \Psi}{\partial \eta} \right) \right] - \frac{\partial}{\partial \eta} \left[b_1 R \frac{\partial}{\partial \eta} (c\Phi) \right] \\ - \frac{\partial}{\partial R} \left[b_2 R \frac{\partial}{\partial R} (c\Phi) \right] + Rd = 0 \end{aligned} \quad (14)$$

The first term is due to convection of the quantity Φ , which may be either Ψ or ω/R , while the second and third terms arise as a consequence of diffusion. The last term may be regarded as a source contribution.

The numerical scheme employed follows closely that of Gosman et al⁴³ with modifications being required to treat the curved boundaries in the region of stenoses. Difference equations are generated by integrating over the control volume surrounding a point P (shown by dotted lines in Figure 2). The difference form which results expresses values at P in terms of the eight neighboring nodes (N, E, S, etc.). Upwind differencing

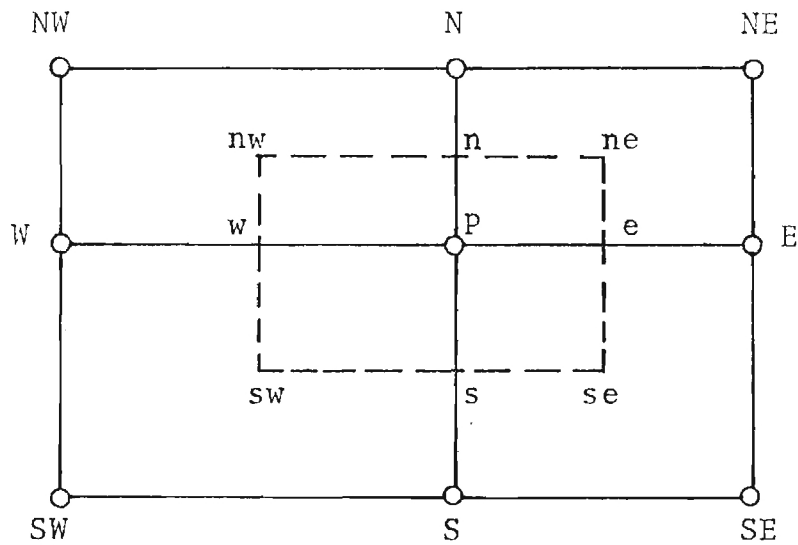


Figure 2. Control Volume for Numerical Scheme

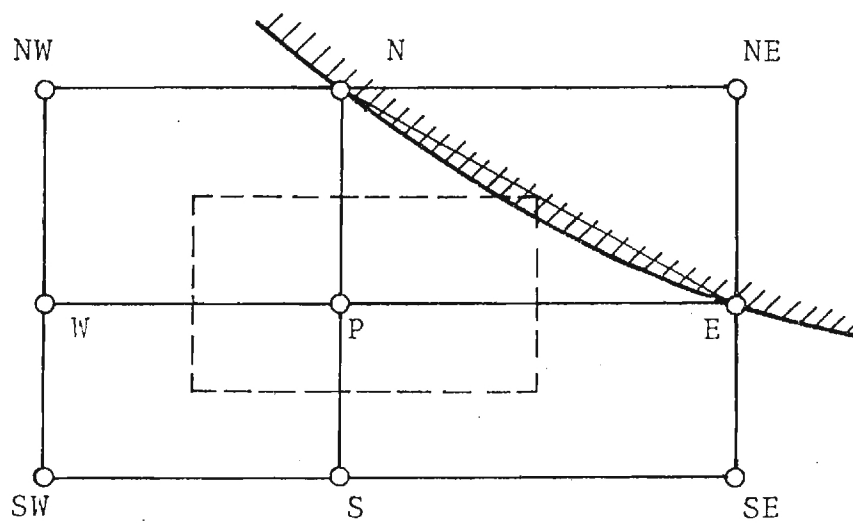


Figure 3. Control Volume Modification Near Curved Boundary

is used in approximating the convection terms. The newly calculated values at P are employed in computations at the next point as the solution proceeds, and iterations over the entire field are required to obtain convergence.

The grid nodes are spaced uniformly in the radial direction, and nodes are made to coincide with the wall boundary to avoid interpolation schemes in locating the surface. This, however, puts some additional restriction in the choice of grid spacing where the boundary is curved since the selection of points in the radial direction then dictates those in the axial coordinate.

Special consideration is given to the integration of convection terms adjacent to the curved boundary. The point n_e (Figure 3), which would be inside the wall if the curvature is convex, is relocated to the wall surface where Ψ is known from the boundary conditions.

The iterations proceed in the following manner. An initial guess is made for the flow field, and boundary conditions on Ψ are imposed. The procedure discussed in Reference 42 is employed to obtain boundary conditions on ω/R at the wall. Then the difference equations are solved for the entire flow to give new values for Ψ and ω . These may then be converted into velocities and pressures if one so desires at this stage. However, this was not actually done until convergence was obtained. This process continues until the differences between successive iterations are less than some small number. (Initially, this was placed at 2×10^{-5} for Ψ and 5×10^{-4} for ω . These constraints were later relaxed as experience was gained in the program).

The numerical procedure was checked for the case of Poiseuille flow with a rather coarse grid spacing consisting of nine points along the radius and 30 points between $Z = -\infty$ and $+\infty$. Initially, guessed values of velocity were taken as zero. After 40 iterations the numerical results differed from the theoretical parabolic profile in the fourth significant digit. There was no difficulty in starting with zero field values and obtaining solutions for Reynolds numbers as large as 10^6 .

In the case of tube geometries containing constrictions, calculations were first done for $Re = 0$, beginning with parabolic profiles at each station. The converged results were then used as the initial profiles for the next higher Reynolds number. This proved to be a convenient and economical procedure rather than a necessity. If results are required for a single large Reynolds number, they can be obtained directly.

For the computations reported here, 31 grid points were taken in the radial direction ($0 \leq R \leq 1$) and the number of axial stations varied from 91 to 111, with a greater number of points being placed downstream of the occlusion. The number of iterations required was usually from 300 to 400. This required four to six minutes of computer time on the UNIVAC 1108. Various numerical experiments were performed using different numbers and spacings of grid nodes to assure that accuracy was consistently maintained.

C. Geometry of Stenoses

The numerical scheme can be applied to axisymmetric contours of arbitrary profile. The form of the stenoses chosen for the present

Table 1. Geometries of Model Stenoses and Reynolds Number Range for Laminar Flow Study

Model	α	Z_o	Area Reduction	Reynolds Number Range for Calculations	Computed Separation Reynolds Number
M0	0.500	1	75%	0 - 300	10.1
M1	0.333	4	56%	0 - 2000	195
M2	0.667	4	89%	0 - 200	17.0
M3	0.667	2	89%	0 - 100	8.75
M4	0.500	2	75%	--*	--

* Not included in Laminar Flow study

studies was

$$R_o(Z) = 1 - \frac{\alpha}{2} \left[1 + \cos \left(\frac{\pi Z}{Z_o} \right) \right] \quad ; \quad -Z_o \leq Z \leq Z_o \quad (15)$$

with

$$R_o(Z) = 1 \quad ; \quad |Z| \geq Z_o$$

where α and Z_o are constants which may be adjusted to allow different lengths and degrees of occlusion. This form corresponds to that employed experimentally by Young and Tsai⁴⁴.

Table 1 lists four of the models studied. The first, Model M0, closely approximates the contour used by Lee and Fung³⁰ while the others duplicate the axisymmetric shapes investigated by Young and Tsia⁴⁴. The table also includes the Reynolds number ranges over which solutions were obtained during the study. It should be emphasized that for all models convergent solutions can be obtained throughout the laminar flow regime so that it is the naturally occurring flow instabilities in the experiments rather than numerical instabilities in the numerical analysis that prevent realistic comparisons at large Reynolds numbers.

D. Results

1. Streamlines and vorticity distribution

A description of the various possible steady laminar flow patterns which may be encountered is perhaps rendered by a display of streamline contours for representative conditions. Figure 4 illustrates curves of constant stream function and vorticity for three such cases. The

contours shown in Figure 4a are for a relatively mild constriction (Model M1) and a Reynolds number lower than the separation value. No recirculation region is present and the flow is but mildly perturbed as it passes through the narrowing. Although asymmetry about the $Z = 0$ plane is not clearly noticeable in the streamline patterns, it is readily apparent in the vorticity contours.

Figure 4b illustrates flow behavior in the region of a more severe stenosis (Model M0) at a Reynolds number sufficiently large to yield separated flow. The recirculation region is confined to the downstream neighborhood of the constriction, separation being initiated distally to the minimum area. Finally, at a much higher Reynolds number (200) the separated flow region is predicted to extend for a considerable distance downstream as shown in Figure 4c. It is emphasized that these figures represent theoretical flowfields under the assumptions given. In particular, no provision has been made for the occurrence of flow instabilities as Reynolds number increases. We shall return to this point in a later section.

2. Separation and reattachment points

Calculations were performed corresponding to the axisymmetric cases reported by Young and Tsai so that a comparison could be made with experimental data. The locations of separation and reattachment in that work were determined visually using dye injection methods. Figure 5 compares the present theoretical predictions with their experimental observations. For model M1, a relatively mild stenosis, the separation Reynolds number is rather high-approximately 200. The theory and experiment agree well for this onset value; and for higher values the locations

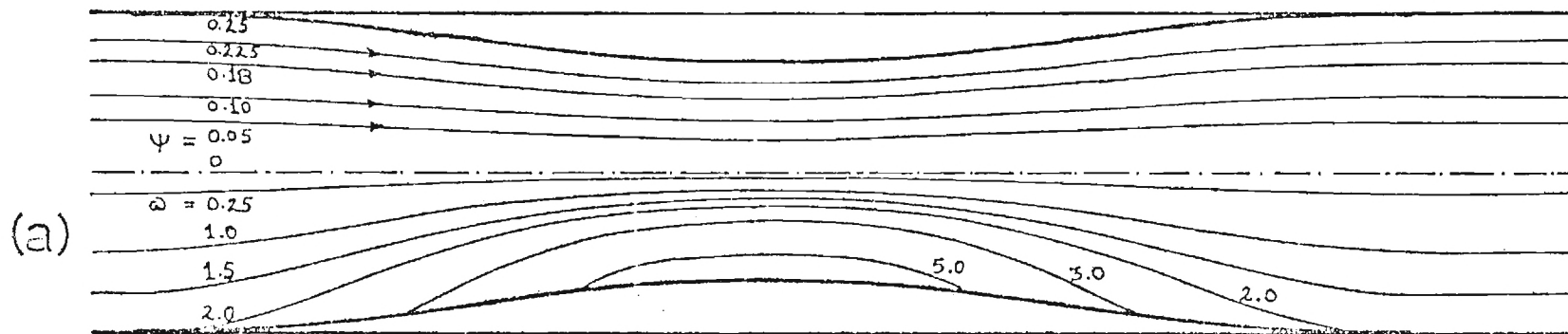
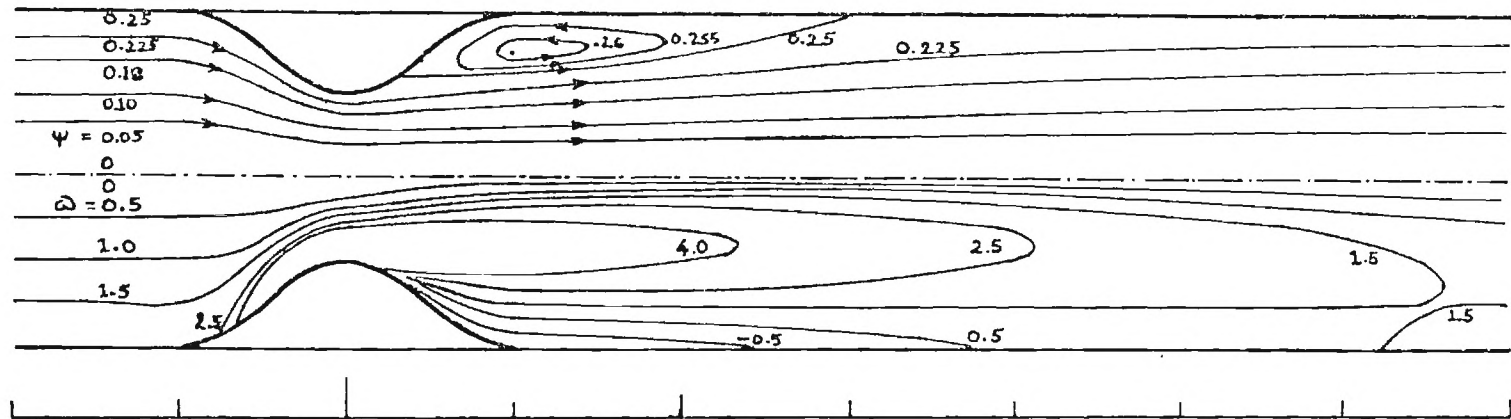


Figure 4a. Stream Function and Vorticity Contours for Model M1
 $Re = 100$

(b)



(c)

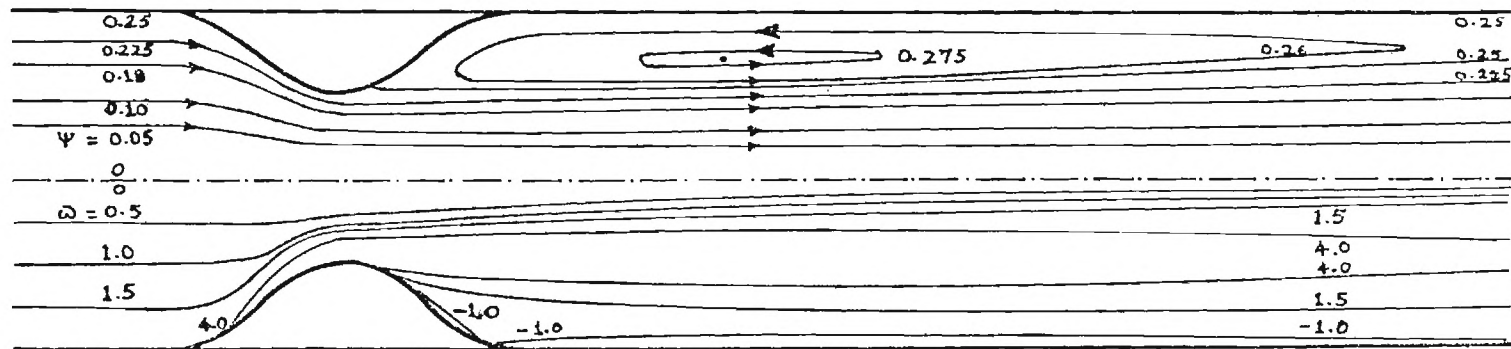


Figure 4b,c. Stream Function and Vorticity Contours for Model M0
(b) $Re = 50$, (c) $Re = 200$

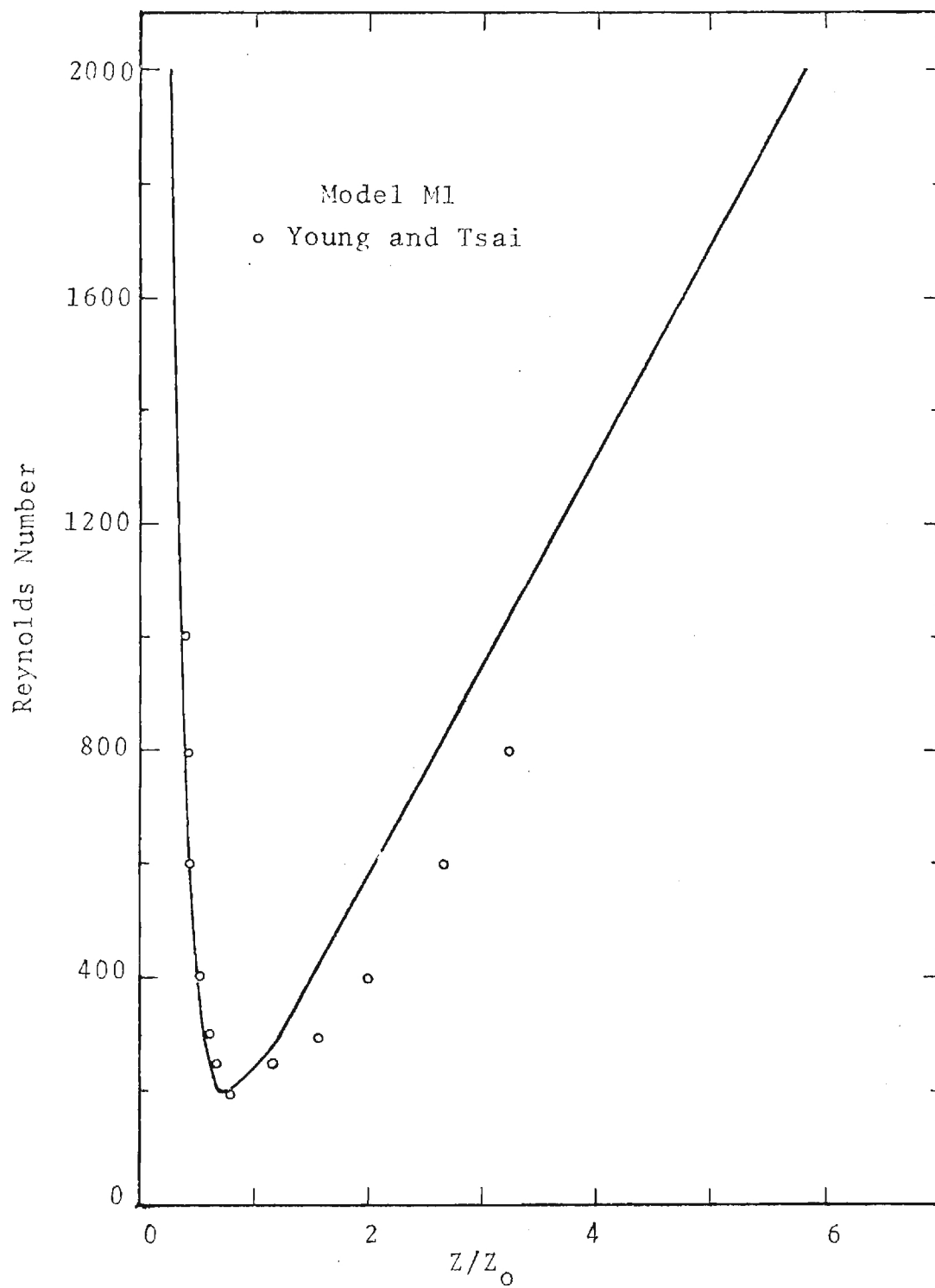


Figure 5a. Separation and Reattachment Points for Model M1

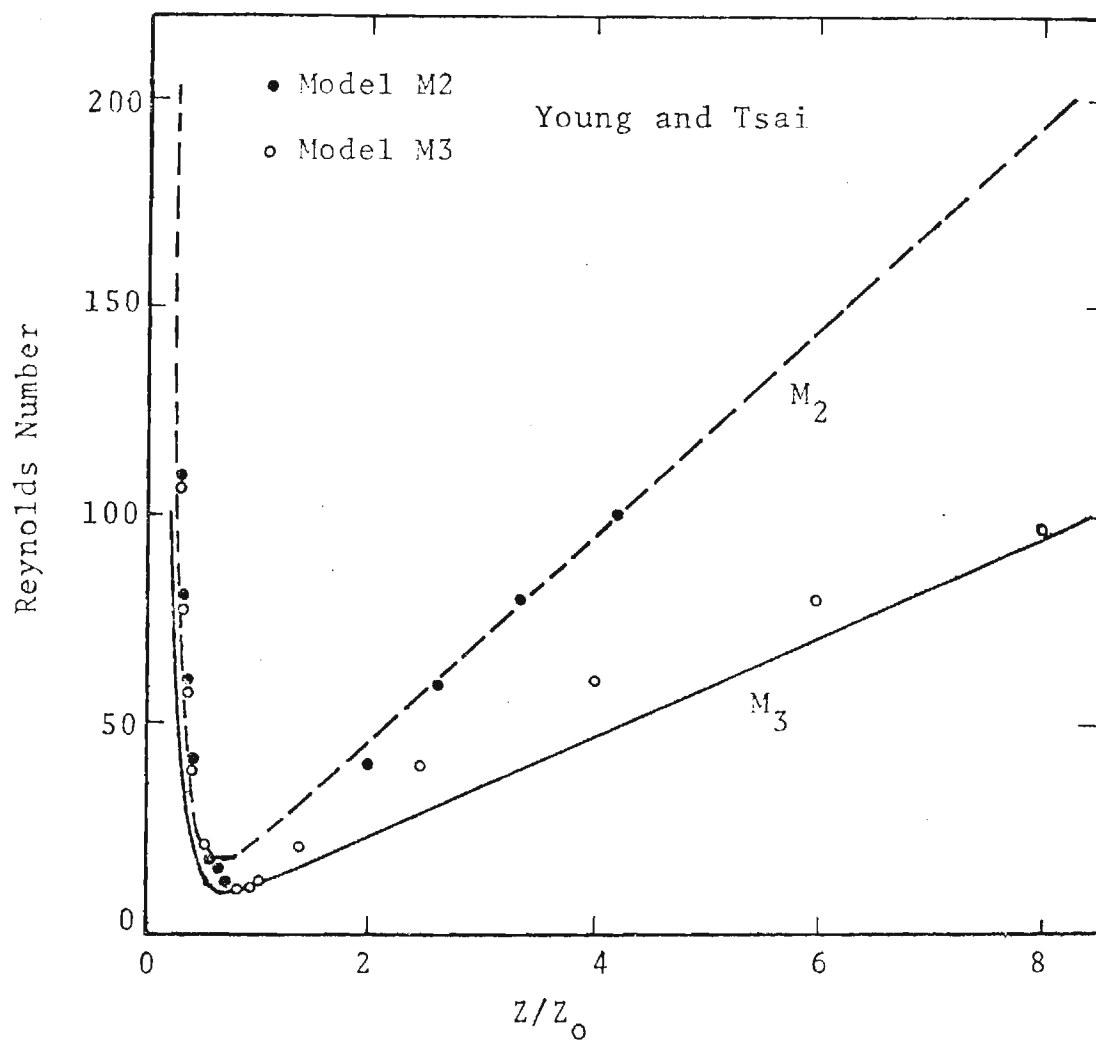


Figure 5b. Separation and Reattachment Points for Models M2 and M3

of the separation points compare favorably (see Figure 5a). A greater disagreement is found for the reattachment points. This is not surprising, however, since Young and Tsia report that flow instabilities were recorded for this case at Reynolds numbers as low as 300. Furthermore, the reattachment points are difficult to ascertain experimentally. One usually observes a reattachment "zone" due to dye diffusion and, for sufficiently high Reynolds numbers, due to intermittency of the dividing streamline.

Figure 5b illustrates the comparisons for models M2 and M3. The agreement here is rather good - and it is noted that flow instabilities were not observed by Young and Tsai over the Reynolds number range depicted in this figure. One point of interest is that the onset of separation was observed experimentally to occur at a Reynolds number of 10 for both of these models, whereas the calculations give values of 8.75 for Model M3 and 17.0 and M2. It is believed that this is adequate agreement considering the experimental difficulties of delineating this onset at such low flow rates.

3. Pressure drop across stenosis

At a given Reynolds number the presence of a stenosis increases the resistance which the flow experiences. Although it would be presumptuous to extrapolate this directly to the in vivo vascular system (due to the presence of compensatory mechanisms such as vasodilation and collateral circulation), there is a tendency for severe stenoses to reduce the supply of blood to distal regions. Thus, the pressure losses through such constrictions are of physiologic interest.

The measurements reported by Young and Tsai were obtained with transducers connected to wall taps located at ± 8 diameters from the plane

of minimum constriction. Values of wall pressure at corresponding locations were obtained from the numerical computations and are compared with the experimental data in Figure 6. The range of Reynolds numbers which the theory and this phase of the experiments have in common is rather limited due to two reasons: (i) the experiment is difficult to perform at very low Reynolds numbers, and (ii) the flow instabilities including transition to turbulence, which are not accounted for in the theoretical model, occur experimentally at moderate values of Re . Where the two results share a common validity, however, the agreement is quite good.

The pressure distribution along the tube is also of interest. Figure 7 illustrates the variation of pressure along the axis and at the surface for a severe stenosis, M3, at two Reynolds numbers. There is a rapid fall in pressure as the occlusion is approached, and for these cases a local minimum in the pressure is obtained just prior to the separation point. The values corresponding to Hagen-Poiseuille flow would be obtained by extrapolating the initially straight segment of these curves through the $Z = 0$ line. Of further interest is the fact that radial pressure gradients are small for these Reynolds numbers. It was only for short and severe stenoses that radial gradients were comparable in magnitude to those in the axial direction. Also, one may note the change in direction of the radial pressure gradient near the region of maximum area reduction.

In all cases the calculations showed a recovery of the pressure gradient far downstream to the fully developed pipe flow result.

4. Wall vorticity (shear stress)

The nondimensional wall vorticity ω_w is of considerable interest

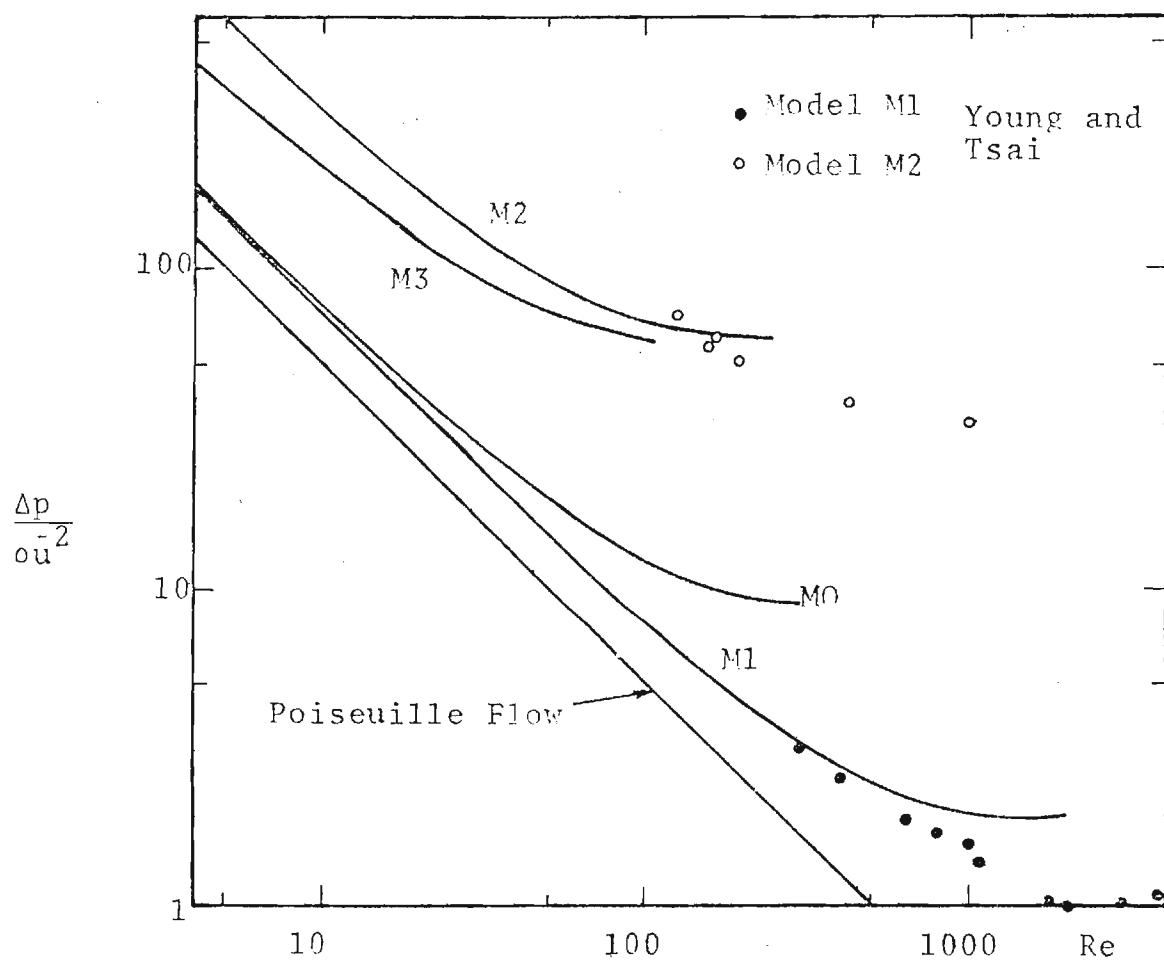


Figure 6 . Pressure Drop Across Stenoses in Laminar Flow

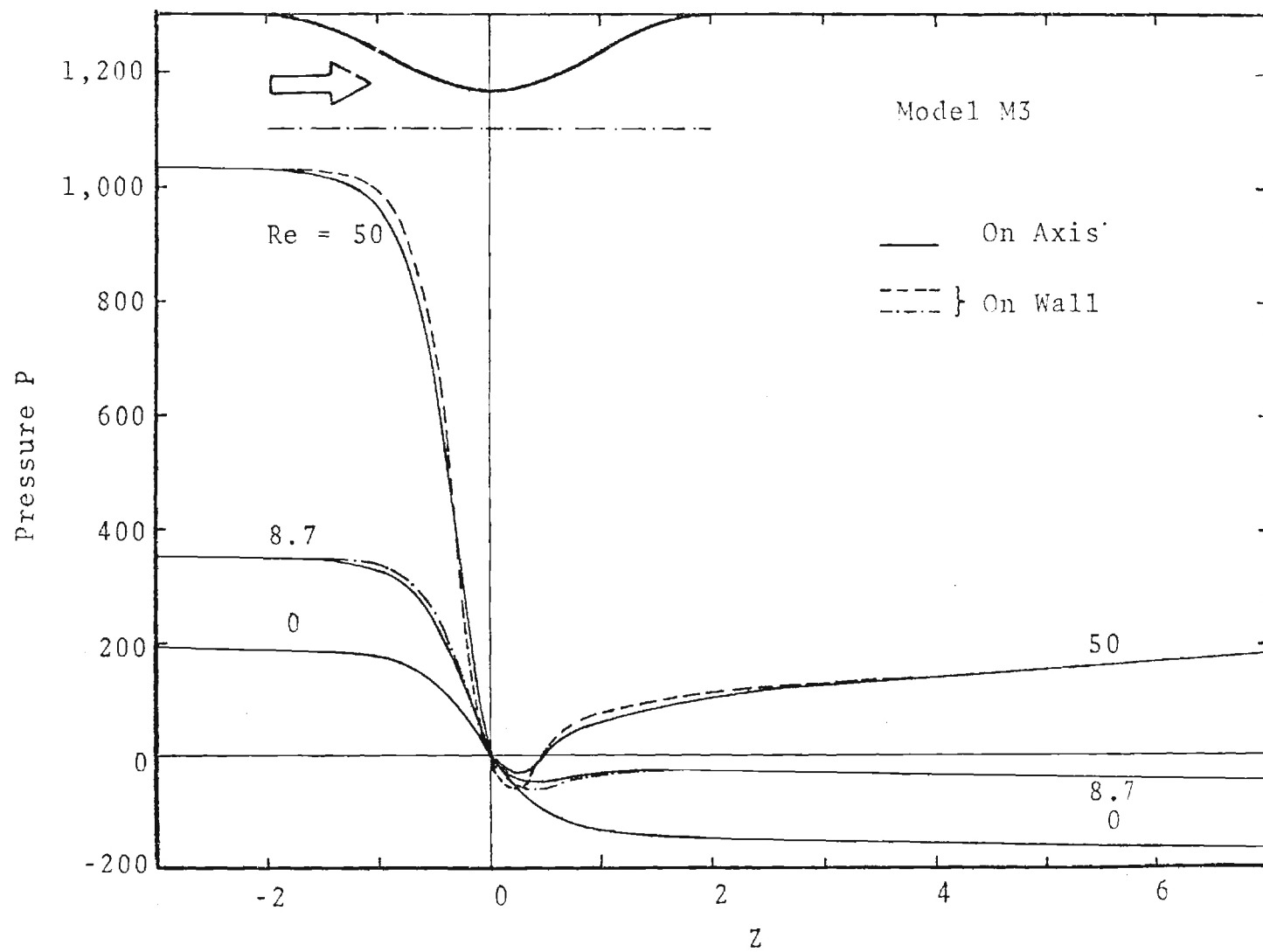


Figure 7. Pressure Distribution in Laminar Flow, Model M3

because of its relation of the value of shear stress acting on the solid surface. The shear stress at the wall is given by

$$\tau_w = \frac{\rho \nu U}{a_o} \omega_w$$

Since there is no reliable method of determining wall shear stress experimentally in regions near the recirculation zone, the theoretical calculations offer some insight into the behavior of this quantity. Figure 8a presents results for Model M0 for four Reynolds numbers. For $Re = 0$ the variation in wall vorticity is distributed symmetrically about the plane of minimum area. As Reynolds number increases, this peak stress shifts upstream slightly. At $Re = 20$ the flow has already formed a separated region as evidenced by negative values of shear stress at the tube surface. This zone increases in extent, both proximally and distally, as the Reynolds number is further increased to 50 and 200.

Figure 8b shows similar curves for Model M3, a relatively severe stenosis. Values for Reynolds number selected for display are 1.0, 8.7, and 100 which correspond to no separation, incipient separation, and extended recirculation region cases, respectively. Note that here, although the peak shear stress has again migrated upstream somewhat with increasing Reynolds number, this movement is scarcely detectable.

Figure 8c illustrates the maximum values of wall vorticity for all four models as a function of Reynolds number. The Hagen-Poiseuille value of 2.0 is shown for comparison. Computational values by Lee and Fung indicated in the figure correspond to their geometry which resembled Model M0. The rapid increase in wall vorticity (and hence wall shear

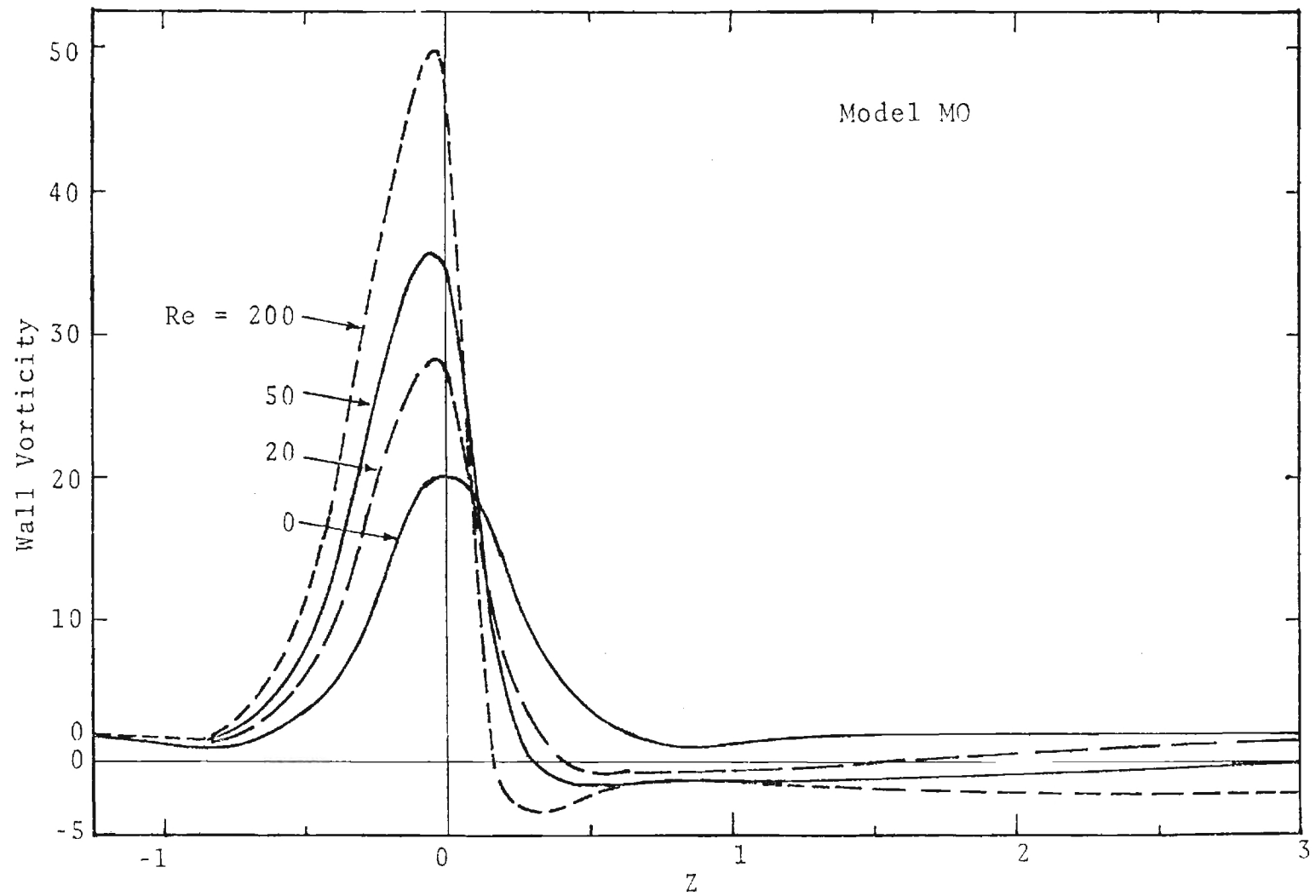


Figure 8a. Wall Vorticity in Laminar Flow, Model M0

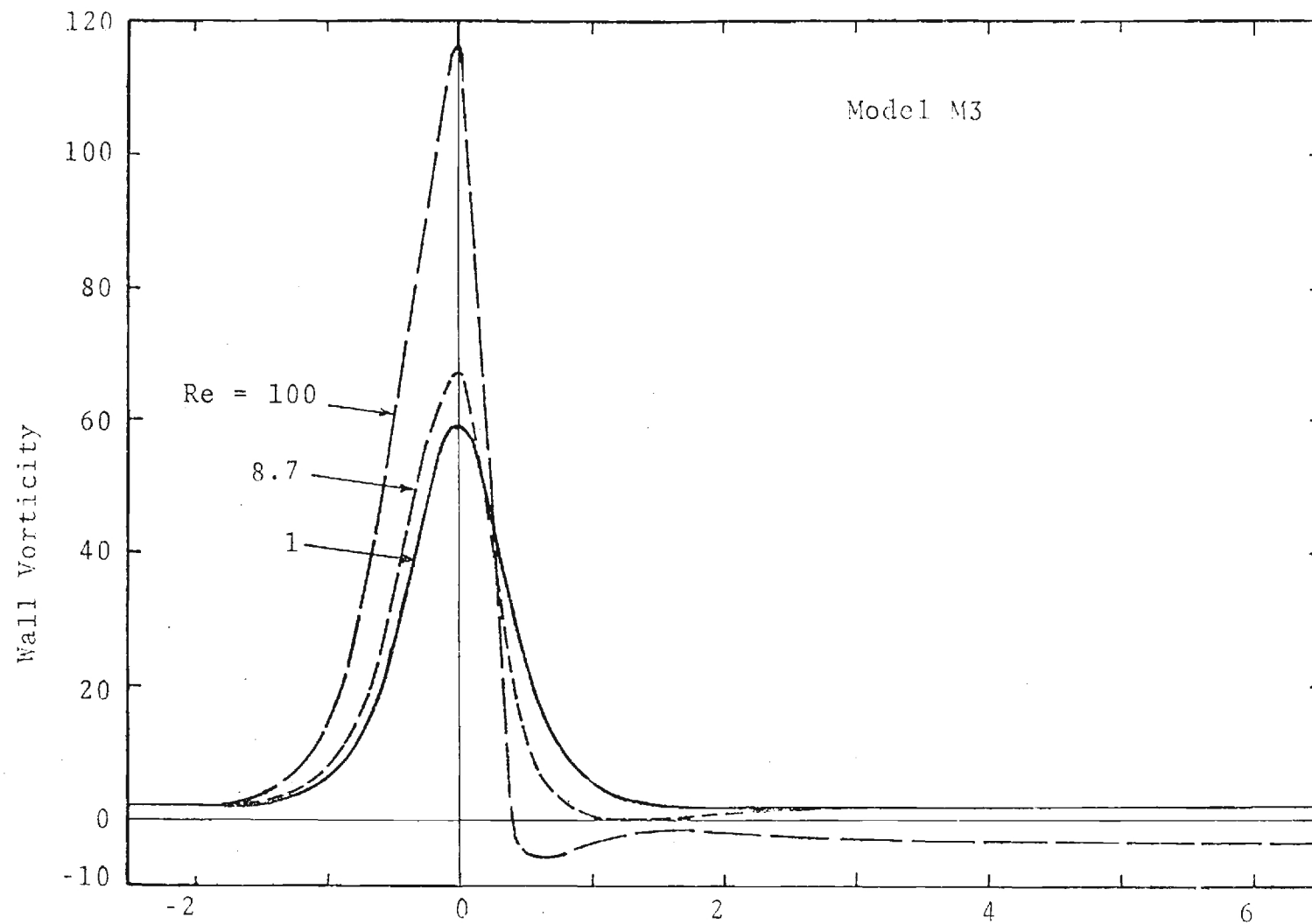


Figure 8b. Wall Vorticity in Laminar Flow, Model M3

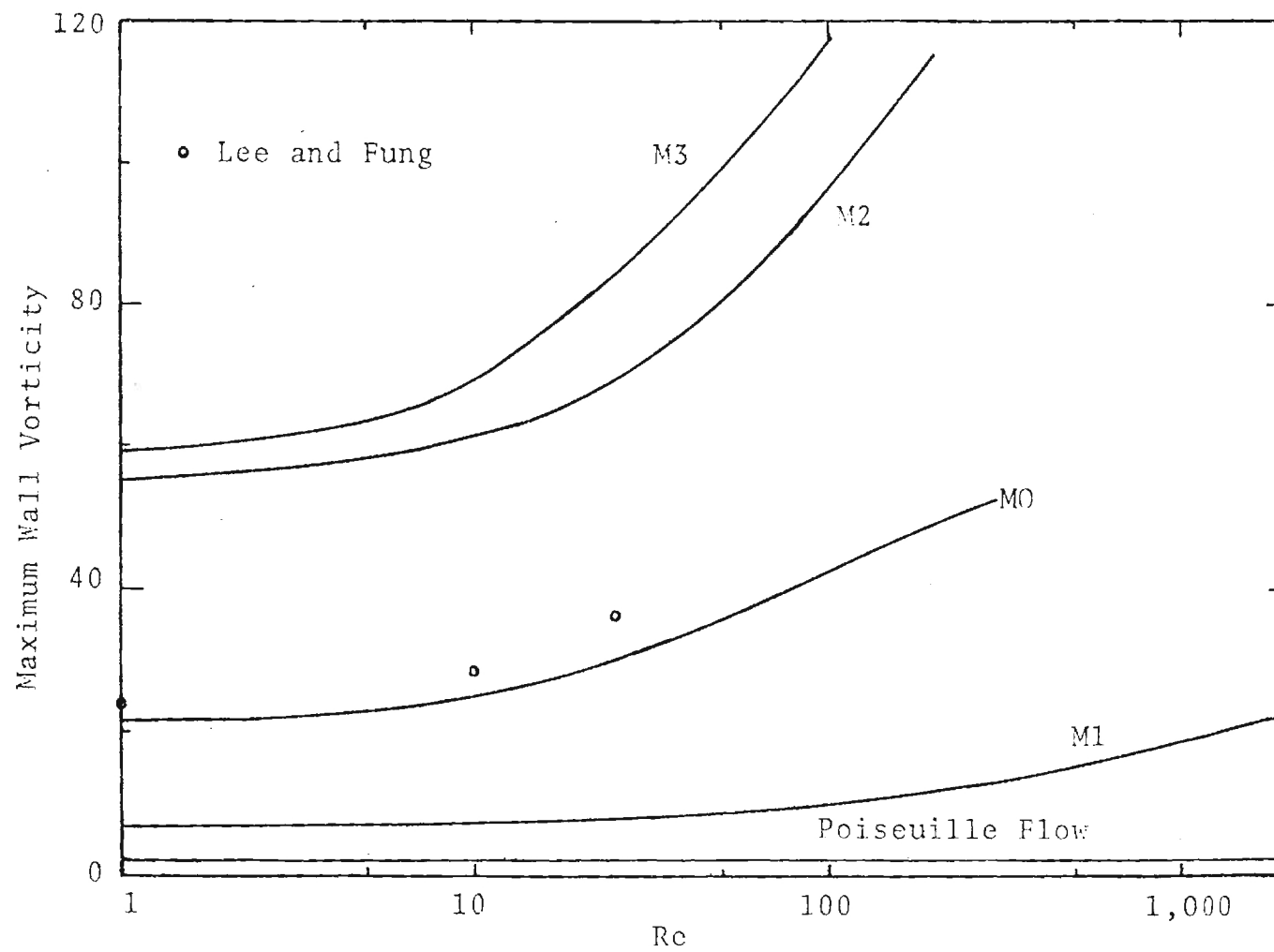


Figure 8c. Maximum Wall Vorticity in Laminar Flow, All Models

shear stress) with Reynolds number for the severe stenoses is quite apparent.

5. Flow velocities

The velocity profiles are also of interest since they provide a detailed description of the flow field. Figures 9a and 9b give examples of the velocity components for Model M2 at $Re = 50$ and 200 . The formation of a jet-like profile in the vicinity of the throat is apparent. However, the fluid is still accelerating at $z = 0$ as evidenced by the slightly negative values of radial velocity. Thus, peak flow velocity is reached just downstream of the minimum constriction.

Regions of reverse flow are clearly seen. Both velocity components undergo a change in sign within the recirculation region at these stations, indicating the strongly elliptic nature of the problem.

Figure 10a shows that the maximum axial velocity may not occur on the centerline axis for all cases. For example, for the relatively short stenosis M0, the peaks occur symmetrically at $R = 0.23$ for $Re = 200$. Figure 10b indicates a rather high value of radial velocity for the same case. At $Z = -0.3$ it is 12 percent greater than the average velocity in the unoccluded tube.

The variation of centerline velocity with axial location is shown in Figure 11 for Model M3 and four representative Reynolds numbers. For $Re = 1$ there is no recirculation region. $Re = 8.7$ corresponds to incipient separation and the two higher values (50 and 100) experience zones of recirculation. For these latter cases the decrease in centerline velocity is approximately linear in Z .

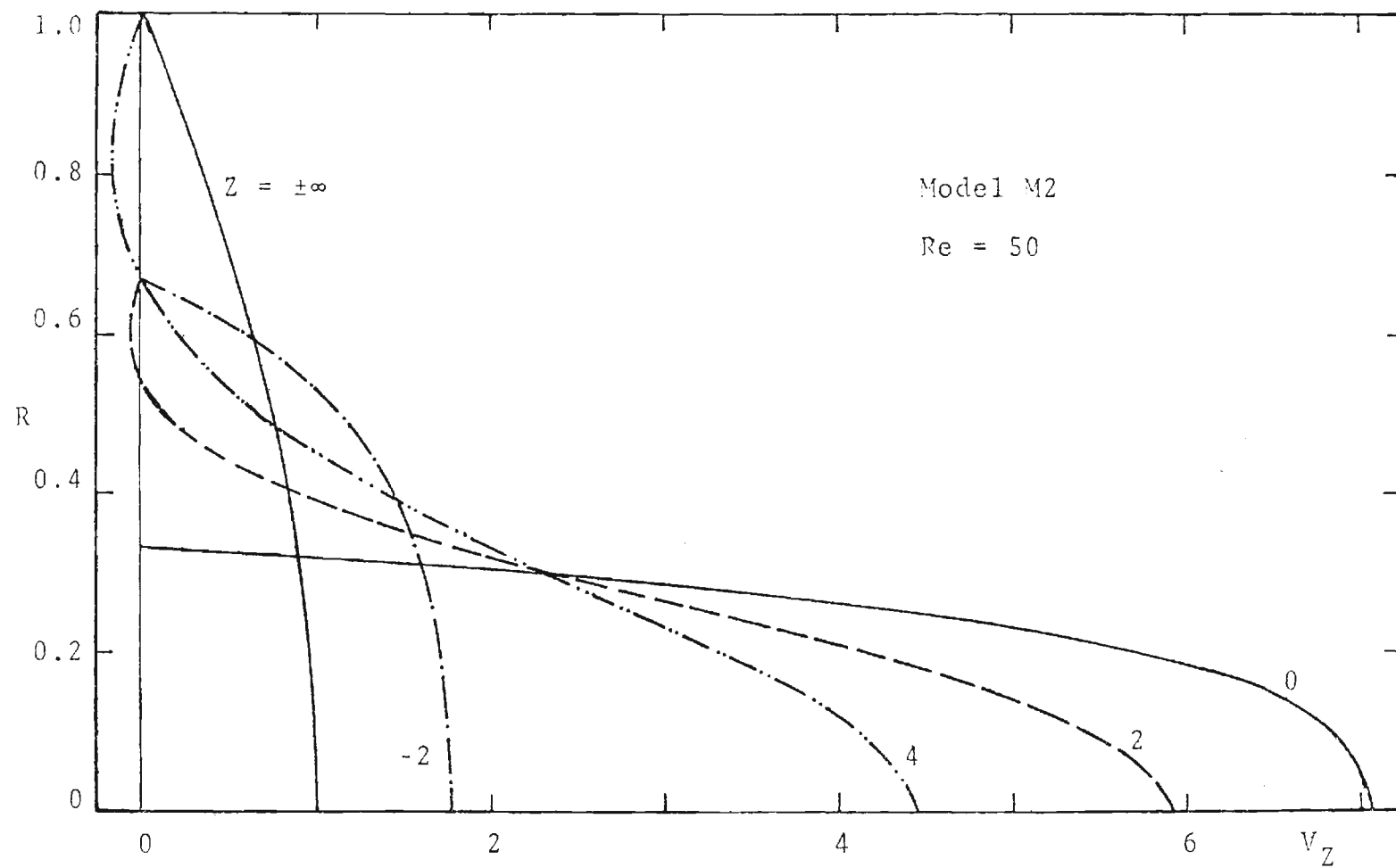


Figure 9a. Axial Velocity Profiles, Model M2, $Re = 50$

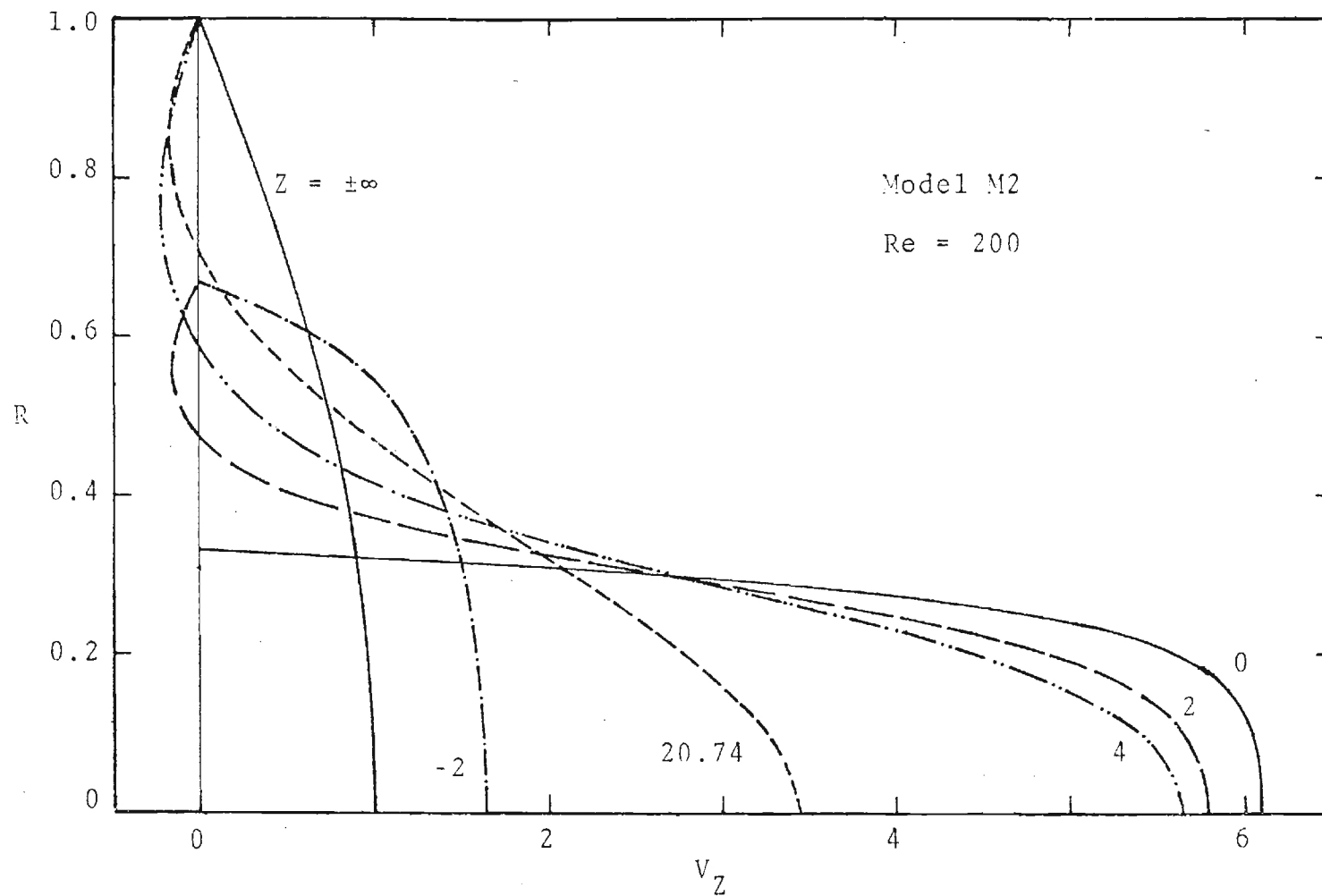


Figure 9b. Axial Velocity Profiles, Model M2, $Re = 200$

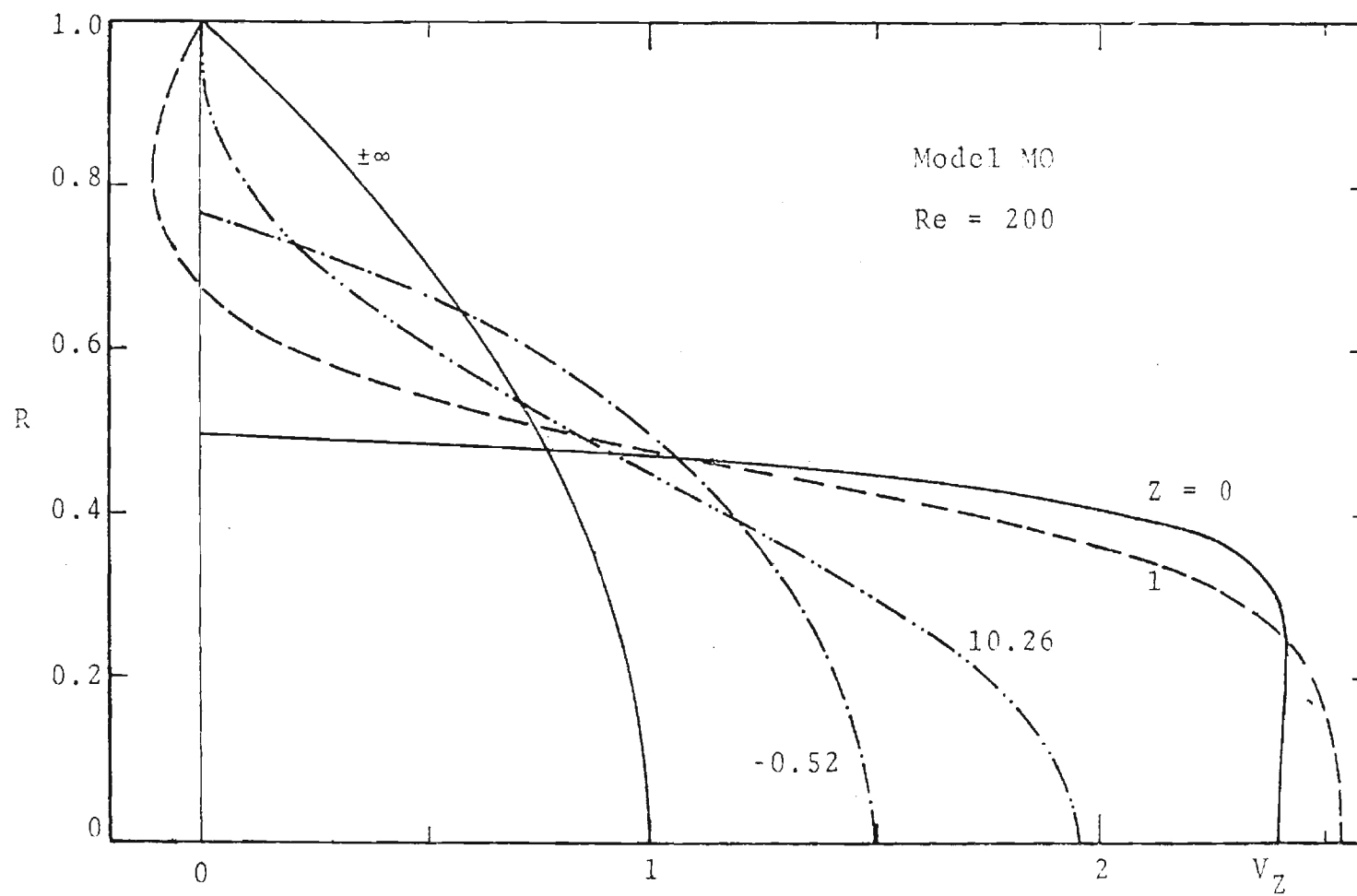


Figure 10a. Axial Velocity Profiles, Model M0, Re = 200

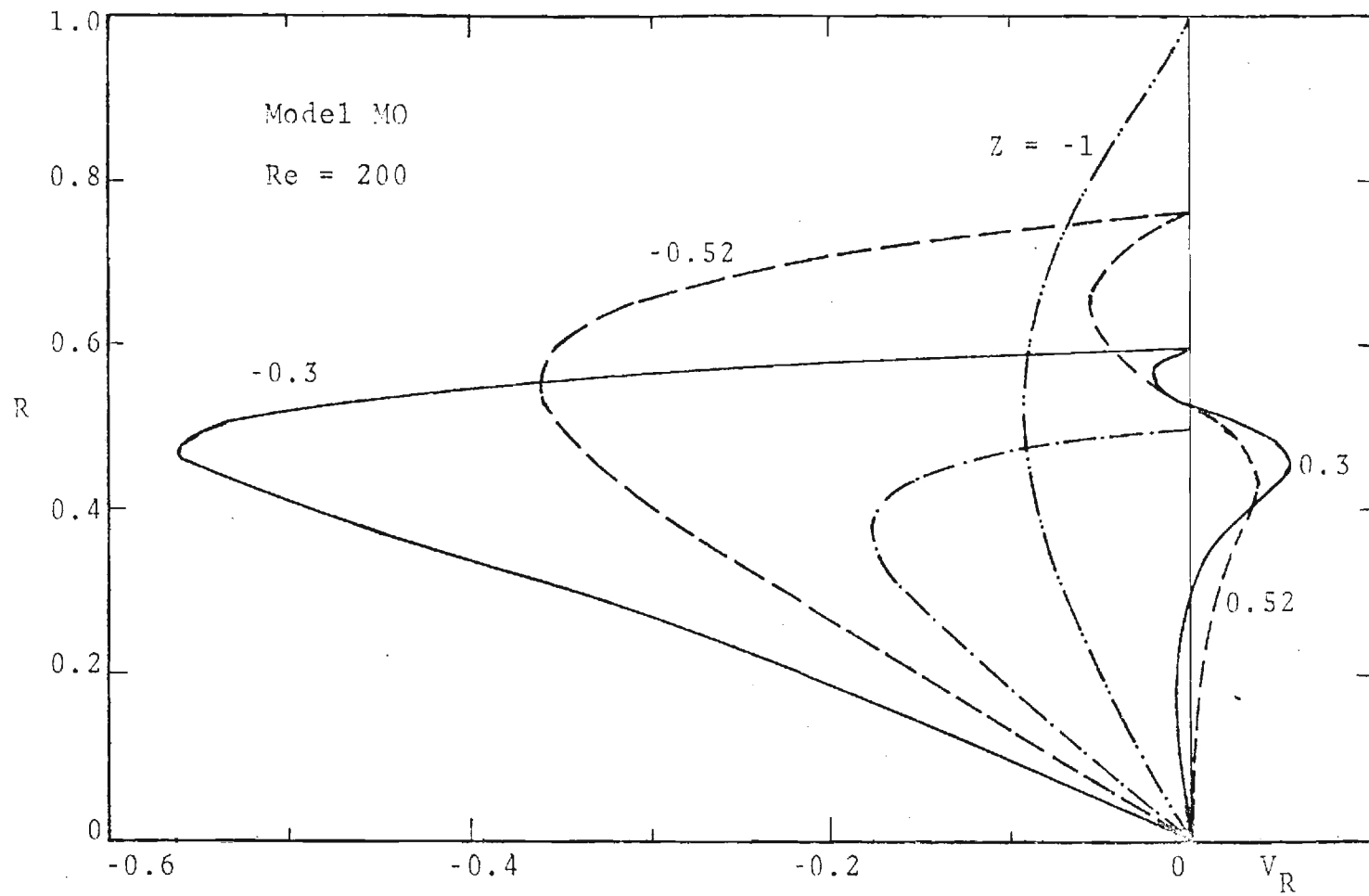


Figure 10b. Radial Velocity Profiles, Model M0, Re = 200

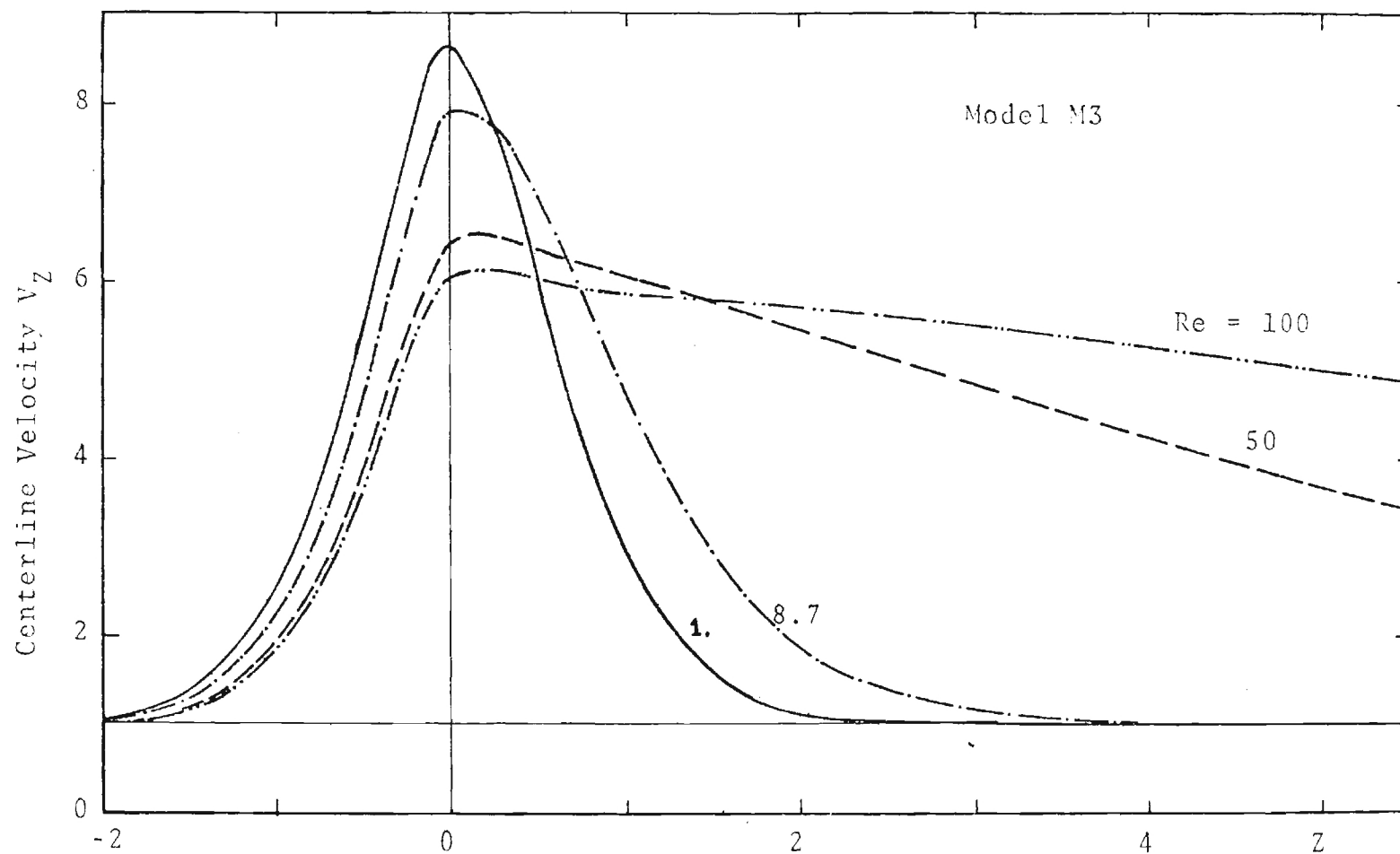


Figure 11.. Axial Variation of Centerline Velocity, Model M3

E. Discussion

The computational results presented here clearly fall short of providing flow field predictions for a realistically physiologic arterial flow. The greatest disparity is that unsteady terms have been omitted. This actually causes two weaknesses. The first is that pulsatile flow is not incorporated. But a second, and very important, consequence is that flow instabilities are not included. Therefore, propagating vortices and transition to turbulence are eliminated from consideration. An enlarging body of experimental evidence, both in vitro and in vivo, indicates that these phenomena are much more prevalent in arterial hemodynamics than had been thought previously.

Another shortcoming is the assumption of axisymmetric stenoses. Lesions which occur in the vascular system are usually irregular in shape and are frequently located near vessel branching or bifurcation. Thus, the biological velocity field is three dimensional with the existence of substantial secondary flow patterns. However, some qualitative observations may be made in the light of the experimental results of Young and Tsai, who studied several nonaxisymmetric stenoses geometries in addition to the axisymmetric contours previously discussed. They proposed that the pressure drop and maximum shear stress for a nonsymmetric stenosis were higher than for the corresponding axisymmetric stenosis with the same degree of occlusion. Further, the separation Reynolds number tends to be lower for the nonsymmetric contour and the flow field distal to this type of constriction appears to be more conducive to the occurrence of instabilities than for the axisymmetric case.

In spite of these deficiencies, the present results have extended steady flow laminar calculations to include contoured, as opposed to unrealistic rectangular, stenoses and have presented a comparison with available experimental data. The range of Reynolds numbers which can be achieved without convergence difficulties or without excessive computer time spans the cases where experimental observations indicate a completely laminar flow. Agreement with measured quantities is good, although hopefully future experimental investigations can provide velocity profiles which would allow a much more detailed comparison.

III. STEADY TURBULENT FLOW THROUGH STENOSES

A. Analytical Studies

1. Turbulence modeling

The continuity and momentum equations are to be solved again. Turbulence stresses, however, are incorporated into the momentum equations; and this is the central problem of any analytical study of the turbulent flows. Due to the difficult nature of this closure problem, several modeling techniques have been proposed^{45,46,47}.

Of these several methods available, the "two-equation turbulence model" was chosen. It derives its name from the fact that two equations are solved to simulate the turbulence phenomena; one equation governing the transport of turbulence kinetic energy k , and a second one governing the transport of another turbulence quantity which, along with k can be used to determine the eddy viscosity ν_e at each point in the field. The second dependent variable chosen here is ϵ -- the rate of dissipation of turbulence kinetic energy k . The k - ϵ model has been used widely by several researchers for engineering computations. Despite its potential shortcomings, this model was chosen as the medium of computation. It is sufficiently general to avoid the necessity of specifying any ad hoc functions; the constants in the equations are tested by several investigators; and it is relatively simple to apply as compared to models using more equations. It is probably the optimum choice for the present recirculating flow predictions until more definitive models evolve in the future.

Governing equations for k and ϵ are taken from the literature along with the constants involved. The coordinate system and the

nondimensional variables of the second chapter are retained throughout; i.e. a_0 and $2\bar{u}$ are used to nondimensionalize length and velocity, where a_0 is the radius of the tube in the unoccluded portion and \bar{u} is the average velocity in this region. Also, k , ϵ and v_e denote the nondimensional variables hereafter in this chapter. When presenting the results, however, dimensional values are employed. The four governing relations can be cast into the standard form of equation (14), repeated here

$$a \left[\frac{\partial}{\partial \eta} \left(\Phi \frac{\partial \Psi}{\partial R} \right) - \frac{\partial}{\partial R} \left(\Phi \frac{\partial \Psi}{\partial R} \right) \right] - \frac{\partial}{\partial \eta} \left[b_1 R \frac{\partial}{\partial R} (c\Phi) \right] - \frac{\partial}{\partial R} \left[b_1 R \frac{\partial}{\partial R} (c\Phi) \right] + Rd = 0. \quad (16)$$

In this equation Φ can be ω/R , Ψ , k or ϵ . The terms in each equation and the numerical values of the five constants C_D , C_1 , C_2 , σ_ϵ are listed in Table 2. The numerical values of these constants quoted in the literature are arrived at by the efforts of numerous investigators who have applied this model to experimentally known flows.

2. Boundary conditions

Appropriate conditions are to be specified all around the boundary for each of the variables ω/R , Ψ , k and ϵ .

On the axis, because of symmetry

$$\omega = \Psi = \frac{\partial k}{\partial R} = \frac{\partial \epsilon}{\partial R} = 0 \quad \text{at} \quad R = 0. \quad (17)$$

Table 2. Governing Equations Given by the k-ε Turbulence Model

$$a \left[\frac{\partial}{\partial \eta} \left(\Phi \frac{\partial \psi}{\partial R} \right) - \frac{\partial}{\partial R} \left(\Phi \frac{\partial \psi}{\partial \eta} \right) \right] - \frac{\partial}{\partial \eta} \left[b_1 R \frac{\partial}{\partial \eta} (c \Phi) \right] - \frac{\partial}{\partial R} \left[b_2 \frac{\partial}{\partial R} (c \Phi) \right] + R d = 0$$

	Φ	a	b_1	b_2	c	d
1	ω/R	R^2	$R^2 N$	$\frac{R^2}{N}$	v_e	$-R^2 \frac{S_\omega}{N}$
2	ψ	0	$\frac{N}{R^2}$	$\frac{1}{NR^2}$	1	$-\frac{\omega}{NR}$
3	k	1	$N \frac{v_e}{\sigma_k}$	$\frac{v_e}{N \sigma_k}$	1	$-G + \frac{C_D \epsilon}{N}$
4	ϵ	1	$N \frac{v_e}{\sigma_\epsilon}$	$\frac{v_e}{N \sigma_\epsilon}$	1	$-C_1 \frac{\epsilon}{K} G + \frac{C_2 \epsilon^2}{KN}$

Where,

Constants

$$C_1 = 1.45 \quad \sigma_k = 1.0$$

$$C_2 = 0.18 \quad \sigma_\epsilon = 1.3$$

$$C_D = 0.09$$

Table 2 (Cont.)

$$N = \frac{\partial \eta}{\partial Z} = K (1 - \eta^2)$$

$$G = \frac{\nu_e}{N} \left[2 \left(\frac{\partial V_R}{\partial R} \right)^2 + 2N^2 \left(\frac{\partial V_Z}{\partial \eta} \right)^2 + 2 \left(\frac{V_R}{R} \right)^2 + \left(\frac{\partial V_Z}{\partial R} + N \frac{\partial V_R}{\partial \eta} \right)^2 \right]$$

$$S_\omega = \frac{2}{R} \left[\frac{\partial^2 \nu_e}{\partial Z^2} \frac{\partial V_Z}{\partial R} - \frac{\partial^2 \nu_e}{\partial Z \partial R} \left(\frac{\partial V_Z}{\partial Z} - \frac{\partial V_R}{\partial R} \right) - \frac{\partial^2 \nu_e}{\partial R^2} \frac{\partial V_R}{\partial Z} \right]$$

$$\nu_e = k^2 / \epsilon$$

$$\kappa = \text{von Karman constant} = 0.4$$

Application of the boundary condition for ω/R on the axis is described in the second chapter.

Downstream boundary conditions are applied at $\eta = 1$ ($Z \rightarrow \infty$) for both stenotic and entrance flow problems. The flow is assumed to be fully developed at this boundary. Fully developed values for all the four variables are computed earlier and stored. Application of these boundary conditions in the gradient form, i.e. specifying that gradients in the Z direction go to zero, did not alter the results significantly.

Imposing the upstream boundary conditions involves an uncertainty which might affect the comparison of theory with the experimental data. Seldom are these boundary conditions measured experimentally in the great detail required for the application of the theoretical models. This always is the case with ϵ . However, it should not be a serious problem away from the upstream boundary. Computations proved that the results in the region away from the upstream boundary are not sensitive to small changes in the inlet conditions. In the stenotic flow case the upstream boundary conditions are applied two radii upstream of the stenosis, i.e. at $Z = -(Z_0 + 2)$. Flow is assumed to have passed through a long tube and thus is taken to be fully developed at this section. These values are available from a fully developed computation as mentioned above.

The wall boundary conditions are the most difficult to specify. This is due to two reasons. Though both k and ϵ go to zero on the wall, this information cannot be utilized effectively as the turbulence models are not applicable in the viscous layer next to the wall. Further, the large gradients of the flow properties in this region require very close spacing of the numerical grid points even if one attempts to extend

the turbulence models into the viscous layer. The usual practice to circumvent this difficulty is to apply the boundary conditions in some approximate form at a point outside the viscous layer where viscous stresses can be neglected in comparison to turbulent stresses. This practice is satisfactory in the boundary layer flows where the law of the wall can be employed to establish certain boundary conditions. The lack of such information in a general flow has led the earlier workers^{48,49} to resort to the same procedure employed in a boundary layer flow even when the flow departs from the boundary layer class.

The value of the stream function on the wall is 0.25. The boundary conditions for the other three variables are applied at the first grid point away from the wall. The logarithmic form of the law of the wall is assumed to be valid and is used to evaluate the wall shear stress τ_w from the known velocity. Then

$$\omega = \partial V_z / \partial Y = \sqrt{\tau_w} / (\kappa Y) \quad (18)$$

where κ is the Karman constant and Y is the nondimensional distance measured from the wall ($Y = R_o - R$). The boundary condition for k is obtained from the transport equation for k by neglecting the convection and diffusion terms and equating generation and dissipation of kinetic energy. This leads to

$$k = \tau_w / \sqrt{C_D} \quad (19)$$

on the wall. The law of the wall is used again to obtain the boundary condition

$$\epsilon = \tau_w^{3/2} / (C_D \kappa Y). \quad (20)$$

In the recirculation region τ_w is negative and equations (18, 19 and 20) cannot be applied. Launder⁴⁹ manipulated these equations in the hope of applying them even when τ_w is negative. In the nondimensional form, equations applied near the wall are finally

$$Y_+ = Y \operatorname{Re} C_D^{1/4} \sqrt{k}$$

$$U_+ = \ln (E Y_+) / \kappa$$

$$\tau_w = C_D^{1/4} \sqrt{k} v_Z / U_+$$

$$u_* = \sqrt{|\tau_w|} \quad (21)$$

$$\omega = u_* \operatorname{sign} (\tau_w) / (\kappa Y)$$

$$\epsilon = \tau_w \omega / C_D$$

$$k = (\epsilon \kappa Y C_D^{1/4})^{2/3}$$

$$E = 9.793$$

These equations have not been compared with any experimental data in recirculating flows and should be considered as only tentative. They give, however, the same results as equations (18, 19 and 20) when τ_w is positive. This makes it very convenient in applying them all along the wall when a recirculation region is suspected to be present adjacent only to a part of this length.

3. Numerical solutions

The four governing relations for ω/R , Ψ , k and ϵ written in the form of equation (16) were solved numerically subject to appropriate boundary conditions. The numerical approach employed was the same as that explained in the second chapter as the form of the governing equations has not been changed. However, it turned out to be more difficult to obtain a converged solution when the number of equations was increased to four. Both a point by point and a line by line elimination method of solution of the difference equations failed to converge. In the line by line elimination method a tridiagonal matrix for each dependent variable Φ was formed on every line of constant η . The form of these linear algebraic equations for the j node is

$$A_j \Phi_{j-1} + B_j \Phi_j + C_j \Phi_{j+1} = D_j, \quad (22)$$

with j being counted in the radial direction. The coefficients A , B , C and D were evaluated from the most recent values of the dependent variables in the iteration procedure. Boundary conditions provide the first and the last value of Φ for each line. Standard recursion relations are available to solve this system⁵⁰. This procedure either failed to

converge or the rate of convergence was very slow and the changes between successive iterations did not reduce beyond a certain limit; the results obtained were not reliable. A modified approach was attempted by rewriting equations for k and ϵ in the form

$$A_j^k k_{j-1} + B_j^k k_j + C_j^k k_{j+1} = D_j^{\epsilon} \epsilon_j + E_j = \bar{D}_j \quad (23)$$

$$a_j^{\epsilon} \epsilon_{j-1} + b_j^{\epsilon} \epsilon_j + c_j^{\epsilon} \epsilon_{j+1} = d_j^k k_j + e_j = \bar{d}_j \quad (24)$$

The presence of the cross terms ϵ and k on the right hand side of the equations for k and ϵ can be seen to be due to the form of the source terms of these equations. In equation (22) these cross terms were eliminated by evaluating them from the values of the previous iteration and lumping them in the coefficient \bar{D} .

A method was devised to solve this coupled tridiagonal-type of system of equations simultaneously. This consists of writing recursion relations similar to those for a tridiagonal form of equations (22) and then evaluating them by proper manipulation. The recursion relations and the details of the derivation are presented in Ref. 42. This technique of solving the equations for k and ϵ simultaneously resulted in a fast convergence and the differences in successive iterations could be made arbitrarily small until round-off errors became a limitation. The importance of the method was that the results were reliable and were obtained with less computing time. The faster convergence rate results in a saving of computing time even though the time required to solve the coupled system of equations simultaneously at each iteration was a little

longer than that required to solve them one after the other. This method of solution also can be used to solve coupled difference forms of equations obtained from the governing relations for ω/R and Ψ .

For the case of flow through stenoses, 31 grid points were uniformly spaced in the radial direction and 75 of them in the axial direction. It required 200 to 300 iterations for the solutions to converge corresponding to about two to three minutes of computer time on the CDC 6600 computer.

4. Results

Theoretical solutions were computed for the four models M1, M2, M3 and M4 (see Table 1). Although the Reynolds number of primary interest was 15,000, computations were also performed at 10,000, 30,000, and 388,000. This allows some insight into flow field variation with changing stenosis geometry and Reynolds number.

Figure 12 gives velocity profiles for Model M4 at the very high Reynolds number of 388,000. Again the maximum velocity in the throat section occurs off-axis. Also, for this case there is no recirculation region predicted. Figures 13 and 14 show profiles for Models M1 and M2 at $Re = 15,000$. Recall that M1 is a milder, and M2 is a more severe, stenosis than the basic model studied, M4. The theory predicts no recirculation region for M1 and there is no off-axis peak in the throat profile. Model M2, which represents a severe constriction, does exhibit a recirculation region and a small, but perceptible, peak off-axis in the velocity profile. Thus, the theory predicts a decreasing size for the recirculation zone with decreasing degree of stenosis (at a fixed Re)

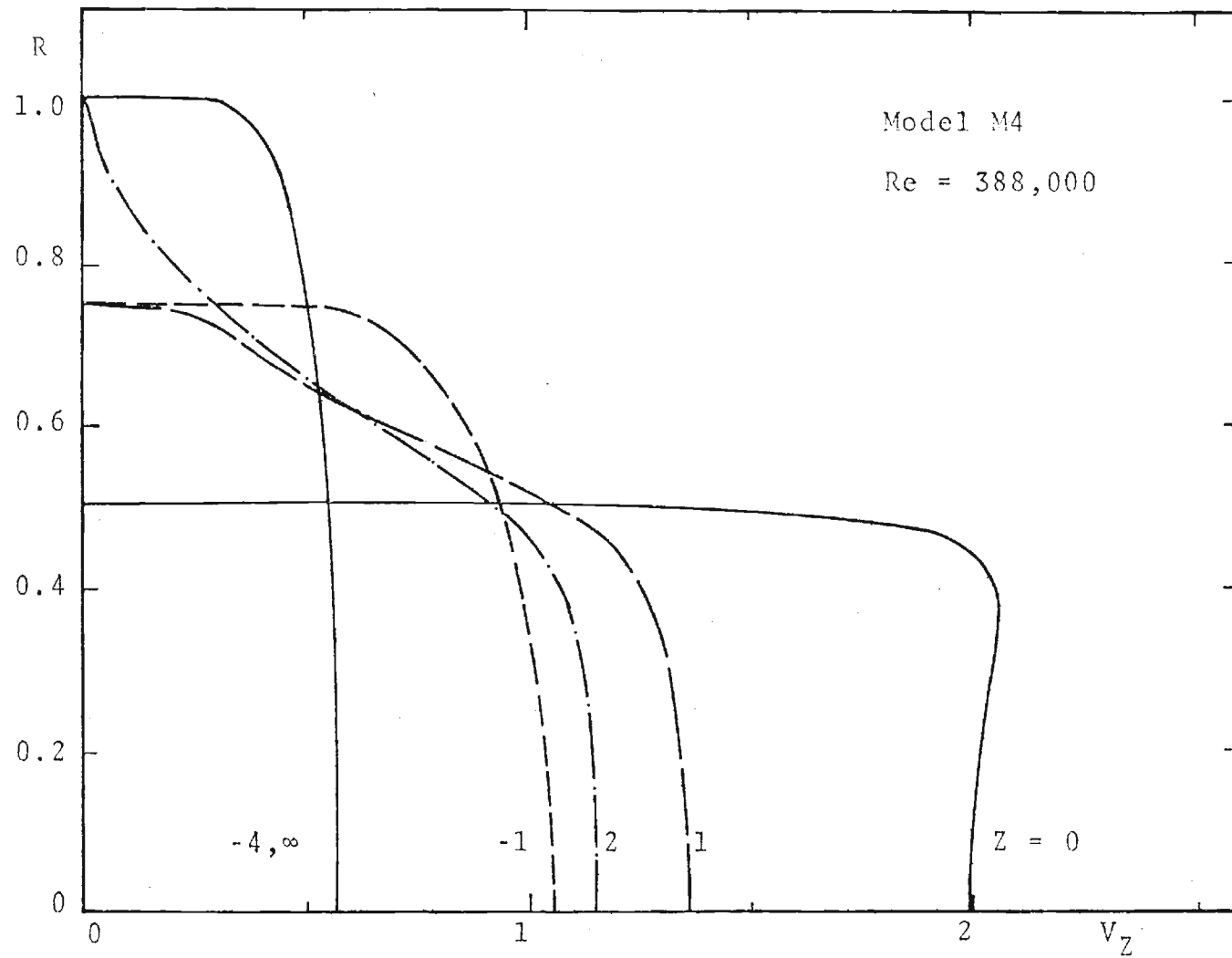


Figure 12. Axial Velocity Profiles, Model M4, Re = 388,000 (Theory)

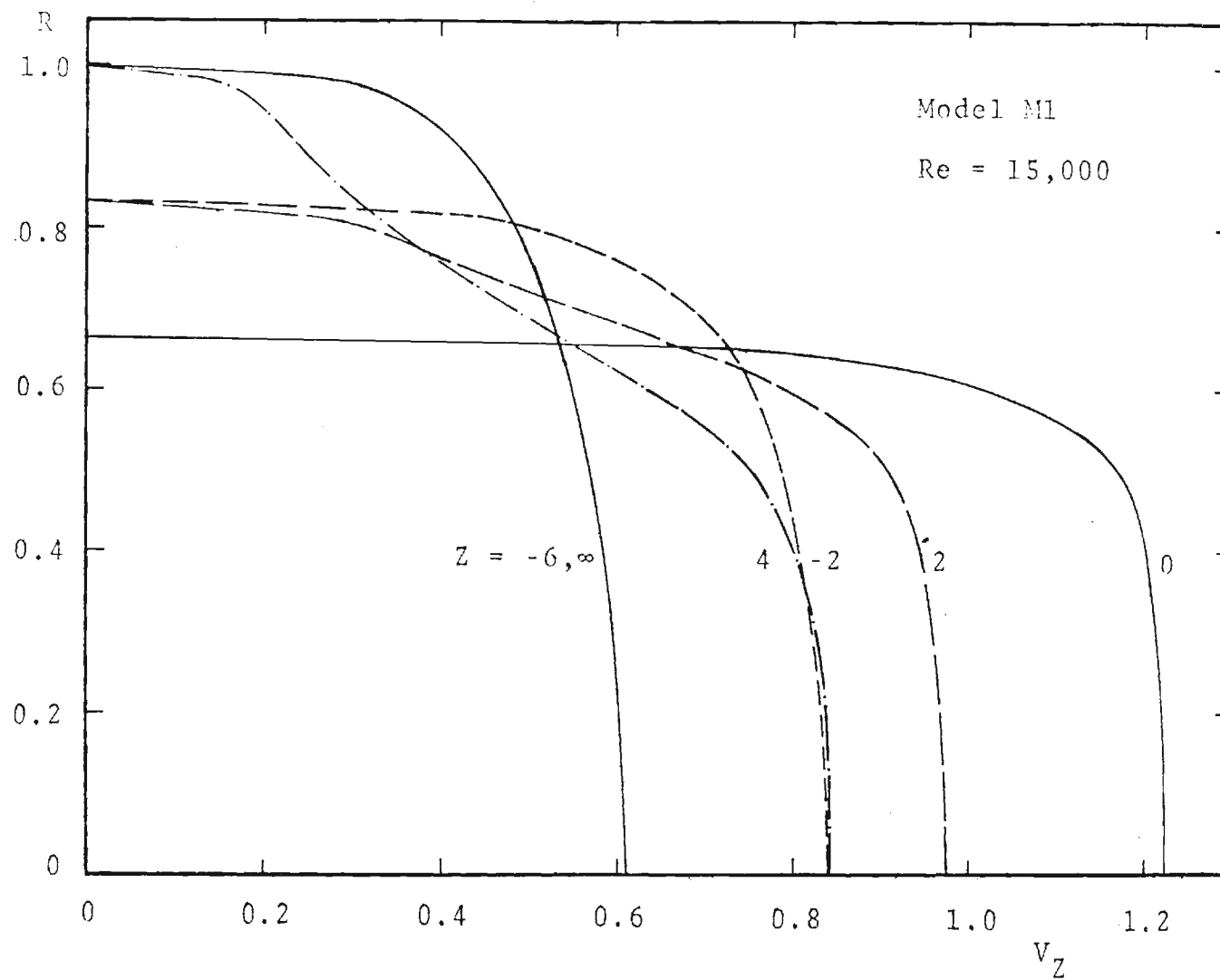


Figure 13. Axial Velocity Profiles, Model M1, Re = 15,000 (Theory)

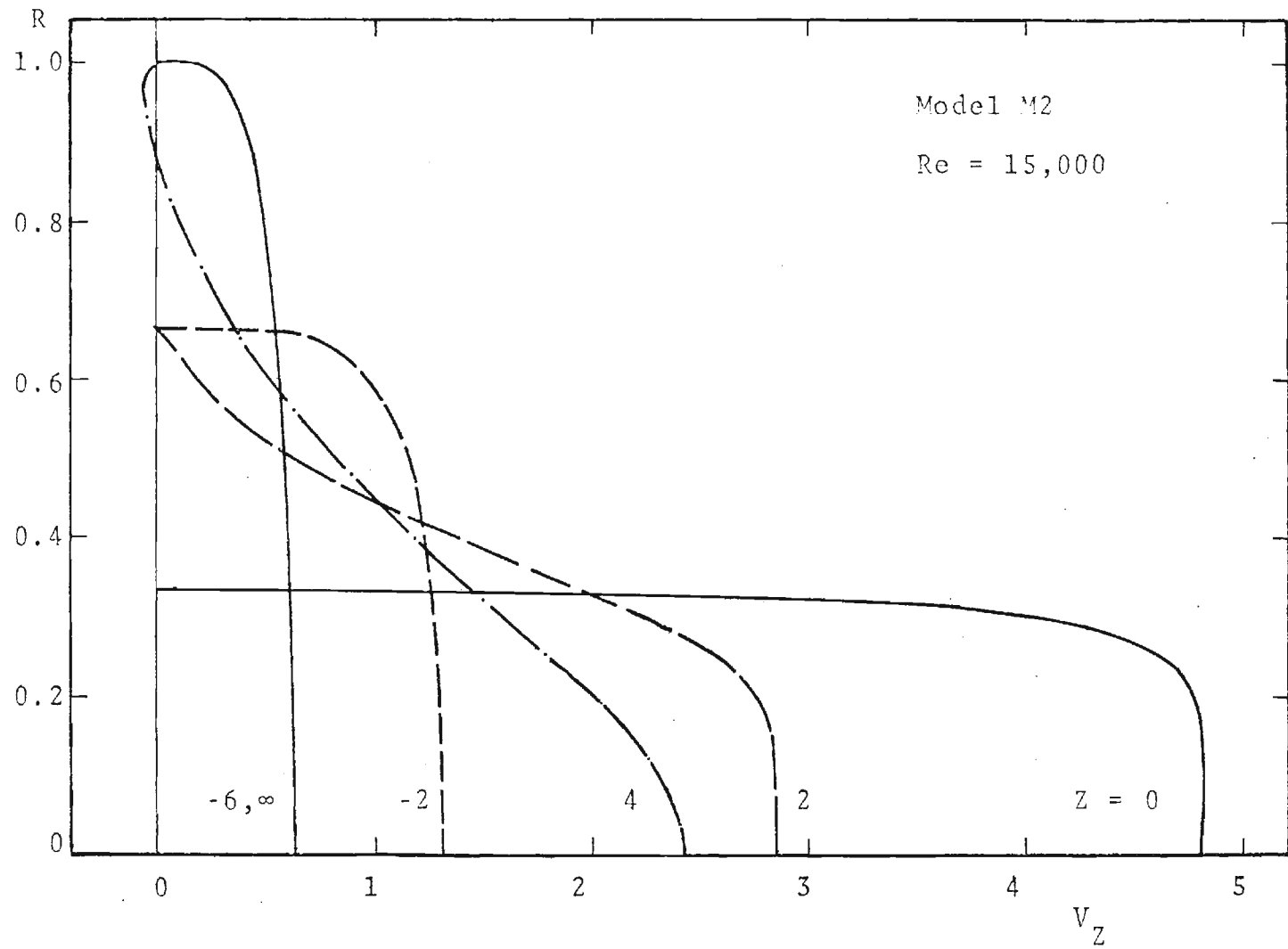


Figure 14. Axial Velocity Profiles, Model M2, Re = 15,000 (Theory)

and with an increasing Reynolds number (at a fixed degree of stenosis). This should occur experimentally, also.

Figures 15 and 16 give the calculated centerline velocities for Models M1 and M2 at two Reynolds numbers, 15,000 and 388,000. It is seen that there is little variation in these curves with Reynolds number, even over such a wide range of values. In this nondimensional form of presenting the data the values of centerline velocity are more elevated, and these persist farther downstream, for lower Reynolds numbers. Again, this is also the trend in the experimental data. Note that the peak velocity in the case of the severe stenosis Model M2 is about four times higher at the same Reynolds number than that for the moderate stenosis M1, but at $Z = 12$ it has returned much closer to the final downstream value. This is caused by a more effective momentum transport arising from increased turbulence intensity for the more severe stenosis.

The predicted nondimensional pressure distribution for Models M1 and M2 is illustrated in Figures 17 and 18. The predicted pressure drop across the stenosis may be expected to be an underestimate. There is very little change in the nondimensional pressure in the converging section when the Reynolds number is increased from 15,000 to 388,000. Changes in nondimensional pressure gradients with Reynolds number are substantial only close to the throat and the diverging portion of the stenosis.

Wall shear stress is of considerable physiological importance. It is difficult to measure this quantity experimentally and hence the theoretical results are valuable. It should be recalled, however, that the law of the wall is employed to assess this quantity and hence the absolute magnitude predicted near the recirculation region is less reliable. The square

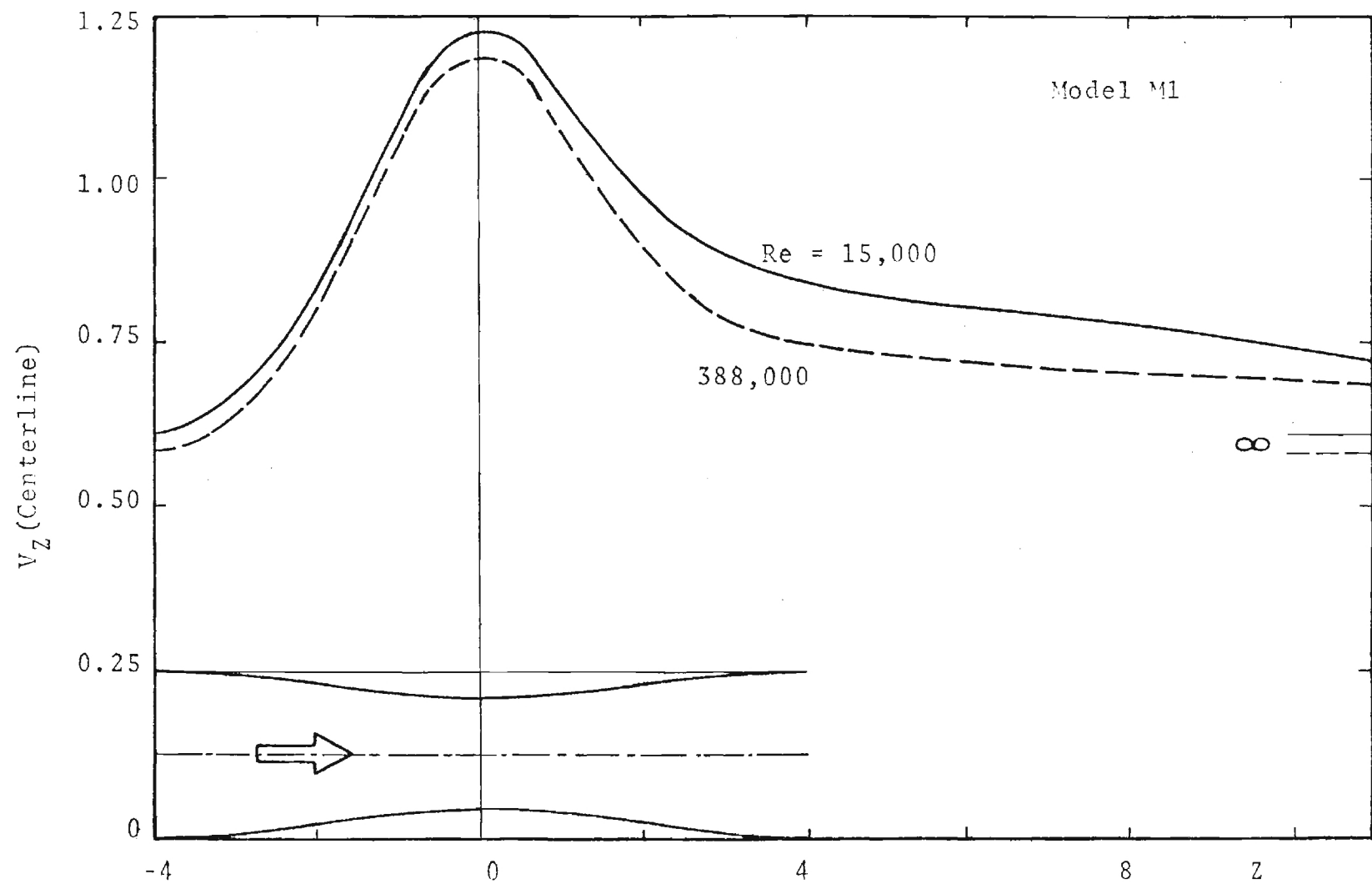


Figure 15. Axial Variation of Centerline Velocity, Model M1, $Re = 15,000$ and 388,000 (Theory)

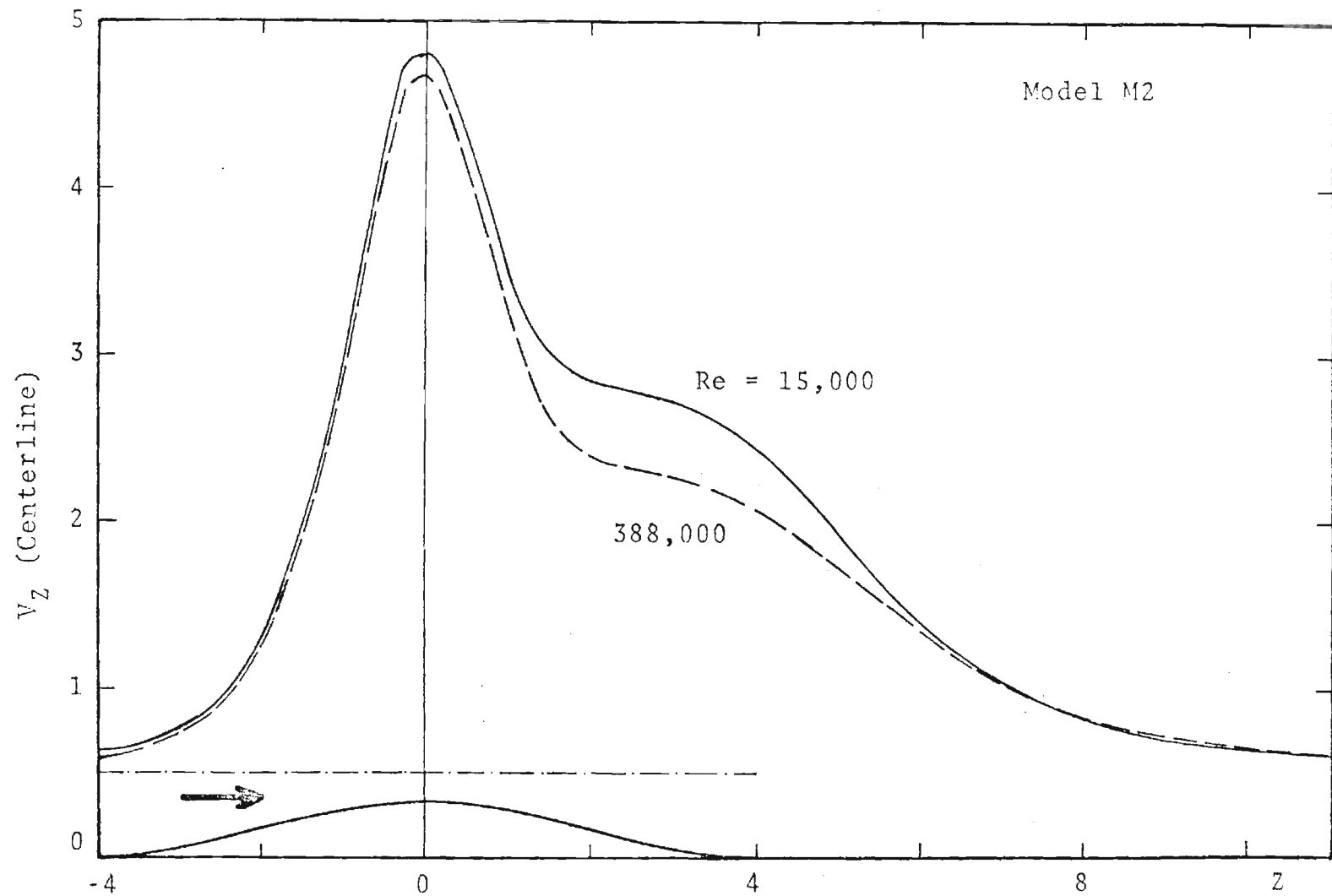


Figure 16. Axial Variation of Centerline Velocity, Model M2, $Re = 15,000$ and $388,000$ (Theory)

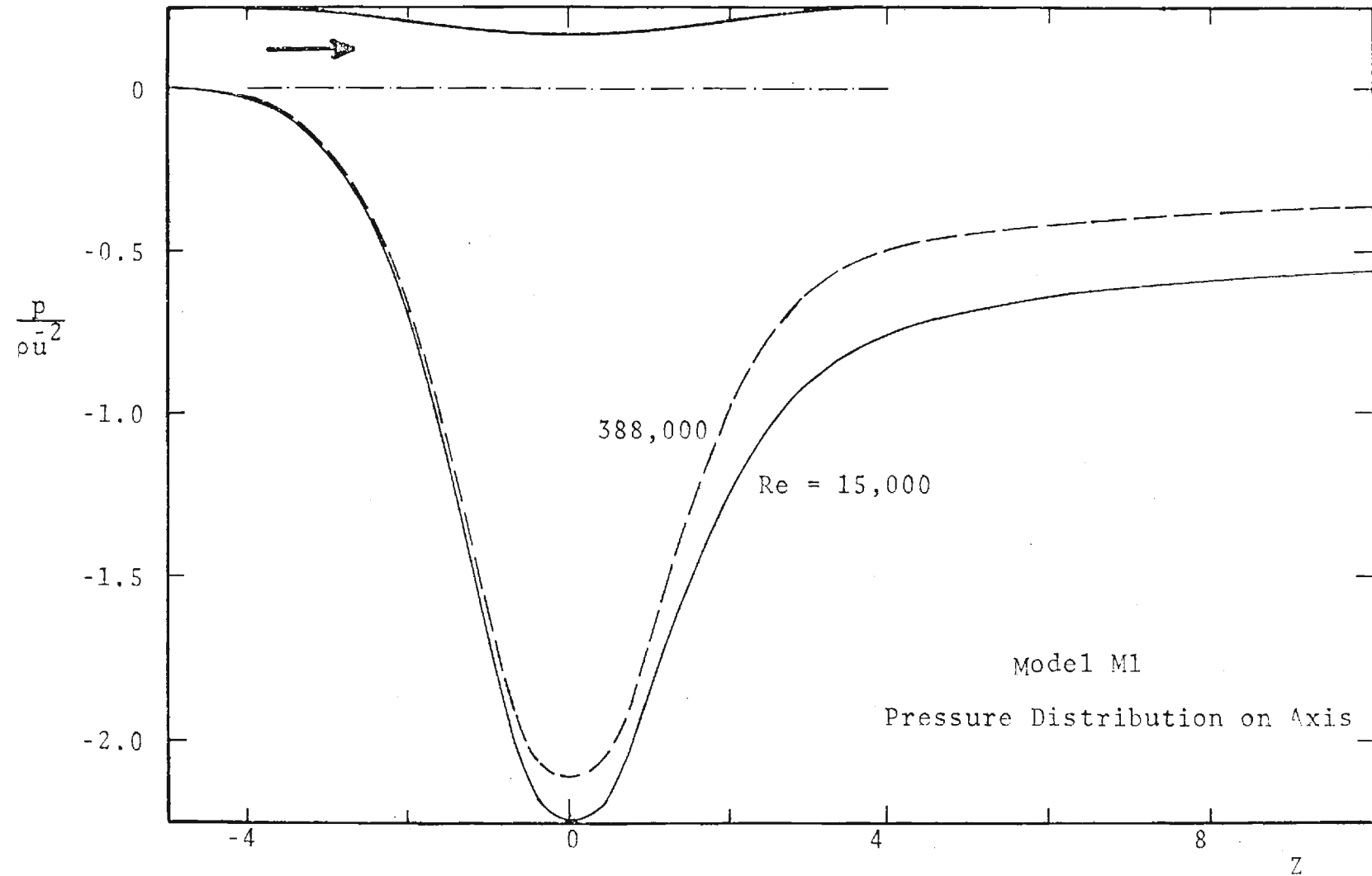


Figure 17. Pressure Distribution Along Tube in Turbulent Flow, Model M1, $Re = 15,000$ and $388,000$ (Theory)

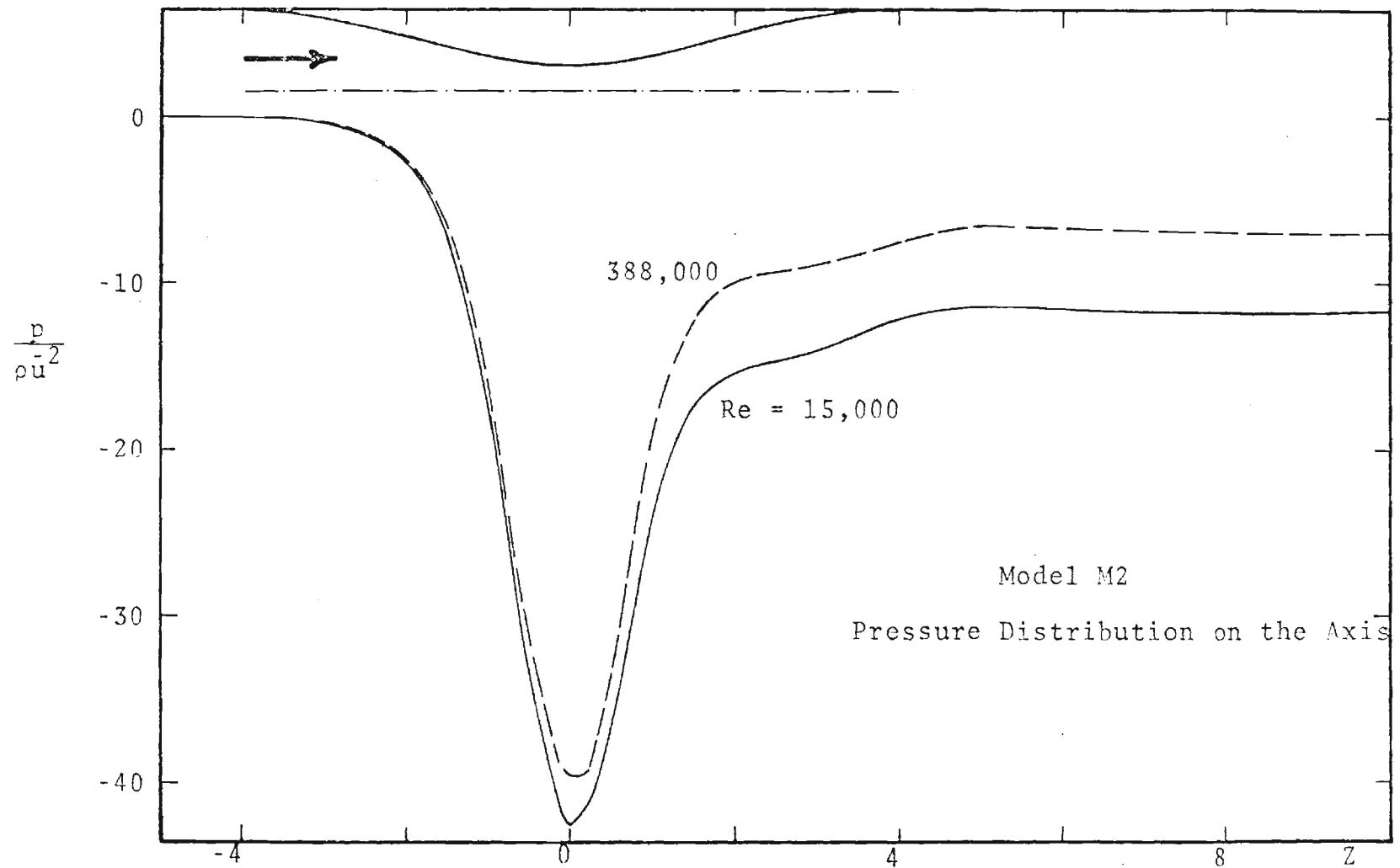


Figure 18. Pressure Distribution Along Tube in Turbulent Flow, Model M2, $Re = 15,000$ and $388,000$ (Theory)

root of this quantity nondimensionalized by the average velocity in the unoccluded tube is plotted for the three Models M4, M1 and M3 in Figures 19, 20 and 21, respectively. The negative square root is used whenever the shear stress τ is negative. Again, a comparative examination for Reynolds numbers 15,000 and 388,000 is chosen.

The behavior of this quantity is somewhat similar to that in the laminar flow. However, it is characterized by a shorter recirculation region and an overshoot in the shear stress distal to the reattachment point before it returns to the fully developed value. The reason for this overshoot in the shear stress is due to the flatter velocity profiles in this region.

The maximum values of the shear stress which are predicted to occur at the throat are compared in Figure 22 for all the four models and the four Reynolds numbers for which computations were performed. The same quantity in a fully developed pipe flow obtained using the Blasius formula is represented by a straight line. The increase in the shear stress with an increase in the severity of the stenosis is evident.

The variation of the turbulence kinetic energy on the centerline is shown in Figure 23 for Model M3 at Reynolds number of 15,000 and 388,000. The trends in the two curves are quite similar, with the $Re = 15,000$ case having higher values when nondimensionalized by the mean velocity, \bar{u} . It can be seen that the predicted values are quite large in the region immediately downstream of the constriction. Since the two-equation model was developed from experience with boundary layer and shear flows with much lower intensities, it is quite likely that the high values predicted here cannot be expected to be quantitatively accurate. The poststenotic

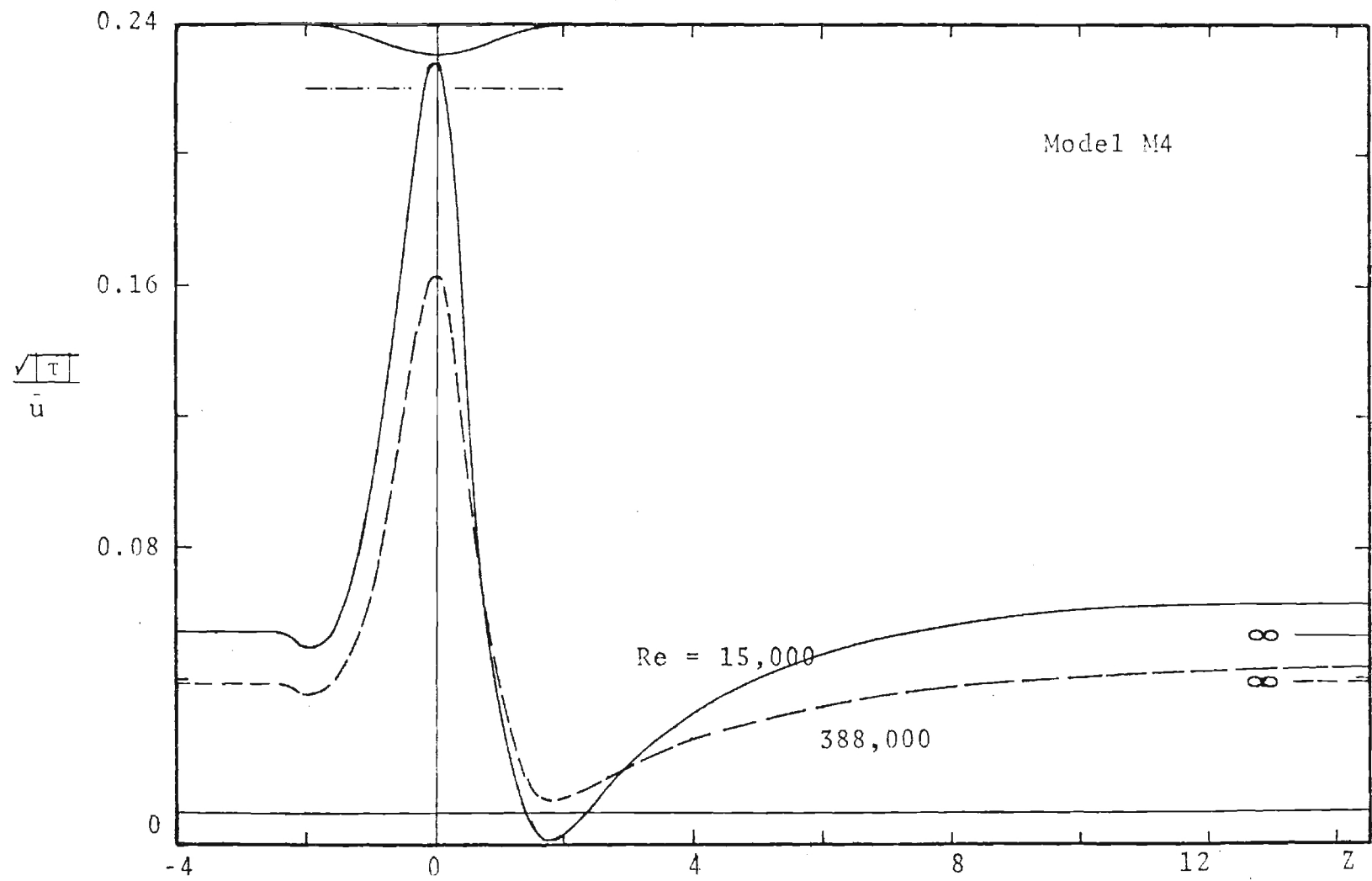


Figure 19. Wall Shear Stress Distribution, Model M4, $Re = 15,000$ and $388,000$ (Theory)

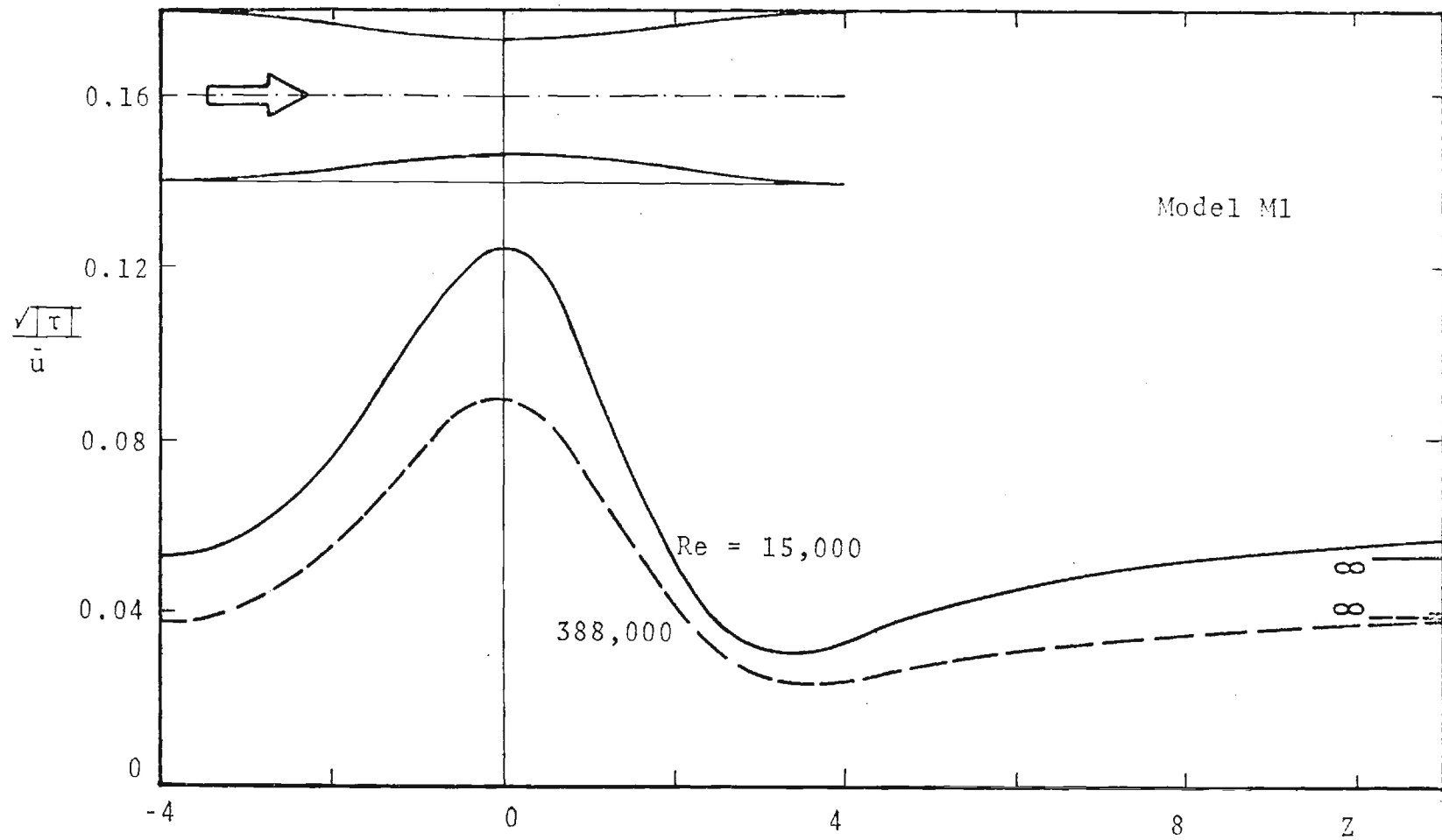


Figure 20. Wall Shear Stress Distribution, Model M1, Re = 15,000 and 388,000 (Theory)

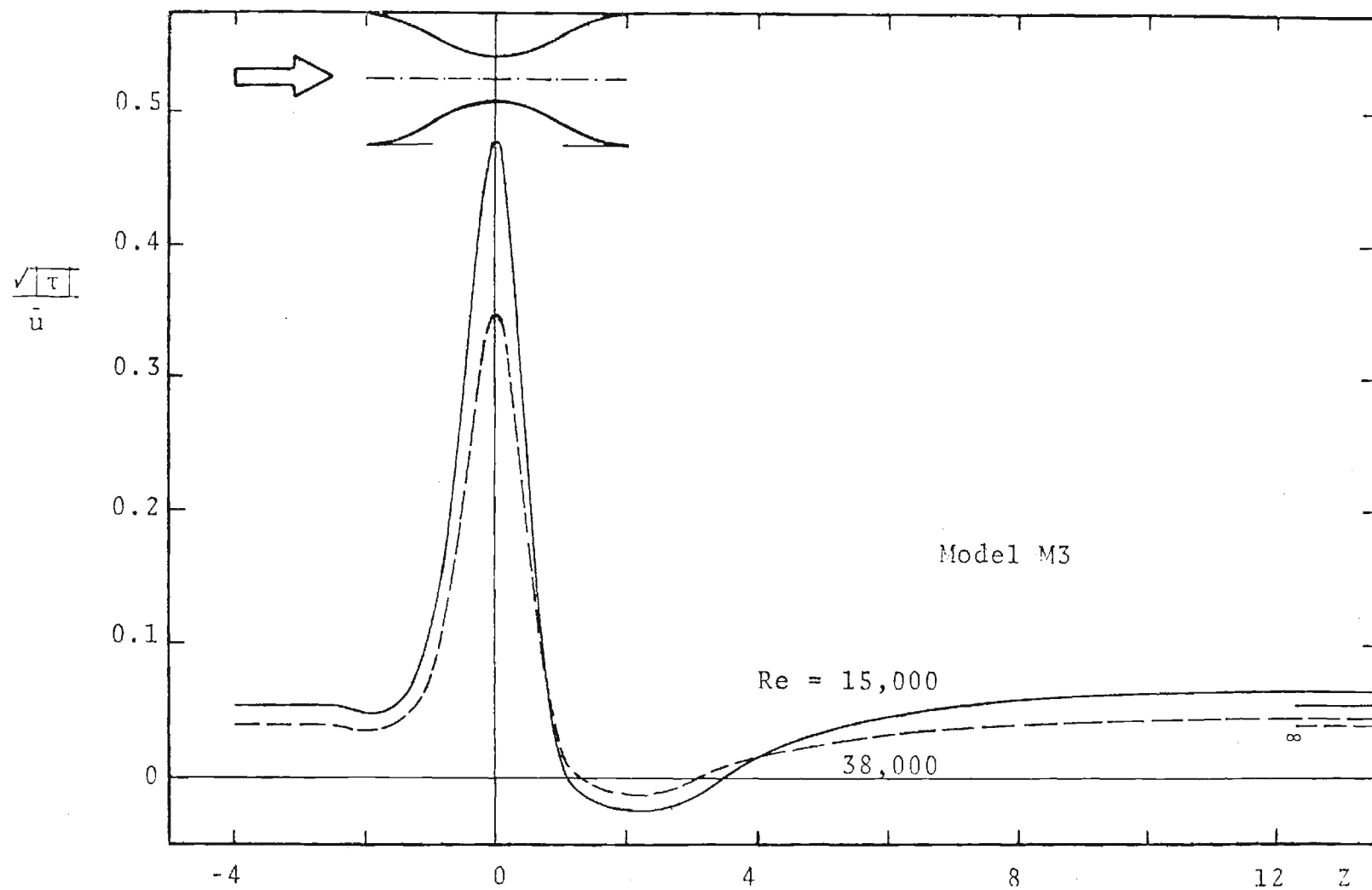


Figure 21. Wall Shear Stress Distribution, Model M3, Re = 15,000 and 388,000 (Theory)

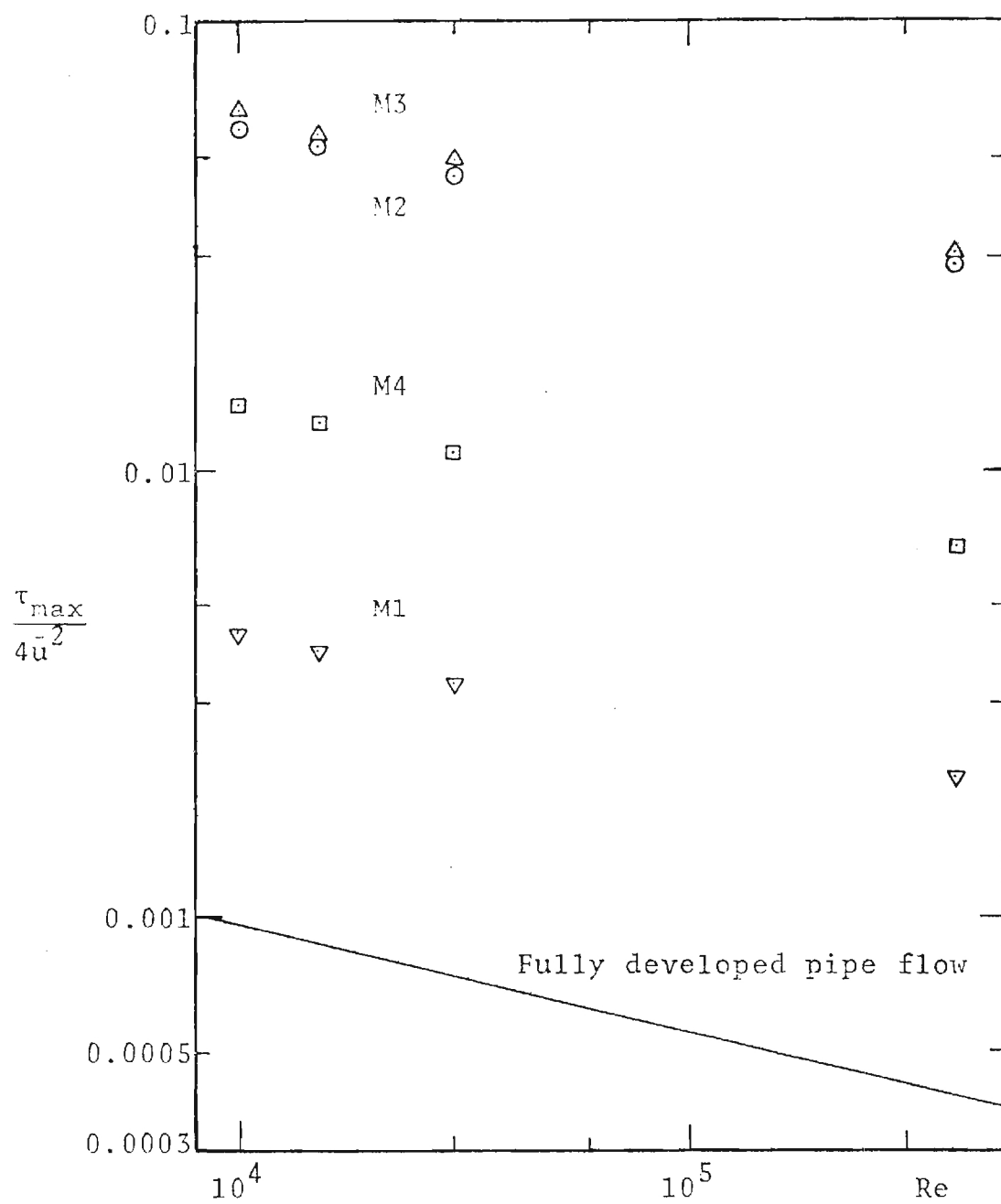


Figure 22. Maximum Wall Shear Stress for Stenoses (Theory)

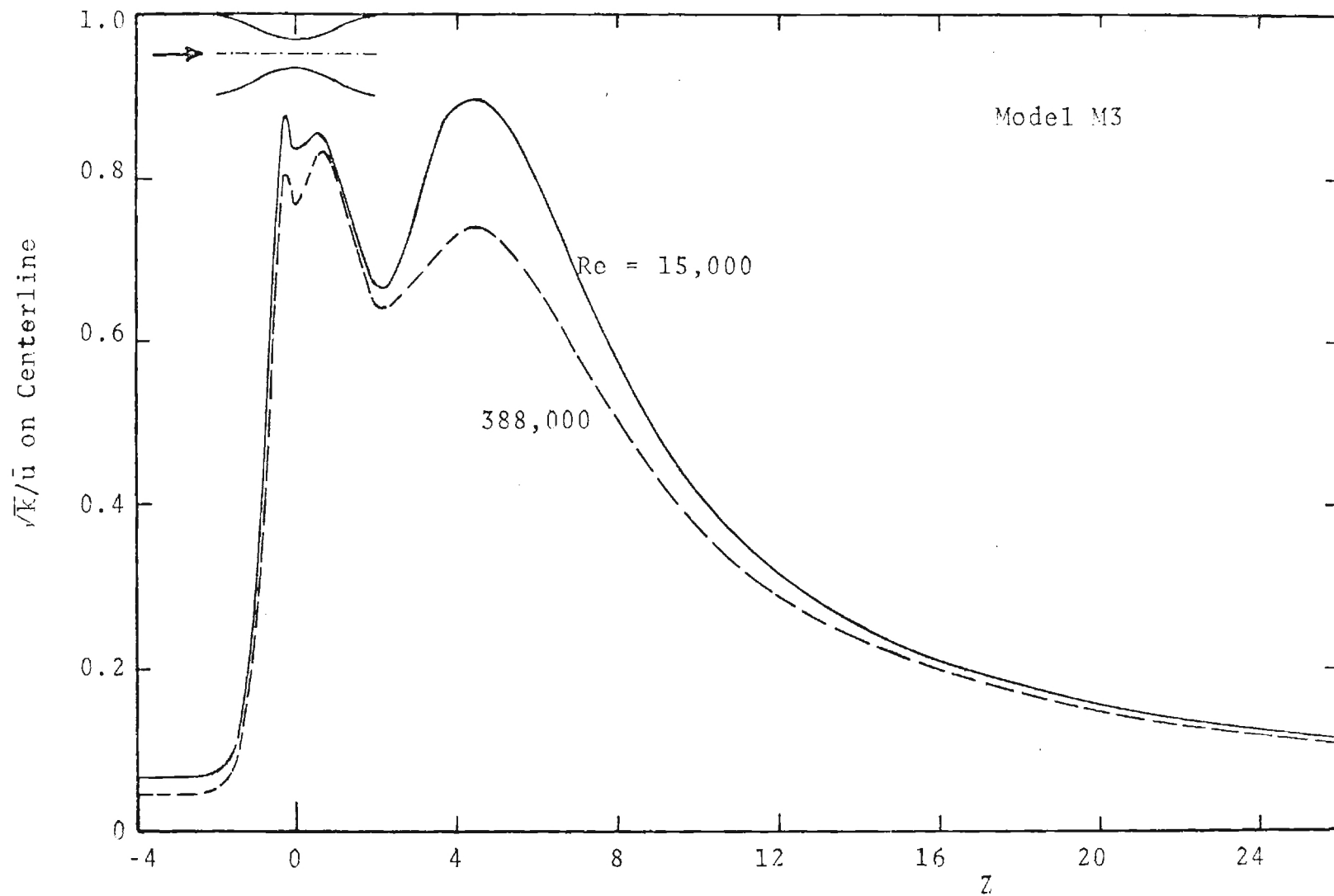


Figure 23. Axial Variation of Centerline Turbulence Kinetic Energy, Model M3, Re = 15,000 and 388,000 (Theory)

flow field for large obstructions may exceed the limits of applicability of the model equation. A comparison with experimental data is planned for future studies. This should be useful in assessing the accuracy of the $k-\epsilon$ model for this flow situation.

At the time of completion of the NSF grant under which this work was accomplished, a comparison of theory with experiment had not been made. Experiments have been in progress, and such a comparison will be included in the Final Report for a follow-on grant, ENG76-23876.

B. Experimental Studies - Hot Film Anemometer

A schematic of the flow system is shown in Figure 24. The stenosis experiments were conducted in 2.54 cm I.D. x 0.318 cm thick wall rigid acrylic tubing into which were inserted the constrictions. The sharp-edged occlusions were thin brass orifice plates and the contoured occlusions were machined from clear acrylic with a cross-sectional shape generated by intersecting circular arcs. Both constrictions were axisymmetric. A smoothly converging inlet which was located immediately upstream of the occlusion assured laminar flow proximal to the occlusion. The velocity profile immediately upstream of the occlusion was flat over 80% of the tube diameter during the steady flow experiments. The flow controls were arranged to provide either a steady flow, a flow upon which was superimposed a sinusoidal pulse from the piston pump, or a more complex pulse waveform which could be provided by the piston pump with the addition of check valves on the inlet and outlet of the pump.

The velocity measurements were made with a commercially available anemometer, linearizer, and miniature conical hot film probe (TSI-1264W) which was frequently calibrated by using a slotted turntable as described

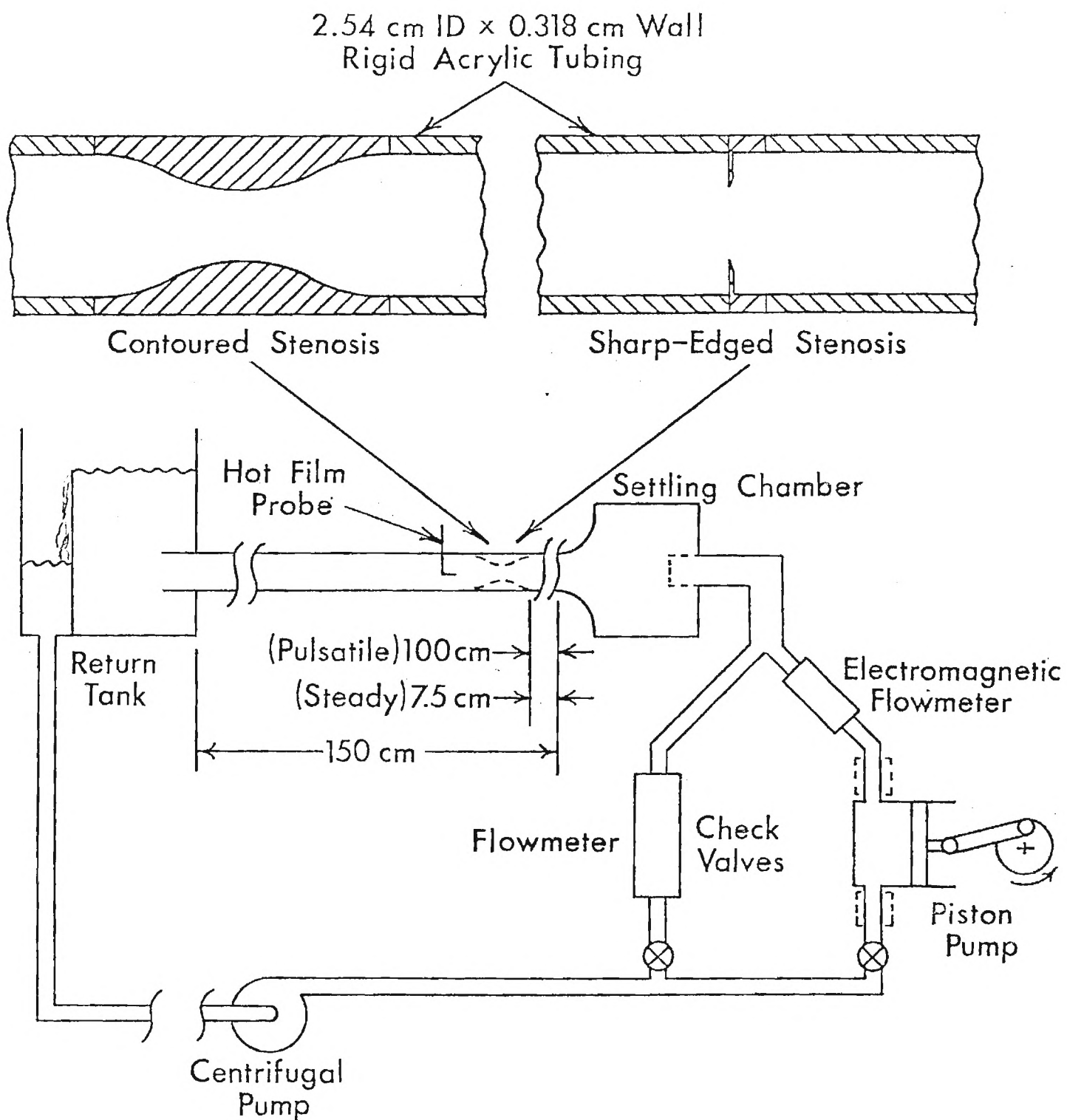


Figure 24. Flow system and stenosis geometries.

by Cassanova⁵¹. The probe was radially adjustable and could be mounted at several axial locations distal to the stenosis. The turbulent energy spectra were obtained by subjecting the entire velocity signal to Fourier analysis using an HP5451A Fourier Analyzer. All spectral data were corrected for variations in analyzer bandwidth settings.

1. Stenotic flow patterns

Figure 25 shows a model of the flow through an axisymmetric constriction in a tube. The flow velocity in the unoccluded tube is denoted by U_p and U_o is the mean velocity through the minimum area. As the flow emerges from the minimum area of the constriction, the effective area of the jet continues to decrease with increasing axial distance and the velocity increases due to the vena contracta effect. The degree to which the velocity increases and the axial location of the maximum velocity in the vena contracta will be influenced by the proximal constriction contour, the proximal velocity profile, and the severity of the constriction. In the region immediately distal to the minimum area and in proximity to the tube wall is a recirculation region containing relatively low energy flow. The flow separation and reattachment points depend on the wall pressure gradient which is a function of the Reynolds number, the constriction shape and the proximal velocity distribution. Roschke and Back⁵² reported measurements of reattachment lengths in flows through an abrupt expansion. In the near-centerline region past the point of maximum velocity in the vena contracta, a system of vortex rings is formed. The eddy size of the vortex rings is governed primarily by the Reynolds number, $Re_d = \rho U_o d / \mu$ with eddy size decreasing with increasing Reynolds

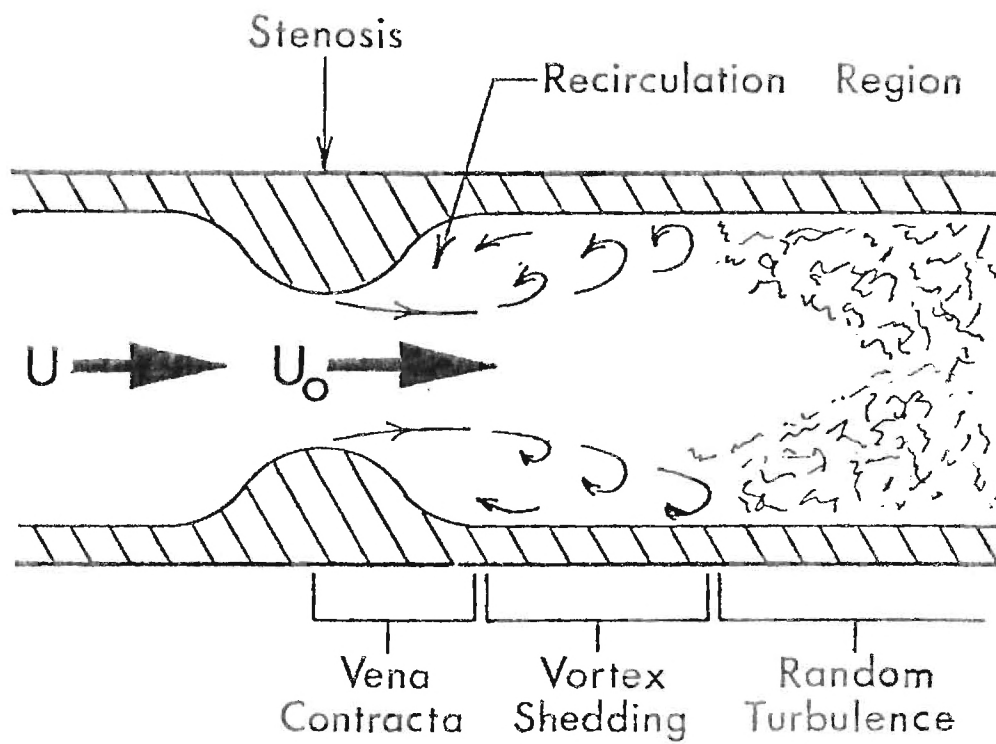


Figure 25. Steady flow through an axisymmetric occlusion.

number. As a vortex ring travels downstream, the tendency is for adjacent ring pairs to coalesce to form a larger ring-like structure and for the propagation velocity to decrease. This causes the observed shedding frequency to decrease with increasing axial distance from the constriction. For high enough Reynolds numbers, this vortex ring system breaks up into a more random distribution of eddy sizes characteristic of turbulence. This breakup of the more ordered structure can occur because: (1) the flow velocity is high enough in the jet to initiate the transfer of energy to eddies of smaller and larger sizes, and/or (2) the vortex rings interact with the tube wall. The interplay of these two factors will, of course, depend on the size of the constriction relative to the unoccluded area. For very low Reynolds numbers, the vortex ring break-up produces few smaller eddies and the ring-like disturbance quickly dissipates upon contact with the wall. If turbulence does result from the breakup, it may (depending on Reynolds number) gradually dissipate at more distal positions or it may reach an energy distribution among the eddies which is characteristic of fully developed turbulent pipe flow. In general, the sharp-edged constriction produced a distinct vena contracta effect while the contoured constriction did not. At a Reynolds number of 318, completely laminar flow with no detectable separation or turbulence formation was observed in the flow through the 50% contoured occlusion. However, the same flow rate through the sharp-edged occlusion produced a distinct recirculation zone and a noticeable flow instability. For $Re_D = 2540$ the sharp-edged constriction produced a vortex ring pattern within one tube diameter downstream of the occlusion. This more orderly flow structure disperses into a random turbulence immediately downstream.

The contoured occlusion, however, produced a more axially elongated recirculation zone and a vortex pattern near the wall which breaks up at approximately 3 diameters downstream from the stenosis site. For the 75% occlusions at $Re_D = 635$, the sharp-edged occlusion produced a comparatively small vortex eddy which disintegrates before the stenotic jet expands to meet the wall. However, the contoured occlusion produced an extremely large recirculation zone and a large scale flow instability which interacts with the tube wall at the reattachment location.

A series of flow visualization experiments was also conducted to determine the effects of wall interference on the formation of vortex rings and the degeneration of the vortex rings into more random fluctuations. In general, the presence of the tube retards the development of vortex rings at the lower Reynolds number by reducing the axial pressure drop and velocity shear that is "felt" by the stenotic jet. However, at higher Reynolds numbers where the amount of shear is sufficient in either case for the generation of a vortex instability, the vortex ring contact with the wall initiates the degeneration of the vortex rings into random turbulence at a lower X/D location than in the free jet case. The presence of the confining, distal wall reduces the magnitude of the vortex-like instability and causes a dissipation of the instability at the wall with no discernable formation of a random turbulence. The flow appears to relaminarize. The free jet with $Re_D = 1270$ shows a very distinct vortex ring pattern which propagates about $3D$ downstream before breaking up. The confined jet with $Re_D = 1270$ also shows a vortex ring structure. However, the relatively large eddies are broken-up by contact with wall at a position 1 diameter downstream from the constriction.

Photographs taken during the flow visualization studies may be found in Reference 51.

2. Velocity measurements

The mean velocity data obtained 3D upstream of the sharp-edged occlusions and 4D upstream of the contoured occlusions are shown in Figure 26. The profiles are flat for about the central 80 percent of the tube diameter for all flow rates.

Figure 27 shows the trends of the centerline mean velocity in the region downstream of the 50 percent occlusions. Also indicated is the velocity at the occlusion minimum area as calculated from the one-dimensional continuity equation using the known total flow rate and the minimum area of the occlusion. It was not possible to measure the velocity at the minimum area location with the hot film probes used in this investigation. There does not appear to be any significant difference in the velocity decrease with axial distance for the sharp-edged or contoured occlusions. However, at x/D 's greater than about 4, the contoured occlusion velocities tend to be slightly greater than the corresponding sharp-edged results.

Figure 28 reveals that for the 75 percent occlusions the velocities for the contoured constriction tend to be slightly higher for d/D greater than about 4. The velocities with the contoured occlusion for x/D less than 1.5 were not measured since the hot film probe mount could not be used any closer to the occlusion minimum area.

Additional results describing the velocity profiles in the radial dimension are given in Reference 51.

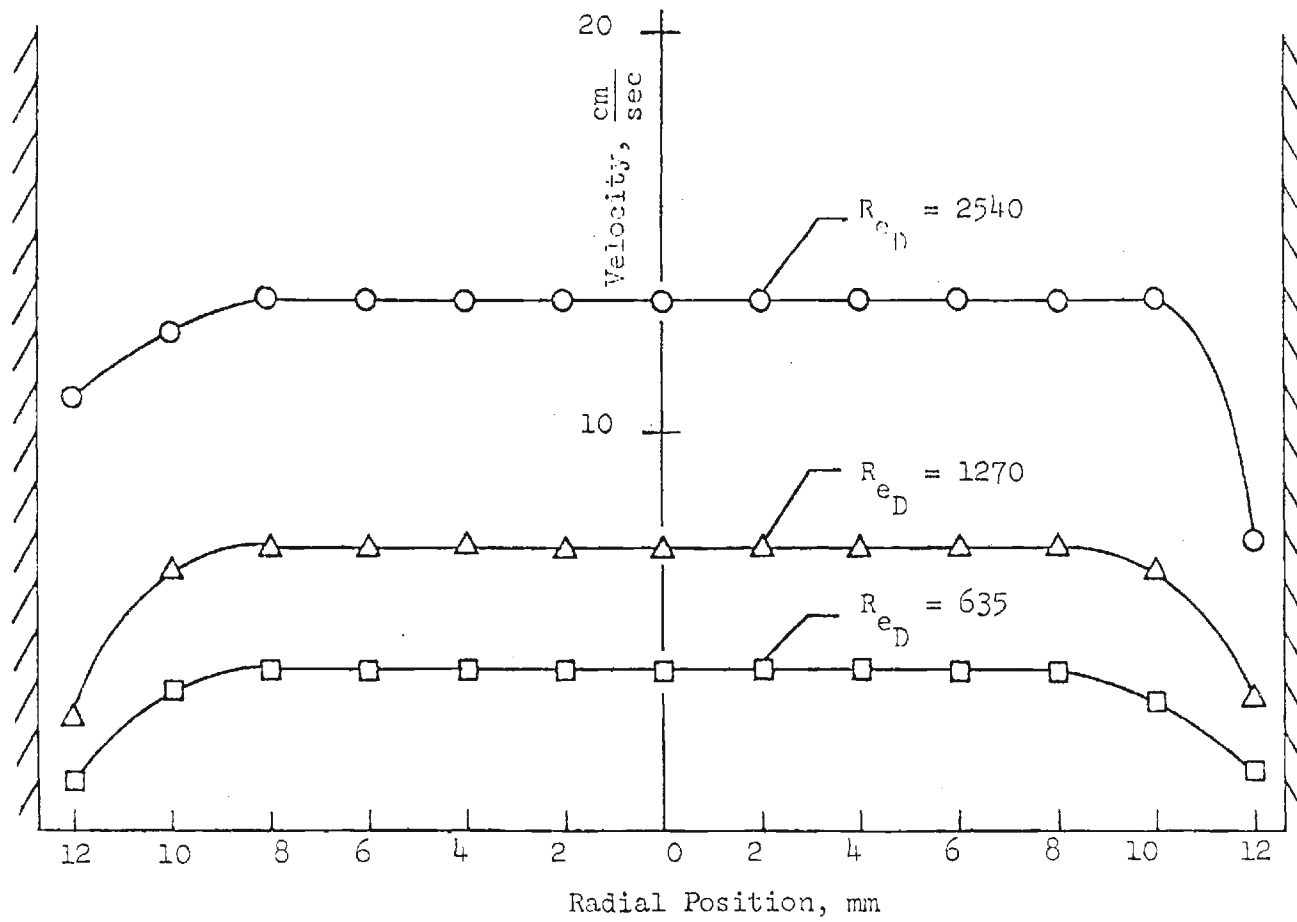


Figure 26. Mean Velocity Profile Upstream of Occlusion

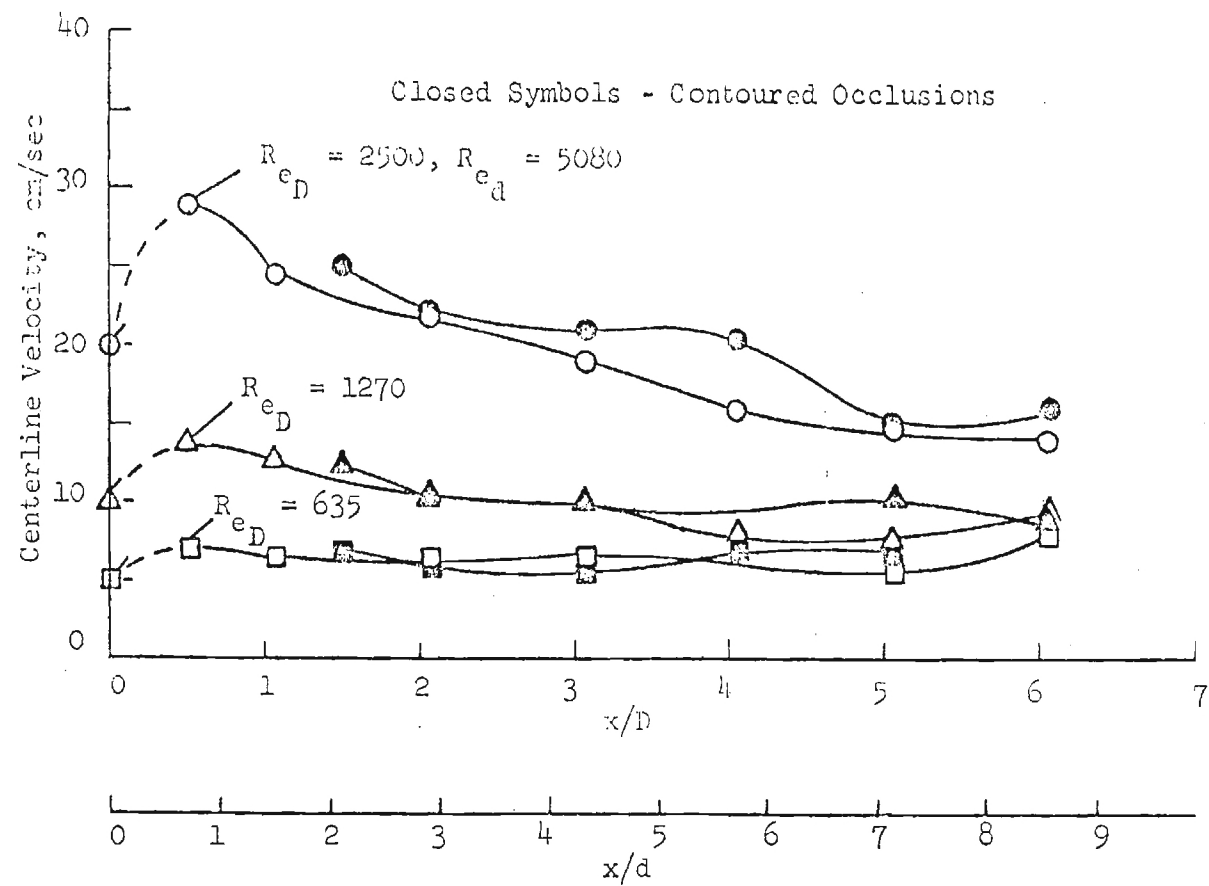


Figure 27. 50% Occlusions, Centerline Axial Velocity Profiles

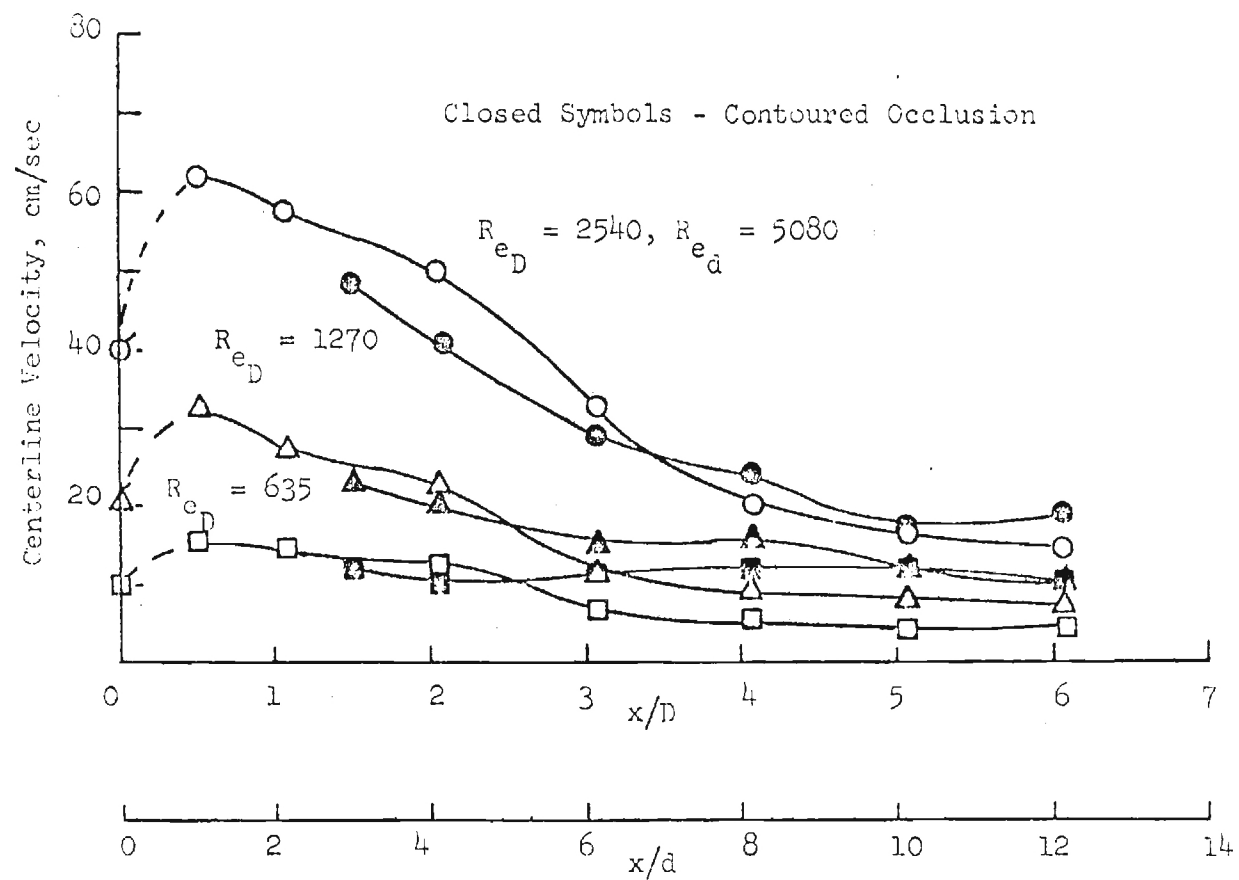


Figure 28. 75% Occlusions, Centerline Axial Velocity Profiles

3. Energy spectra

The velocity fields distal to the constrictions may contain a mixture of laminar flow, unstable or disturbed flow with large eddies and highly turbulent flow with a random distribution of eddy sizes. The measurement of the velocity at a point is a sensitive indication of the nature of the flow. The energy spectrum of the velocity signal is a measure of the kinetic energy contained within a specified frequency bandwidth and is a sensitive indication of the type of flow instabilities which are present. For instance, the fluctuations produced by vortex shedding result in an energy spectrum which contains a concentration of energy within a narrow frequency band; whereas, the more randomly distributed eddies in highly turbulent flows produce an energy spectrum which exhibits a continuous decay in intensity with increasing frequency. The occurrence of different shapes of energy spectra and velocity waveforms in distal stenotic flows and the effects of the distal wall on the occlusive jet and of a pulsatile mean flow are illustrated in the following sections. All spectral analyses in steady flow utilized a Fourier analyzer bandwidth of 1 Hz. Other methods of waveform analysis were discussed by Giddens et al¹⁰.

The proper Reynolds number and nondimensional length scale for duplication of flow conditions in a free jet or in a confined, stenotic jet in the near centerline region are, in most cases, based on the constriction conditions, U_o and d . However, from the viewpoint of studying degenerative vascular disease a more appropriate parameterization would be to hold the unoccluded flow conditions, U and D , constant while the degree of occlusion is allowed to increase. Such a comparison of the resulting

energy spectra at $Re_D = 2540$ is shown in Figure 29 for a fixed axial location. As the degree of constriction increases from 50% to 75%, the magnitude of the fluctuation energy increases noticeably and the character of the spectra changes from a peaked spectra caused by vortex shedding to a more dispersed spectra indicative of highly turbulent flow. The sharp-edged occlusion produced significantly higher intensities than did the contoured geometry. The 25% occlusion did not produce any disturbances at this position which were of measurably higher intensity than the unoccluded flow. At a given location in the near distal region the result of increasing the amount of constriction is an increase in the centerline mean velocity due to the stenotic jet effect. Subsequently, the amount of shear at the edge of the jet and at the wall reattachment point is higher which enhances the likelihood of the development of instabilities and transfer of kinetic energy into fluctuations.

As the measurement point is moved radially outward from the centerline at a particular axial location, the energy spectra change as shown for the 50% sharp-edged stenosis in Figures 30 and 31. At the near distal position, $X/D = 1.125$, the spectra exhibit a vortex shedding peak at the near centerline positions, $r = 0$ and 4 mm, while the spectra obtained near the wall, $r = 8$ and 12 mm, are more dispersed and of higher overall intensity than those near the centerline. This intense turbulence near the wall is indicative of the transfer of energy from the vortex ring eddies into larger and smaller eddies which was initiated by the stenotic jet reattaching to the distal wall. The effects of the wall on the stenotic jet characteristics are discussed in more detail later in this paper. As the flow progresses downstream, the randomized turbulence which was formed

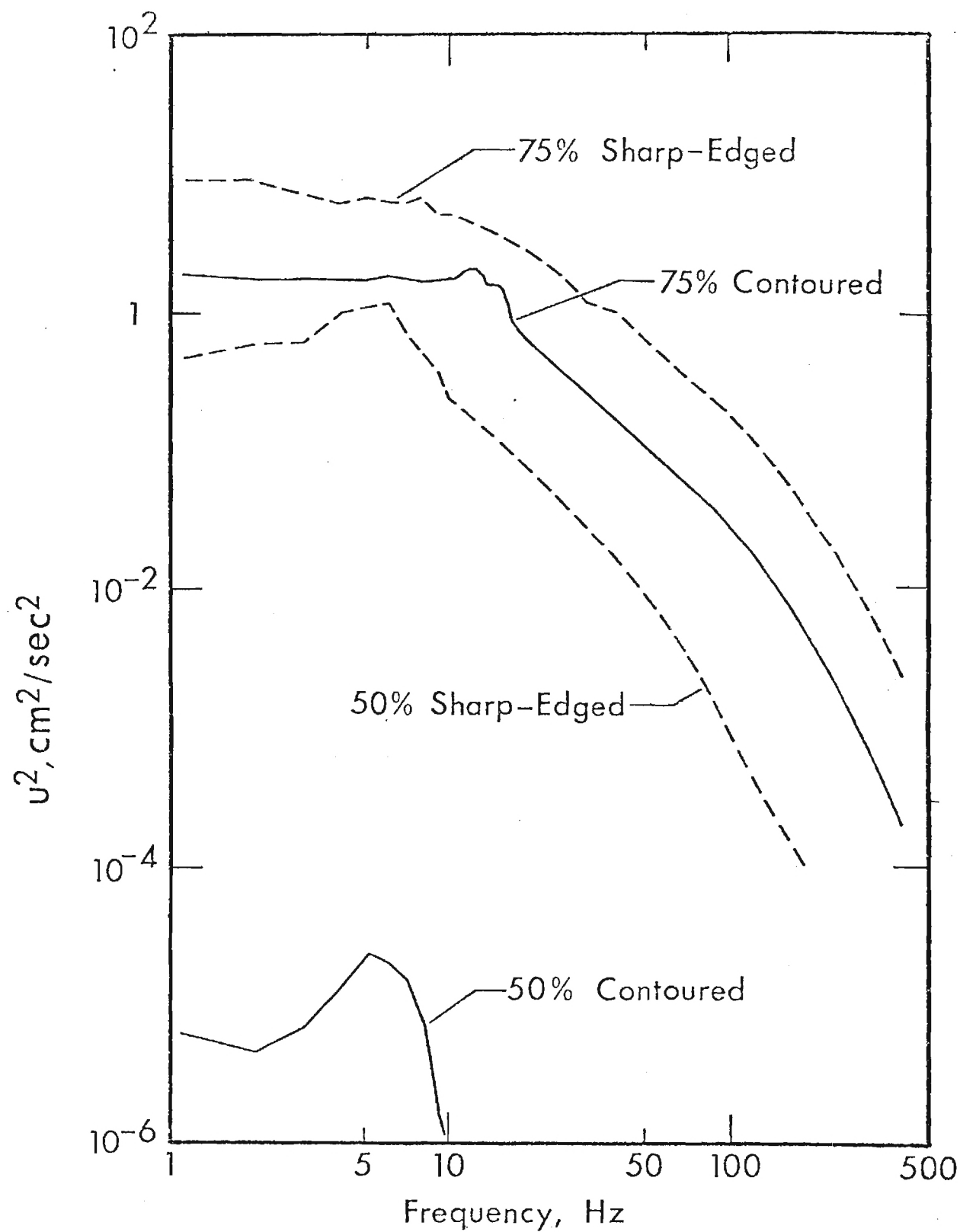


Figure 29. Energy spectra measured at $X/D = 2.125$ for $Re_D = 2540$.

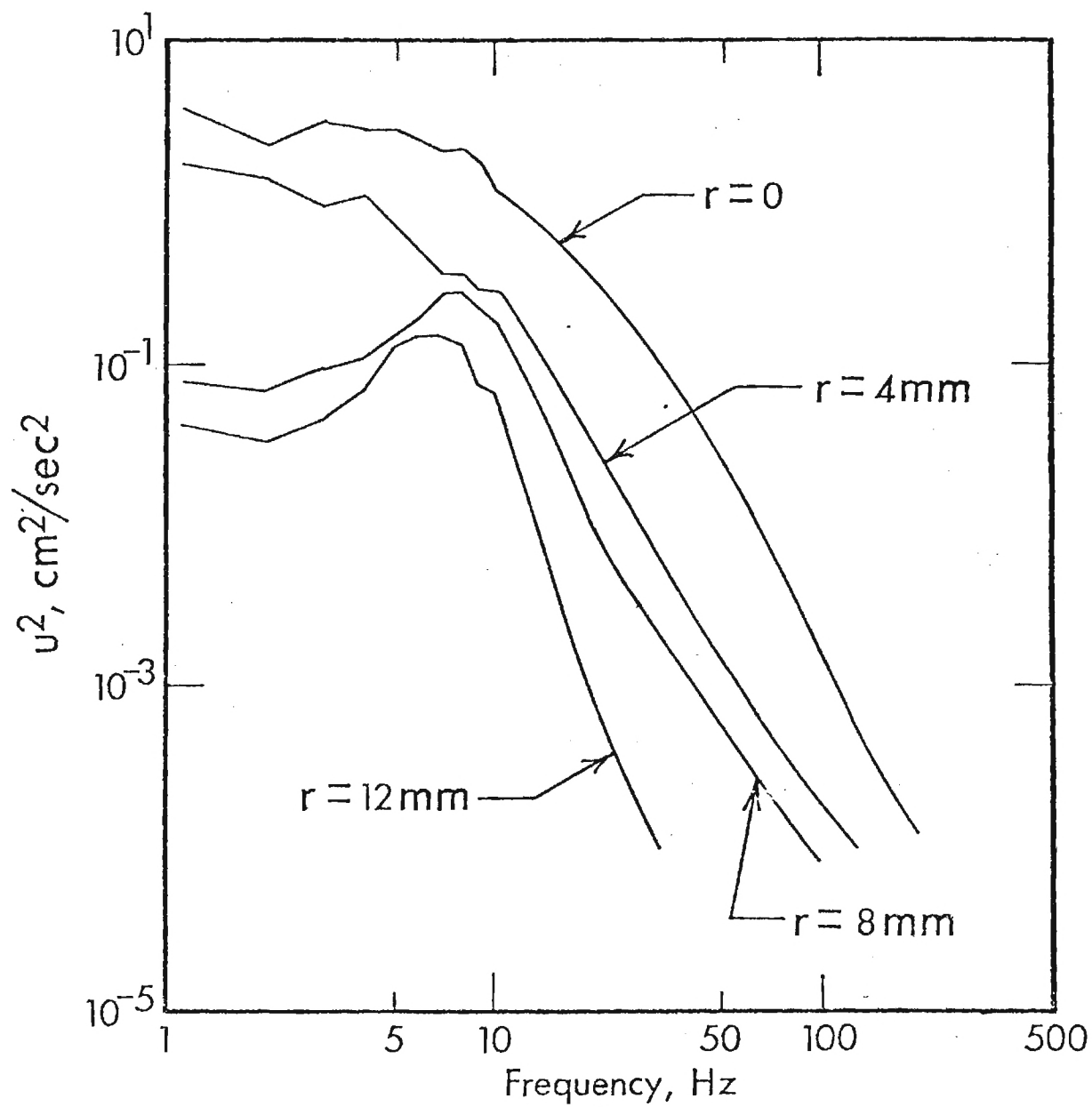


Figure 30. Radial variation of energy spectra for the sharp-edged stenosis at $X/D = 1.125$ for $Re_D = 2540$, $Re_d = 3592$.

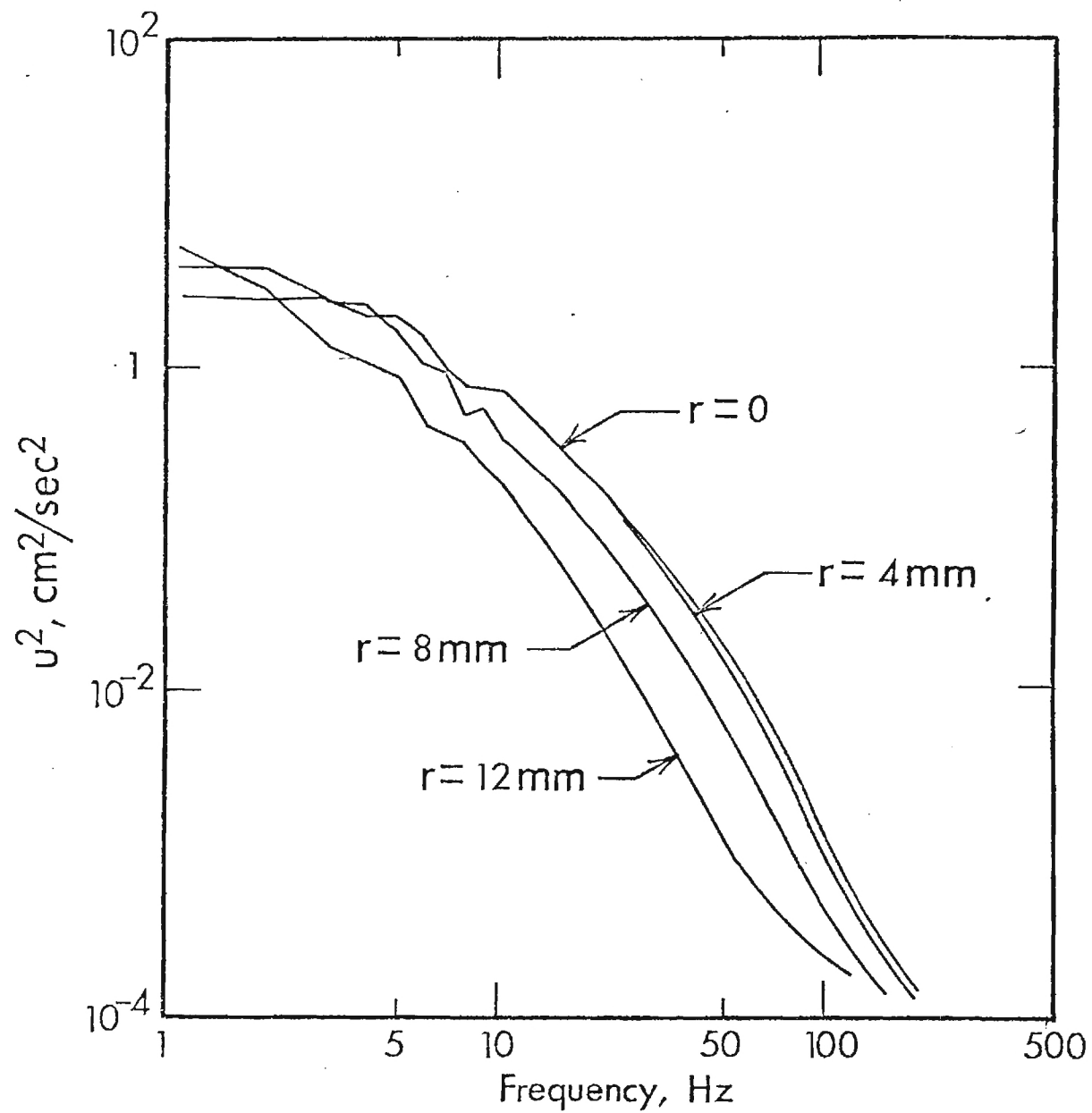


Figure 31. Radial variation of energy spectra for the sharp-edged stenosis at $X/D = 3.125$ for $Re_D = 2540$, $Re_d = 3592$.

near the wall is carried by convection and diffusion toward the center-line. Eventually the large vortex ring eddies are completely obliterated by the random turbulence as is shown in Figure 31. The peaks in the energy spectra which are caused by vortex shedding eddies are completely absent from the spectra at $X/D = 3.125$ and the overall intensity of the spectra is lower near the wall.

The influence of the wall on the initial formation of vortex rings and break-up of the vortex rings into random turbulence is less pronounced for greater degrees of occlusion where the stenotic jet shear layer is farther removed from the wall. As the wall interference effects are reduced, the vortex ring growth and the degeneration of the vortex ring system by "natural" instabilities approaches the behavior of the free jet case. The effects of the distal confining wall on the development of the stenotic flow disturbances are illustrated in Figures 32 through 34. Figure 32 shows the energy spectra for the 50% sharp-edged occlusion for $Re_D = 635$. The energy spectra for the free jet shows the growth of a spectral peak as the measurement location moves downstream from the constriction. This is characteristic of the formation of vortex rings. The confined jet, however, only shows a spectral peak immediately downstream of the constriction at $X/D = 0.5$. Farther downstream, the vortex-like instability dissipates without significant transfer of energy to smaller eddies. This result indicates that for low Reynolds numbers and moderate degrees of occlusion, the presence of a downstream confining wall has the effect of stabilizing flow instabilities.

Figure 33 shows the spectral results for the same 50% occlusion at a higher Reynolds number of $Re_D = 1270$. The confined jet produced

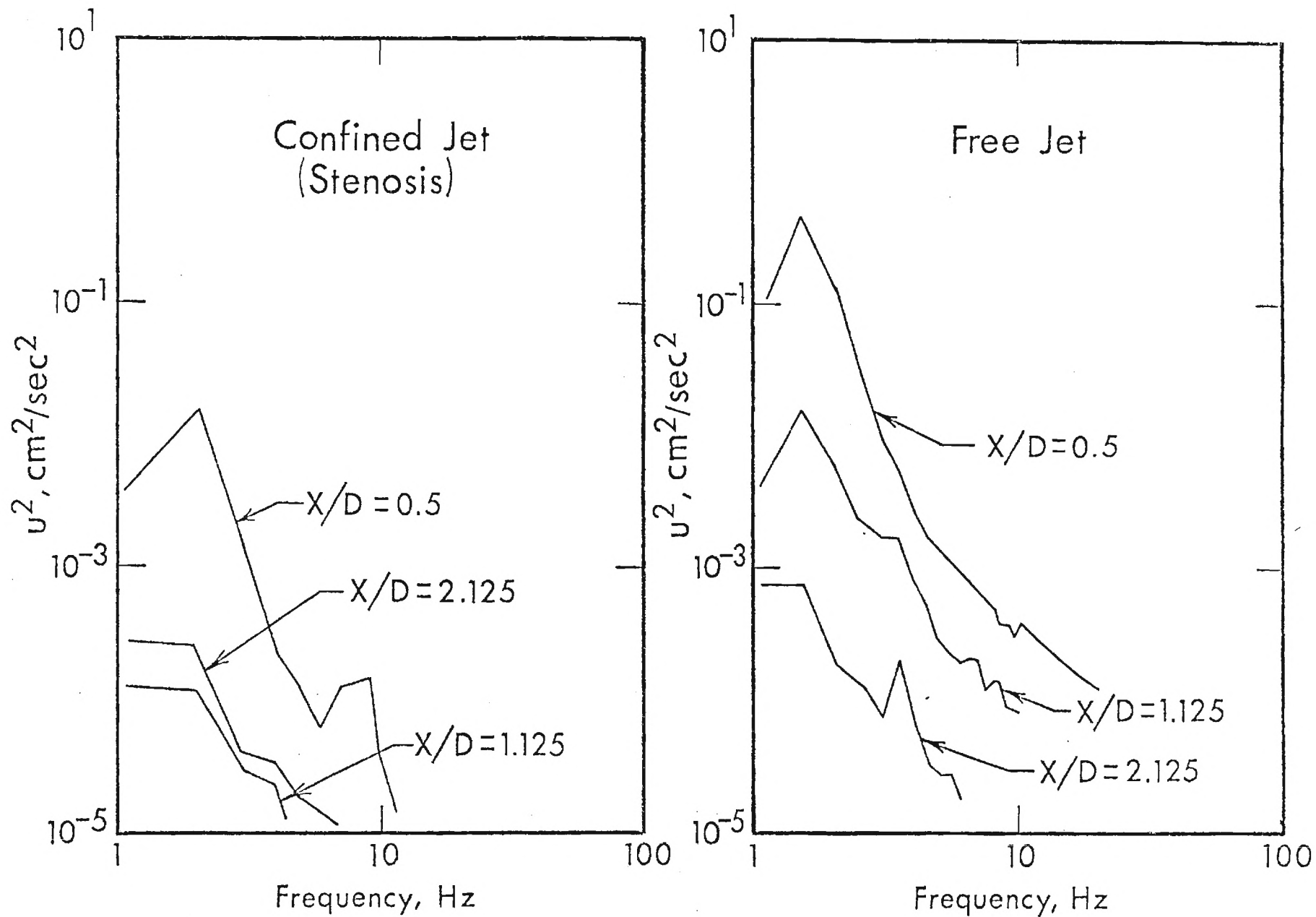


Figure 32. Comparison of the centerline energy spectra produced by stenotic and free jets flowing from the 50% sharp-edged constriction at $Re_D = 635$, $Re_d = 898$.

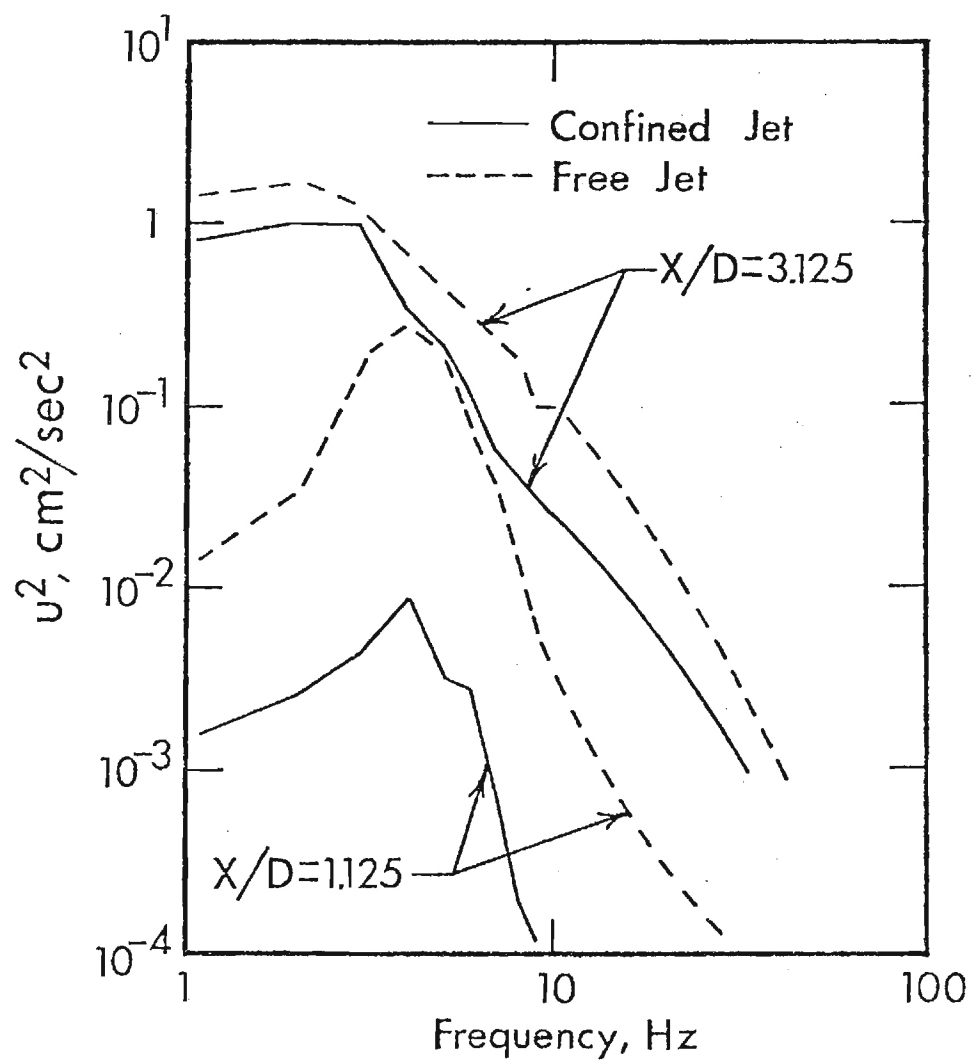


Figure 33. Comparison of centerline energy spectra produced by confined (stenotic) and free jets flowing from the 50% sharp-edged constriction at $Re_D = 1270$, $Re_d = 1796$.

a spectral peak which increases in intensity as the flow progresses downstream. However, the velocity fluctuation energy contained in the free jet vortex ring system is greater than the confined jet system. At this higher Reynolds number, the presence of the wall has served to suppress, but not eliminate, the growth of the vortex ring system. Farther downstream at $X/D = 3.125$, the two cases produce a more randomly distributed energy spectra with the free jet having a slightly higher overall magnitude.

Figure 34 shows the energy spectra for the 75% sharp-edged occlusion at $Re_D = 1270$. In the near distal region at $X/D = 1.125$, the spectral distributions are very similar for the two cases. For this degree of occlusion, the downstream wall is far enough removed from the vortex ring system so that the wall has little or no effect on the initial development. However, as the jet expands radially at the more distal locations, the confined jet shear layer contacts the wall. The contact with the wall breaks up the vortex system into a random turbulence. This effect can be seen at $X/D = 2.125$ where the free jet spectra still contain a distinct spectral peak while the confined jet spectra do not. Farther downstream at $X/D = 3.125$, both spectra are nearly identical since the free jet vortex system has also degenerated into random turbulence due to natural dissipative mechanisms.

The purposes of correlating the energy spectra are: (1) to determine the applicability of nondimensional parameters to the scaling of the distal flow field, (2) to compare the relative intensities of the velocity fluctuations produced by the two stenosis geometries, and (3) to relate the Strouhal number of the vortex shedding frequency to the data cited

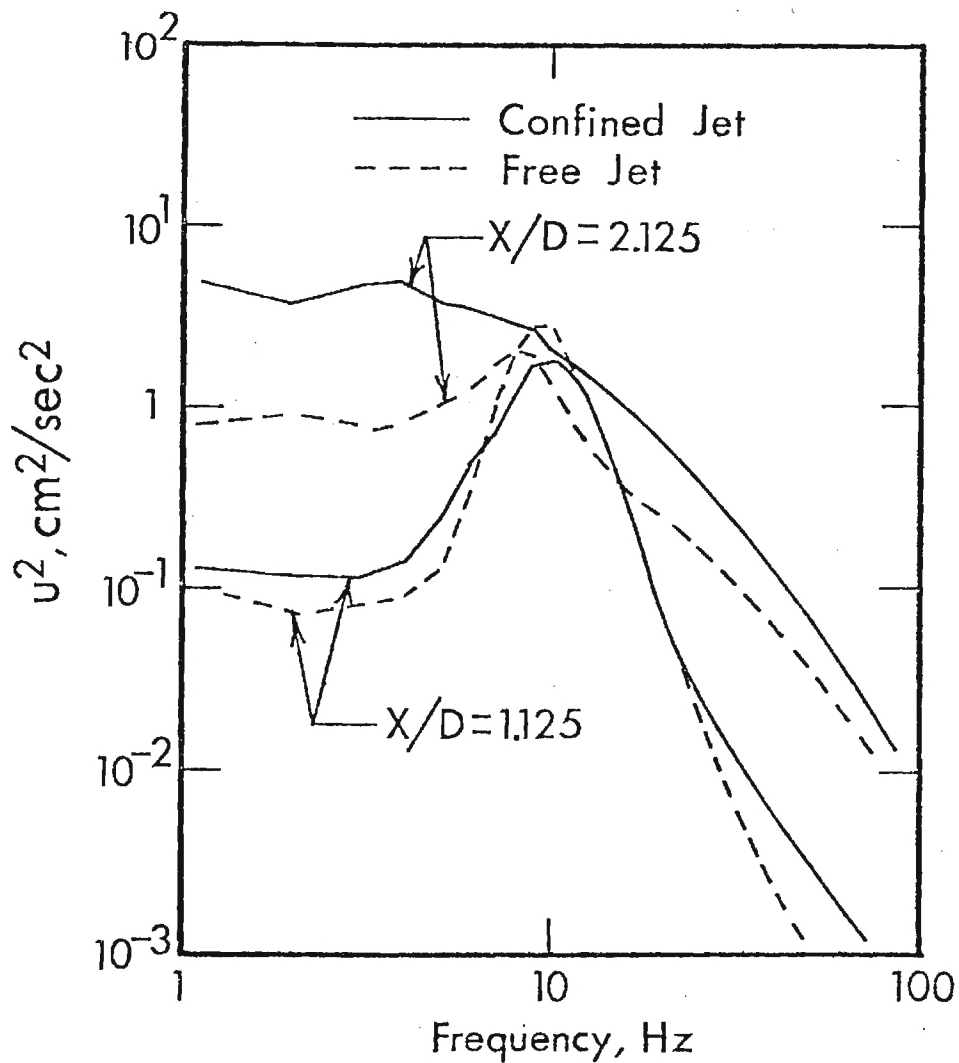


Figure 34. Comparison of centerline energy spectra produced by confined (stenotic) and free jets flowing from the 75% sharp-edged constriction of $Re_D = 1270$, $Re_d = 2540$.

in the literature.

Since the data presented in the references is often correlated with a Strouhal number based on conditions at the jet orifice or pipe exit, it is appropriate that the present data be nondimensionalized in a similar manner. The energy and frequency are nondimensionalized by the mean velocity at the constriction minimum area, U_o , and the constriction diameter, d .

Figure 35 shows the Strouhal number comparisons for the 50 percent occlusions at $Re_D = 2540$, $Re_d = 3592$. In the near distal field ($X/D = 0.5$) of the sharp occlusion, the Strouhal number of the spectral peak is about 1.0 and decreases to a value of about 0.5 to 0.6 at the more distal positions ($X/D = 1.125$ and 2.125) before the onset of the turbulent-like dispersed spectra at $X/D = 3.125$. The intensity of the spectral peak also reaches a maximum at $fd/U_o = 0.6$. The contoured occlusion data show the spectral peak occurring at a Strouhal number of about 0.5 to 0.6 at all positions shown. The dominant Strouhal number of about 0.6 for both geometries agrees with the correlations published in the literature for confined and free jets (Johansen⁵³; Beavers and Wilson⁵⁴). However, the sharp-edged occlusion yields more intense spectral peaks, as compared to the total kinetic energy available at the occlusion, U_o^2 , than did the contoured occlusion. Likewise, the correlations of the free jet spectral peaks would also yield a Strouhal number of about 0.6 and indicate an even higher transfer of energy into the vortex fluctuation. Similar Strouhal number correlations can be demonstrated for the 75 percent occlusions and for lower Reynolds number flows. As the constriction Reynolds number, Re_d decreases, the

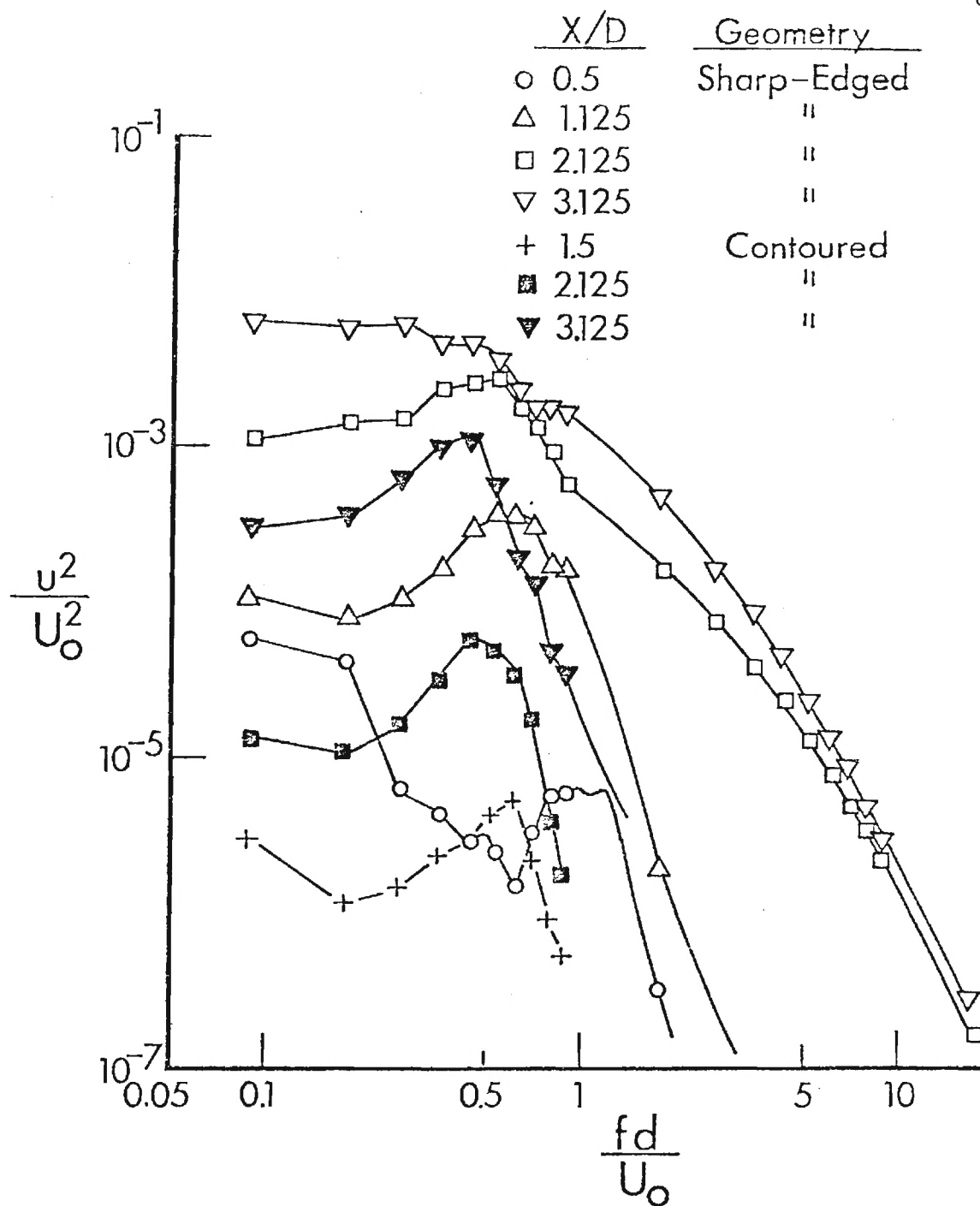


Figure 35. Strouhal number and nondimensional spectral energy measured on the centerline distal to the 50% stenosis at $Re_D = 2540$, $Re_d = 3592$.

differences in the nondimensional intensities of the spectra produced by the two geometries are more pronounced (Cassanova, 1975).

In the near-distal region of the flow field where wall interactions are minimum, the conditions for similarity of the energy spectra are that $X/D = \text{constant}$ and $Re_d = \text{constant}$ for a given stenosis geometry. This is demonstrated in Figure 36 for three different degrees of occlusion. The centerline energy spectra for the 75 and 90 percent occlusions which were obtained at the same $Re_d = 2540$ and $X/d = 4.25$ have similarly dispersed spectra which correlate by using this particular nondimensionalization. However, the 50 and 75 percent occlusion data which have the same $Re_d = 1270$ and $X/D = 2.125$ do not correlate at all since the spectra are not similar. The spectrum for 50 percent occlusion indicates that the flow at this location is dominated by laminar vortex shedding, whereas, the 75 percent occlusion spectrum indicates a more randomly dispersed turbulent flow.

The correlation of the steady flow energy spectra in the near-distal region indicate that the mechanisms controlling the formation of instabilities and turbulence are dominated by the constriction conditions, i.e., Re_d and constriction geometrical shape, in a manner which is similar to free jets. Farther downstream where the interaction of the jet with the wall has destroyed the "memory" of the flow, a similarity relationship between occlusion sizes would not be expected since the observed characteristics would no longer possess a unique dependence on the constriction conditions.

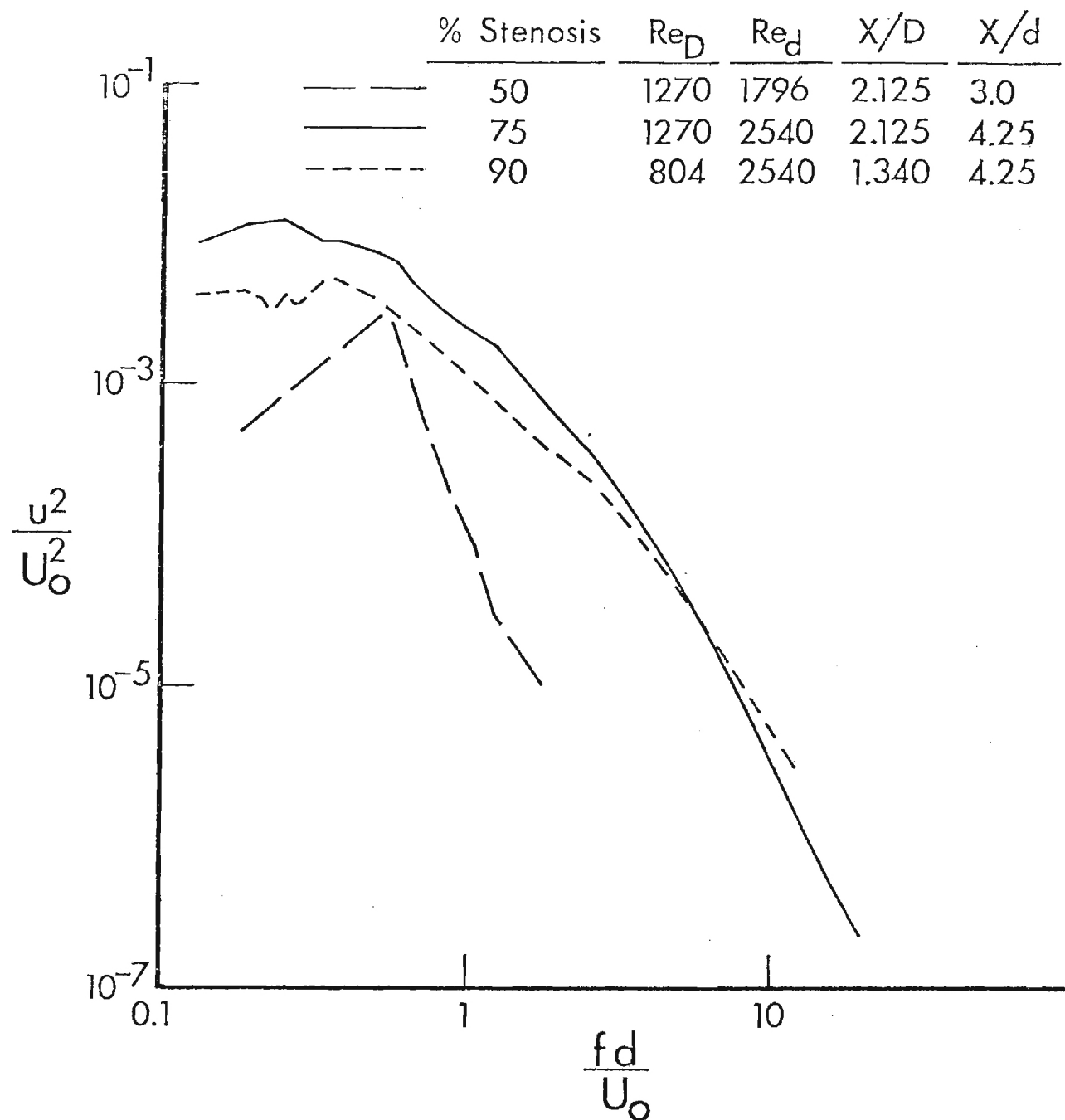


Figure 36. Correlation of the Strouhal number and nondimensional spectral energy with stenosis size for the sharp-edged stenoses.

C. Experimental Studies - Laser Doppler Anemometer

There are certain limitations in employing the hot film anemometer for velocity measurements in a poststenotic flow field. The recirculation region cannot be studied since the conical probe is accurate only for flows which are essentially parallel to the probe axis. For the same reason, the measurements of a fluctuating velocity in a region where fluctuations are large must be viewed as qualitative in nature, since large v' and w' components mean that the instantaneous angle of the flow with respect to the sensor will vary considerably. Also, of course, it is recognized that the hot film probe is an invasive instrument. Its presence in a flow, particularly one as complex as a poststenotic field, may affect the measurements being attempted. Finally, the hot film is a tedious instrument with which to work. Recalibration must be done frequently, and it is difficult to change the axial location of the probe.

For these reasons the Biofluid Dynamics group at Georgia Tech decided to purchase a DISA Mark II Laser Doppler Anemometer (LDA). This instrument has been installed in our laboratory. At the time of completion of the NSF grant period covered by this report, no measurements of poststenotic flows had been completed. Since the termination of that grant measurements have been made and will be reported upon in the Final Report for our present grant, ENG76-23876.

IV. DISORDER IN PULSATILE FLOWS

An important goal of this research program was to develop methods for describing disorder in pulsatile flows and to apply these methods to data obtained from in vitro and in vivo experiments.

From the fluid dynamics viewpoint the problem of disordered flow in the arterial system is particularly intriguing. Several factors combine to create complexities which often do not arise in other engineering applications. The most dominant of these factors is the pulsatility of the flow. Because of this, the traditional approach of averaging quantities for a period of time sufficiently long to obtain constant mean values must be modified. In arterial flows the "mean" velocity of interest is usually not the average over a long time, but is rather the basic pulsatile waveform itself. Further, this waveform is not of a particularly convenient shape for engineering analysis. Under certain conditions the sharp increase in velocity during systole may be followed by a reverse flow phase and a subsequent secondary forward flow peak. The general waveform shape is such that many harmonics of the fundamental heart rate are present, so that flow disorder or turbulence which occurs at, say, ten Hertz may be difficult to distinguish from an harmonic of the basic waveform. Finally, an additional complication is the presence of biological variability. The basic velocity waveform is not strictly periodic since each heartbeat may differ slightly (or significantly) from all others. Coupled with this is the fact that it is often difficult to maintain a subject in a relatively constant state for a time sufficiently long to allow a reliable description of flow disorder. For this reason, the problem of separating flow disorder from biological

disorder is of importance.

Thus, at the outset of this study there was a need for well-defined methods of analysis of turbulence and flow disorder in arterial flows. Recently, several investigators have independently pursued such development. The earliest approaches were to compute energy spectra of the entire velocity waveform without regard to a development with time of events or to the separation of a disturbance velocity component. Examples of this are Nerem et al², Falsetti⁵⁵, Giddens et al⁹, and Cassanova⁵¹. Subsequently, interest was drawn to a more detailed analysis of the flow. For example, Pawel³⁹ has studied the problem of turbulence produced by velocity pulsations in an elastic tube of circular cross-sectional area. Using a hot film anemometer to measure velocities, he divided the simulated heart cycle into several segments and determined a time-development of the disturbance energy spectra. These data showed short "bursts of turbulence" during and immediately after systole for a pulse rate of 71 beats per minute and a more developed turbulence at a higher rate of 112 beats per minute. These findings were very sensitive to the values of Reynolds number, frequency parameter, and the harmonic composition of the periodic velocity waveform. Parker⁴⁰ has given results taken from in vivo data in the descending thoracic aorta of dogs which show instabilities during the initial deceleration phase of systole. Giddens et al¹⁰ have reported on the development with time of the energy spectra of the total velocity and on time-varying ensemble average waveforms for flow distal to varying degrees of stenosis. These results indicated substantial disorder during flow deceleration, even for mild stenoses.

A. Theory

Most fluid dynamic studies of turbulence deal with flows which have steady mean values. That is, if time averages are formed of any particular variable, this average value is a constant. This is best illustrated by consideration of a velocity measurement at a fixed point in a turbulent flow. The output of an anemometer might look like that shown in Figure 37a. If the average reading is formed, by determining the integral

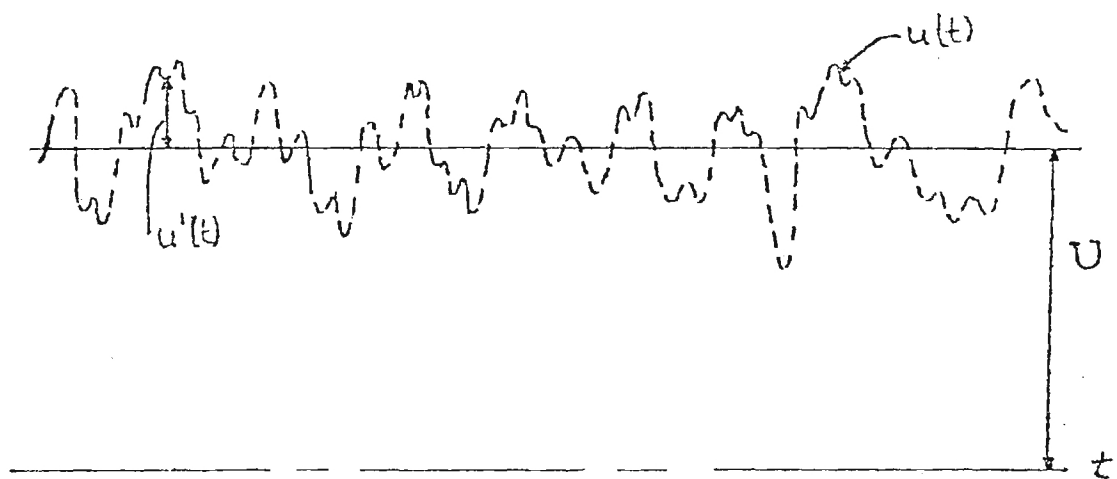
$$\frac{1}{T} \int_0^T u(t) dt = U \quad (25)$$

where $u(t)$ is the instantaneous velocity and t is the time, then one finds that for large time T , the value of U approaches a constant. This is then termed the mean velocity of the flow at that point in space. Typically, then, one writes

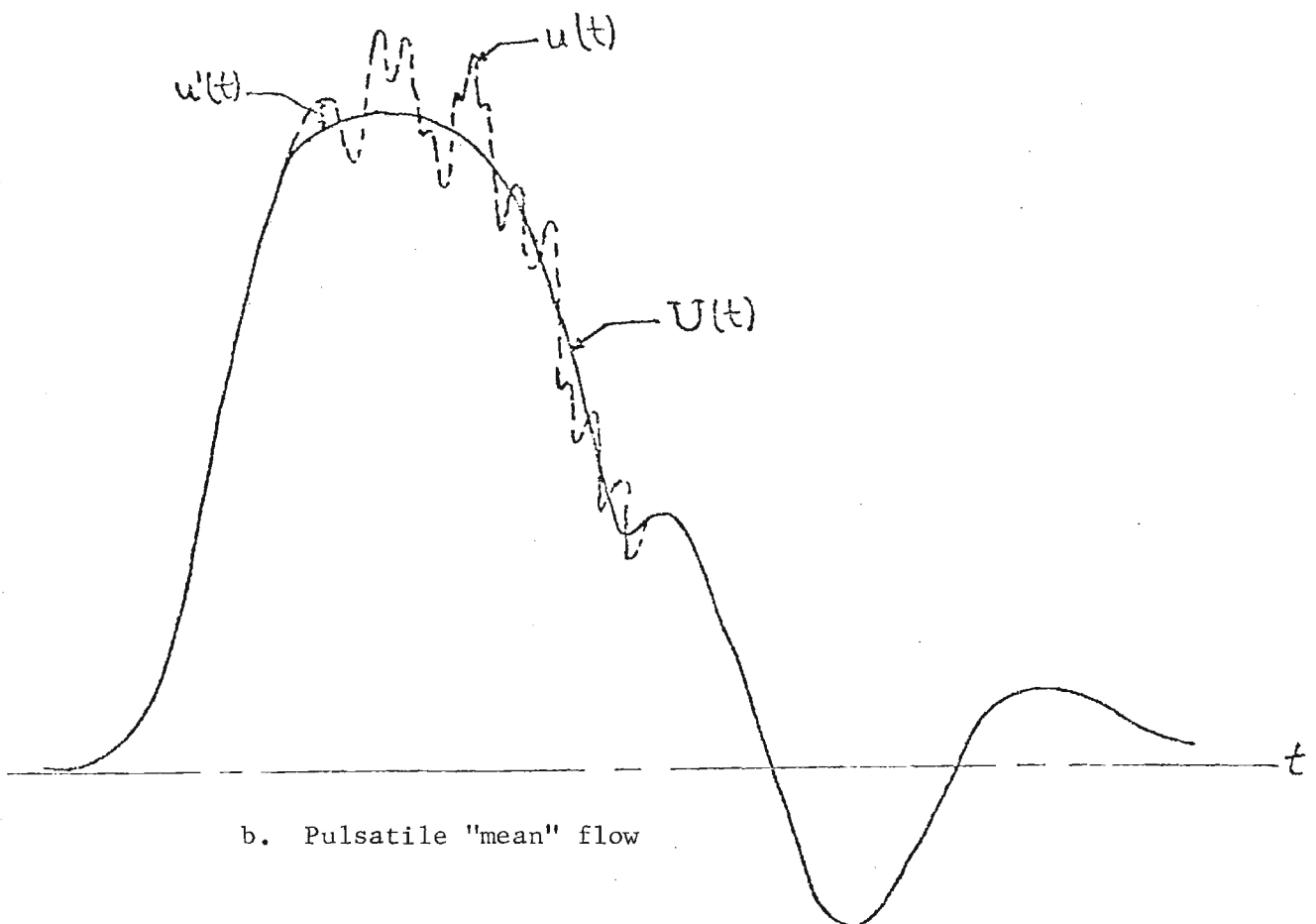
$$u(t) = U + u'(t) \quad (26)$$

as a representation of the instantaneous velocity at a point. The quantity $u'(t)$ is a disturbance velocity, and by definition its time average is zero. This same representation may be used for other flow variables such as pressure, temperature, and additional velocity components. Furthermore, in most treatments of turbulent flows the magnitude of $u'(t)$ is considerably less than that of U .

In studies of ordered structures in a turbulent flow a further breakdown of contributions to the velocity is prescribed. For such flows a velocity is considered to be composed of mean, periodic, and turbulent



a. Steady Mean Flow



b. Pulsatile "mean" flow

Figure 37. Illustration of disturbances in "steady" and pulsatile flows.

components. The periodic disturbance is often "buried" in the turbulence and an important problem is to extract the ordered structure from a seemingly random pattern. Examples of this approach are given by Hussain and Reynolds⁵⁶.

When the problem of arterial flows is considered, immediate complications arise. First of all, only at the crudest level of description -- namely, mean blood flow delivered -- is it useful to define a mean velocity such as that of Equation (25). The flow is essentially periodic rather than essentially steady. Furthermore, the heart is not a perfectly reproducible pump. Each heart beat may be slightly different so that a "biological disorder" is present, as described earlier. Fortunately, in a carefully controlled experiment heart rates and ejection characteristics which are reasonably periodic can be maintained. It is thus possible, under proper conditions, to define a time-varying ensemble average waveform by

$$U(t) = \lim_{N \rightarrow \infty} \frac{1}{N} \sum_{n=0}^{N-1} u(t + n P) \quad (27)$$

where P is the period of the waveform, the inverse of the fundamental heart rate. Note that if every heartbeat produced exactly the same waveform (i.e., no biological disorder) and if there were no fluid dynamic disorder, then $u(t) = u(t + NP)$ for all values of the integer n .

Having defined such a deterministic ensemble average waveform given by $U(t)$, it is possible to describe disturbances or deviations from this. For any given waveform the velocity may be expressed as

$$u(t) = U(t) + u'(t) \quad (28)$$

where $u'(t)$ is the disturbance velocity, to be treated as a random variable. This is illustrated in Figure 37b. It is not a straightforward matter to define turbulence, in the strictest sense, for such a flow. For example, to achieve a developed turbulent flow the time scale over which $U(t)$ varies significantly should be much longer than that over which $u'(t)$ varies. Also, a condition for maintaining turbulence throughout most of a cycle is that the instantaneous Reynolds number be sufficiently high. If the dissipation time is short in comparison with the heart rate period, any so-called turbulence which is generated during systole, for example, would not persist throughout diastole. Furthermore, in the case of stenoses in particular, periodic low frequency disturbances such as vortex shedding may be generated and then break up as they proceed downstream.

For situations in which the disturbances exist over only a part of the cycle there is the additional complication that $u'(t)$ is not a stationary random variable. Therefore, computations of energy spectra, correlation functions, and rms disturbance velocities depend upon the time intervals selected for analysis. In fact, it is precisely this dependence which provides information on the development of disorder. Although the concept of energy spectra which are time-varying is perhaps unusual, there is precedent for such a notion, given by Priestly⁵⁷.

For these reasons, the flow through a stenosis in a relatively large vessel is such that it is frequently misleading to term it turbulent. Thus, we have chosen to call these "disturbed" or "disordered"

flows, meaning by this a departure of the individual waveforms from their time-varying ensemble average. Turbulence falls, of course, under such a definition, as do vortex shedding and transitional flows. However, the existence of a disturbance velocity $u'(t)$ in an arterial blood velocity waveform can by no means be construed as signifying turbulence. Simple deviations from perfect reproducibility among heartbeats may give u' results which, upon superficial analysis, seem to resemble turbulence. In fact, separation of biological disorder from fluid dynamic disorder is a most difficult problem.

As discussed previously several types of analyses are useful in describing disordered arterial flows. Among these are

- a) determination of time-varying ensemble average waveforms
- b) computation of energy spectra and correlation functions of the total velocity component, $u(t)$
- c) computation of energy spectra and correlation functions for the disturbance velocity component, $u'(t)$
- d) analysis of (b) and (c) as a functions of the time interval within the cycle
- e) determination of rms values for the disturbance velocity component and the variation of this quantity with time.

It is inappropriate to select any one of these as the most significant method for analysis. Each has information to offer and, together, they complement each other to form a total description of the flow. The following sections will focus upon the extraction and analysis of disturbance velocities as applied to poststenotic flow field measurements.

B. Pulsatile Flow Studies - In Vitro

This section discusses results obtained in an in vitro study employing hot film anemometers for velocity measurements in the flow facility described earlier. At the time these experiments were performed, we had not yet implemented the analysis techniques for examining the development of disorder with time in the pulsatile cycle. Therefore, all the spectral data presented in this section were obtained from a study of the entire velocity waveform. In the next section on in vivo measurements we present results obtained from examining several intervals within the flow cycle.

1. Flow description

The behavior of pulsatile flow through constrictions in tubes is more complex than the steady flow case since the velocity pulse waveform typical of those found in a physiological situation is relatively complex in that it is composed of a number of harmonics of the fundamental pulse rate, and may have a reverse flow component. For the purpose of illustrating the basic phenomena present in post stenotic flow, a simpler sinusoidal-like waveform is employed.

A pulsatile velocity waveform proximal to the partial occlusion is represented by the solid line shown in Figure 38. The resulting velocity pulse through the minimum area of the occlusion is depicted by the dashed curve. The peak pulse velocity proximal to the occlusion is denoted by U_p ; and U_{op} is the peak pulse velocity at the minimum area of the occlusion. The difference between U_{op} and U_p depends not only on the geometrical area change, but also on the shape of the occlusion upstream of the minimum area. This shape influences the

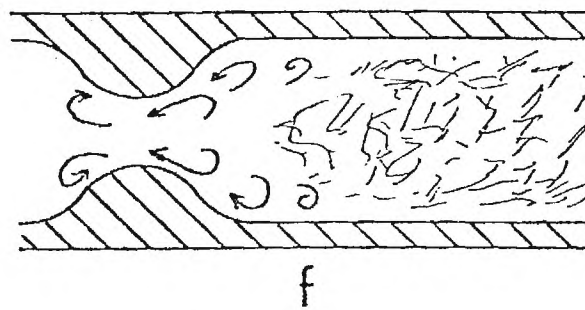
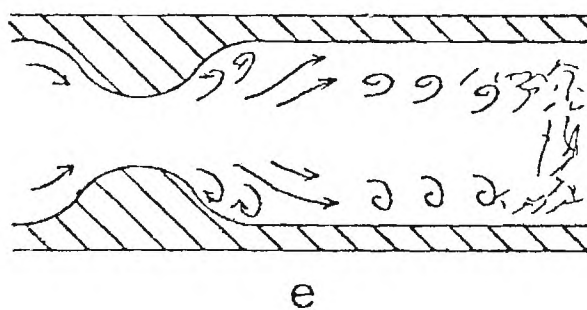
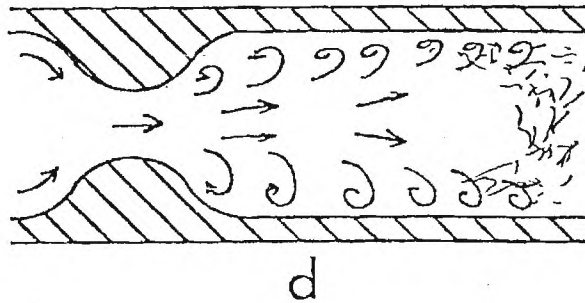
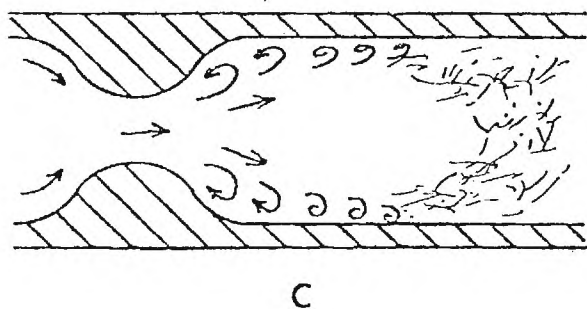
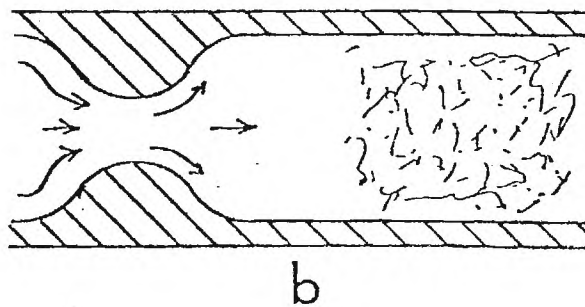
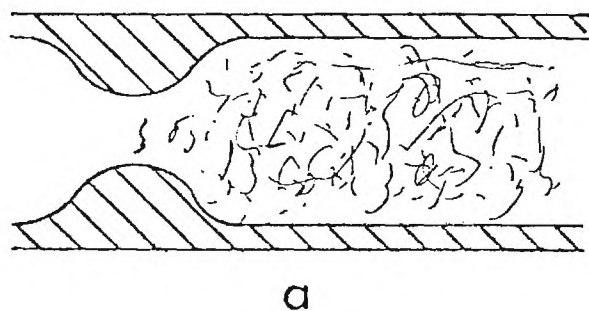
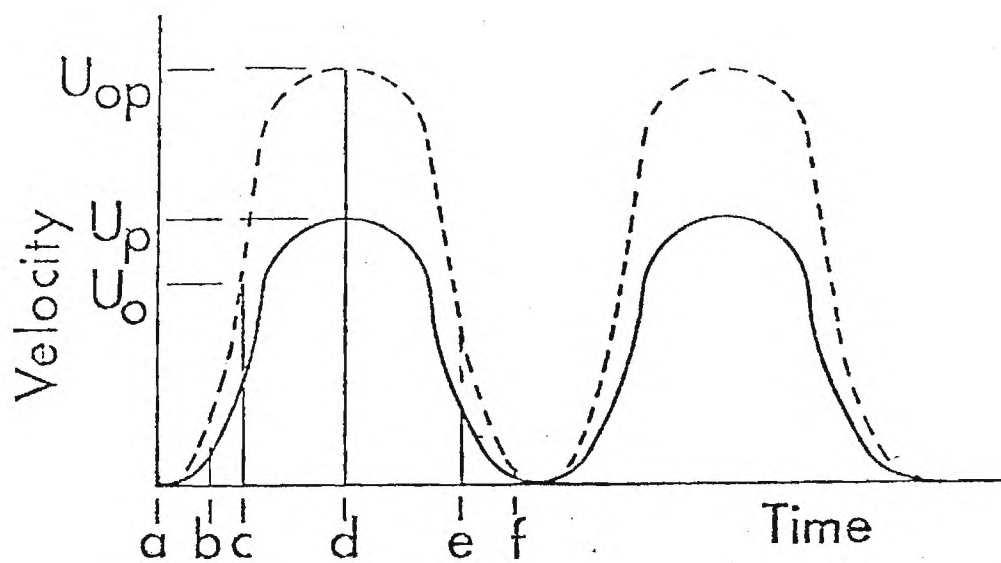


Figure 38. Development of flow disorder distal to a stenosis in pulsatile flow.

vena contracta, or effective minimum area, of the occlusion. At time (a) the mean velocity is zero and some turbulence generated in the previous pulsation lingers in the region distal to the occlusion. At time (b) the velocity through the occlusion has not reached that required for separation and the turbulent field from the previous pulse is being moved downstream. At time (c) the separation velocity U_s , is reached in the minimum area and vortices are shed which dissipate to form a turbulent field as they move downstream. From the times (c) through (d) and (e), vortices are continually shed to form random turbulence downstream. At time (d) the velocity through the minimum area reaches a maximum, U_{op} . The shedding frequency of the vortices at a given time is dependent on the instantaneous Reynolds number based on the conditions at the minimum area of the occlusion. For low peak Reynolds numbers, a large vortex ring can form downstream of the minimum area and swirl toward the center of the tube. The size of the vortex ring depends on the pulsation rate of the main flow and the degree of occlusion. It is emphasized that, contrary to a steady flow case where the separation region can be filled with a low velocity, low turbulence flow, the pulsatile "separation region" can be filled with a relatively violent, swirling vortex ring during a portion of the flow pulse. The shape of the occlusion (sharp versus rounded) will probably influence the shedding frequency but this factor has not been investigated extensively. As the velocity decreases from (e) to (f) the flow reattaches to the surface and the turbulent eddies and vortices are carried downstream. At time (f) when the mean velocity is essentially zero, the vortices and turbulent eddies near the stenosis can actually recirculate flow back through the

minimum area. These eddies are then moved downstream as the mean velocity begins to increase in the next pulse and the process repeats. The length of time and distance that the turbulent eddies persist in the subsequent pulsation is dependent on the fluid viscosity, the degree of occlusion and the waveform of the driving velocity pulse. The degree of occlusion, and to some extent the occlusion shape, influence the point at which the relatively large vortices of the turbulent jet interact with the wall and dissipate into smaller scale turbulence.

2. Velocity measurements

The following discussion illustrates further some of the salient features of the flow disturbances created by a pulsating mean flow. The proximal flow had a sinusoidal-shaped waveform with a pulse rate of 0.2 Hz, a frequency parameter of 15 and a peak Reynolds number of 2540. While this waveform approximately duplicates the physiologically normal frequency parameter with the relatively large tubing size that was used in the experiments, the pulse rate is considerably lower than normal. Therefore, the acceleration and deceleration rates of the pulse were also lower than would be normally encountered in the human cardiovascular system. The entire velocity waveform was sampled by the Fourier analyzer to obtain the energy spectra with a frequency bandwidth of 0.2 Hz. It should be noted that the conical hot film probe cannot be utilized successfully in periodically reversing flows. All data reported herein were obtained in regions where forward flow over the probe was assured for the entire cycle.

Figure 39 shows the centerline waveform at several axial positions

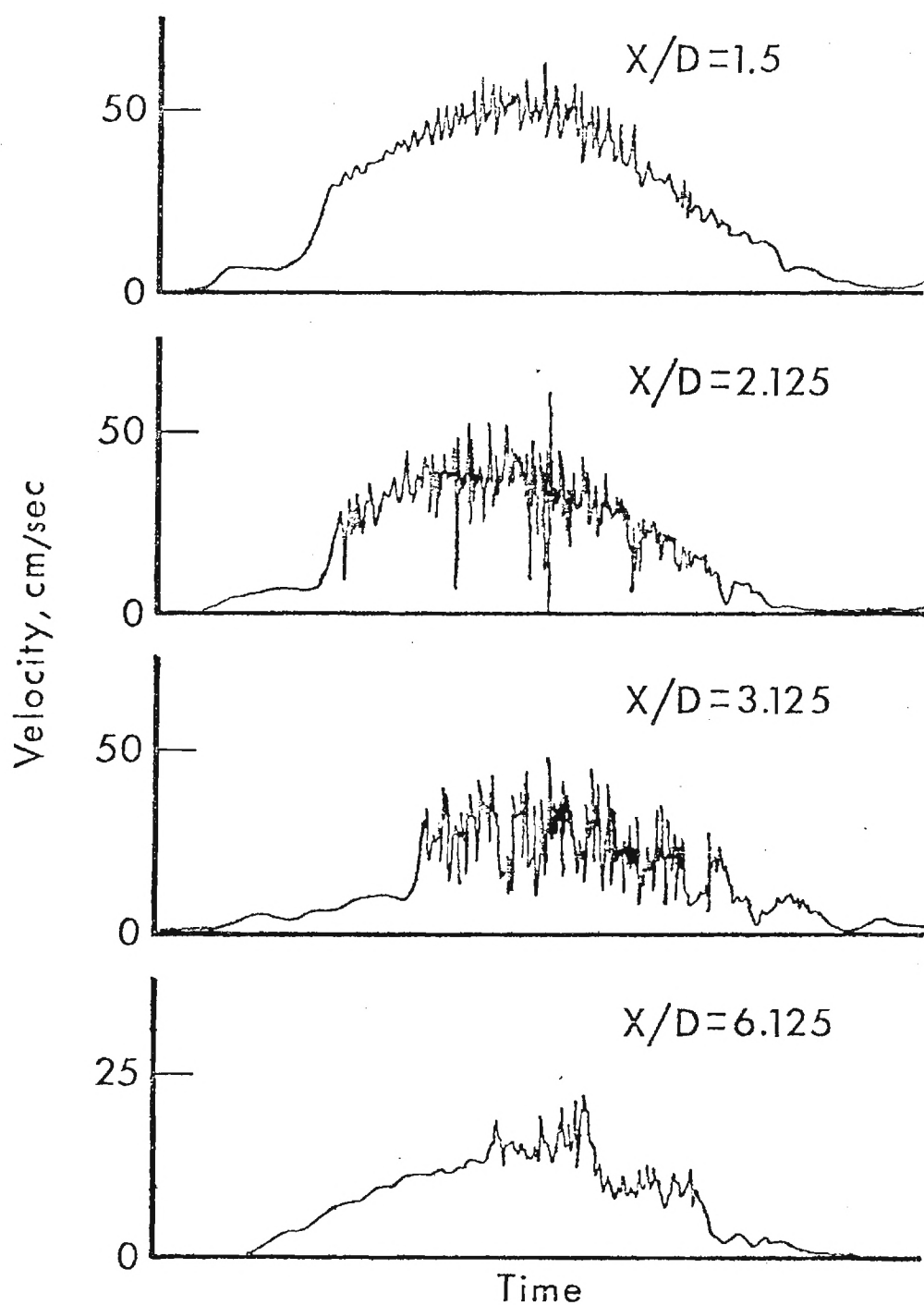


Figure 39. Axial variation of the centerline velocity waveforms distal to the 75% contoured stenosis with $\alpha = 15$, $Re_{DP} = 2540$.

distal to the 75% contoured occlusion. The development of flow disturbances during the higher velocity portion of the pulse is evident. The intensity of the disturbance increases and the mean velocity decreases as the measurement point moves downstream to $X/D = 3.125$. The disturbances essentially dissipate during the low velocity portion of the pulse at all locations. The disturbances which were created at the stenosis do not reach the farthest downstream position, $X/D = 6.125$, until the mean velocity nears the maximum.

The typical radial variation of the waveform and the occurrences of large vortex rings in the initial phase of the pulse can be seen in Figure 40 which are data obtained with the 50% sharp-edged occlusion. The large, low frequency fluctuation which occurs during the acceleration phase at $r = 8$ and 12 mm is caused by the starting vortex ring swirling into the region near the wall which is a recirculation region in the steady flow case. The intensity and frequency of the velocity fluctuations in the high shear region at $r = 8$ and 12 mm increase as the mean velocity increases and then dissipate before the beginning of the next pulse.

The relatively slight degree of occlusion, i.e. 25%, did not produce any measurable flow disturbances in the steady flow experiments. However, when the pulsatile flow was utilized, the flow visualization showed an increase in the amount of flow reversal during the low velocity phase in the near distal region of both 25% occlusion geometries and the formation of flow disturbances near the tube wall. The disturbances near the wall which are formed, for the most part, in the low velocity decelerating portion of the pulse propagate toward the centerline as the

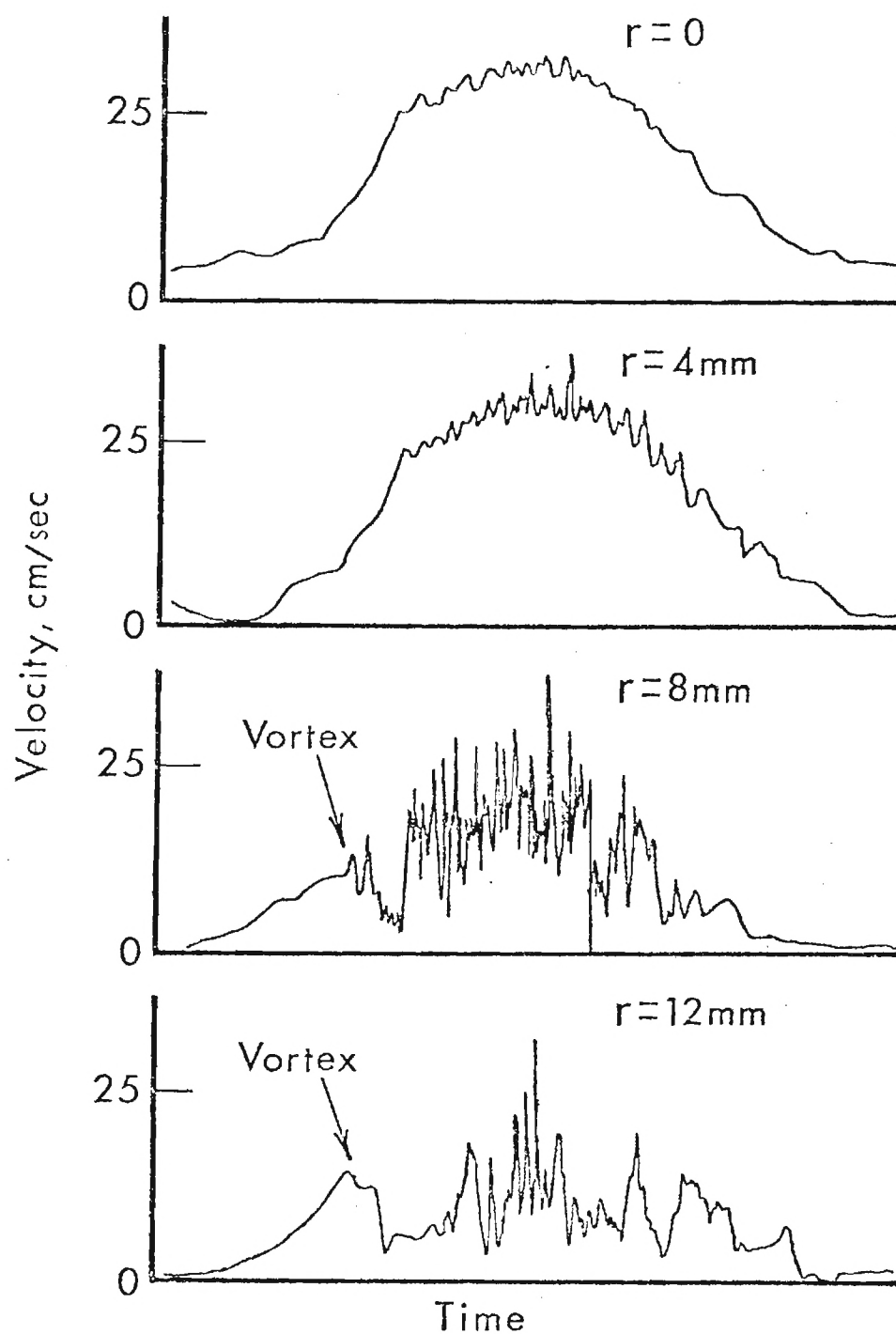


Figure 40. Radial variation of the velocity waveforms at $X/D = 1.125$ distal to the 50% sharp-edged stenosis with $\alpha = 15$, $Re_{DP} = 2540$.

mean velocity begins to increase in the following pulse. In Figure 41 the flow disturbance is seen at $X/D = 1.5$ as a velocity fluctuation at the minimum velocity point of the pulse. As the disturbances propagate toward the centerline and are carried downstream by the mean motion of the fluid, the velocity fluctuations appear during the acceleration phase of the following pulse at the $X/D = 6.125$ location.

3. Energy spectra

The occurrence of measurable flow disturbances distal to slight stenoses in pulsatile flow is further illustrated in Figure 42 which shows the energy spectra obtained distal to the sharp-edged occlusion. The intensity of the no stenosis spectra decreases rapidly with increasing frequency from the fundamental pulse rate of 0.2 Hz. The type of spectral curve indicates that the flow was essentially laminar in nature with very little energy in higher frequency fluctuations. The 25% occlusion produced a noticeable increase in the spectral energy at higher frequencies. As the degree of flow constriction is increased to 75%, the spectral energy distributed at the higher frequencies likewise increases. The more random spectral distribution which is characteristic of turbulence begins at an intensity considerably below the 0.2 Hz peak and no distinct harmonic peaks can be seen. Similar spectral trends were reported for the contoured occlusions by Cassanova⁵¹. These results are in contrast to the in vivo results (Giddens et al¹⁰) which indicated significant energy in the first few harmonics. This characteristic of the in vivo data is due to the complex velocity waveform present in the experimental animals.

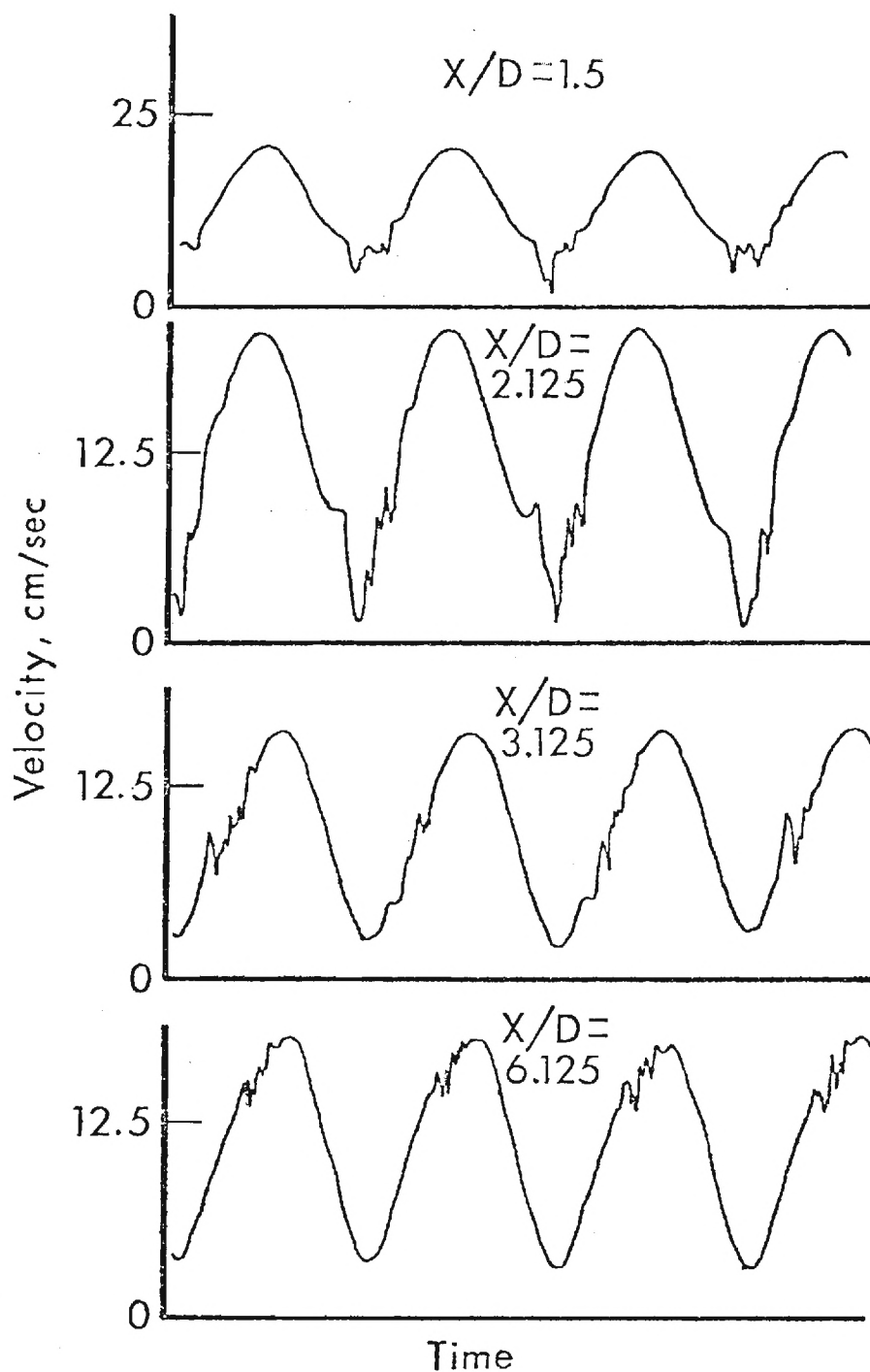


Figure 41. Axial variation of the centerline velocity waveforms distal to the 25% contoured stenosis show the development of flow disorder during the decelerating phase of the pulse.

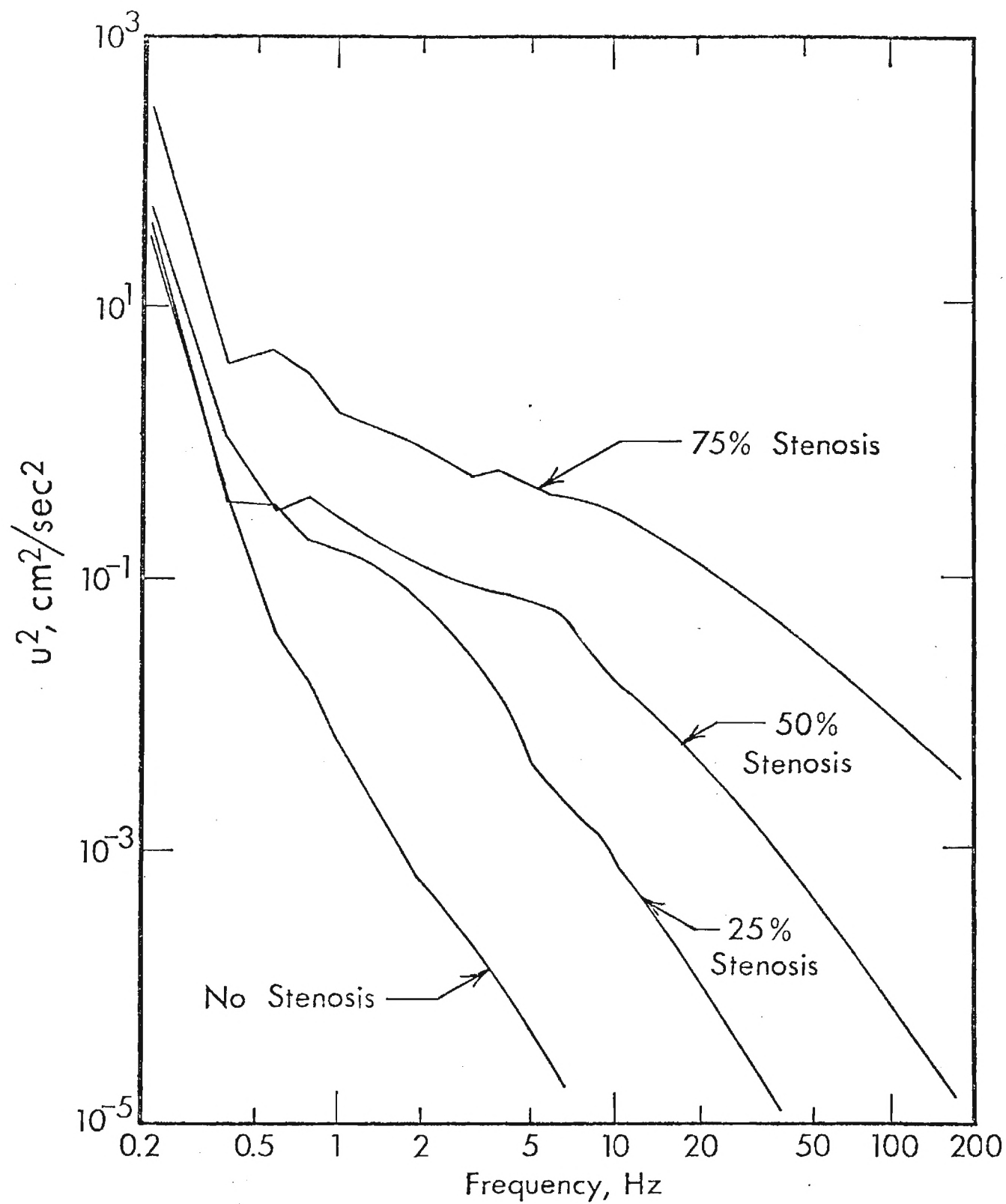


Figure 42. Centerline energy spectra at $X/D = 2.125$ distal to the sharp-edged stenoses in pulsatile flow.

Figures 43 and 44 show evidence of vortex shedding in the pulsatile flow through the sharp-edged occlusions. Similar data are available for the contoured occlusions (Cassanova⁵¹). The near-centerline spectra show peaks which indicate that discrete vortex shedding is occurring over a significant portion of the flow pulse. The frequency of the vortex shedding for the 75% occlusion corresponds to the steady flow frequency which was obtained at the same Reynolds number corresponding to the peak Reynolds number of the pulsatile flow. The spectra shown in Figure 44 which were measured with the 50% occlusion exhibit harmonics of the fundamental vortex shedding frequency.

Giddens et al¹⁰ measured the distal energy spectra in vivo and were able to show a correlation of energy spectra in a limited distal region by using a "semi-local" Strouhal number. These will be discussed in a subsequent section. Since the present pulsatile data were obtainable in simpler, more repeatable flow conditions than would normally be encountered in in vivo experiments, a correlation of the present data serves as a step in developing an understanding of a similarity concept of disordered cardiovascular flows with a minimum complicating factors, such as vessel wall elasticity and complex waveforms.

In the region within approximately one pulse length from the stenosis minimum area, the flow characteristics are dominated by the jet emerging from the constriction. A condition for similarity of the energy spectra is that the energy is distributed in a similar manner amongst the eddy sizes. The data show the energy to be "similarly distributed" by 2 or 3 diameters downstream from the constriction site in pulsatile flow. In general, this region is also the location of most intense turbulence.

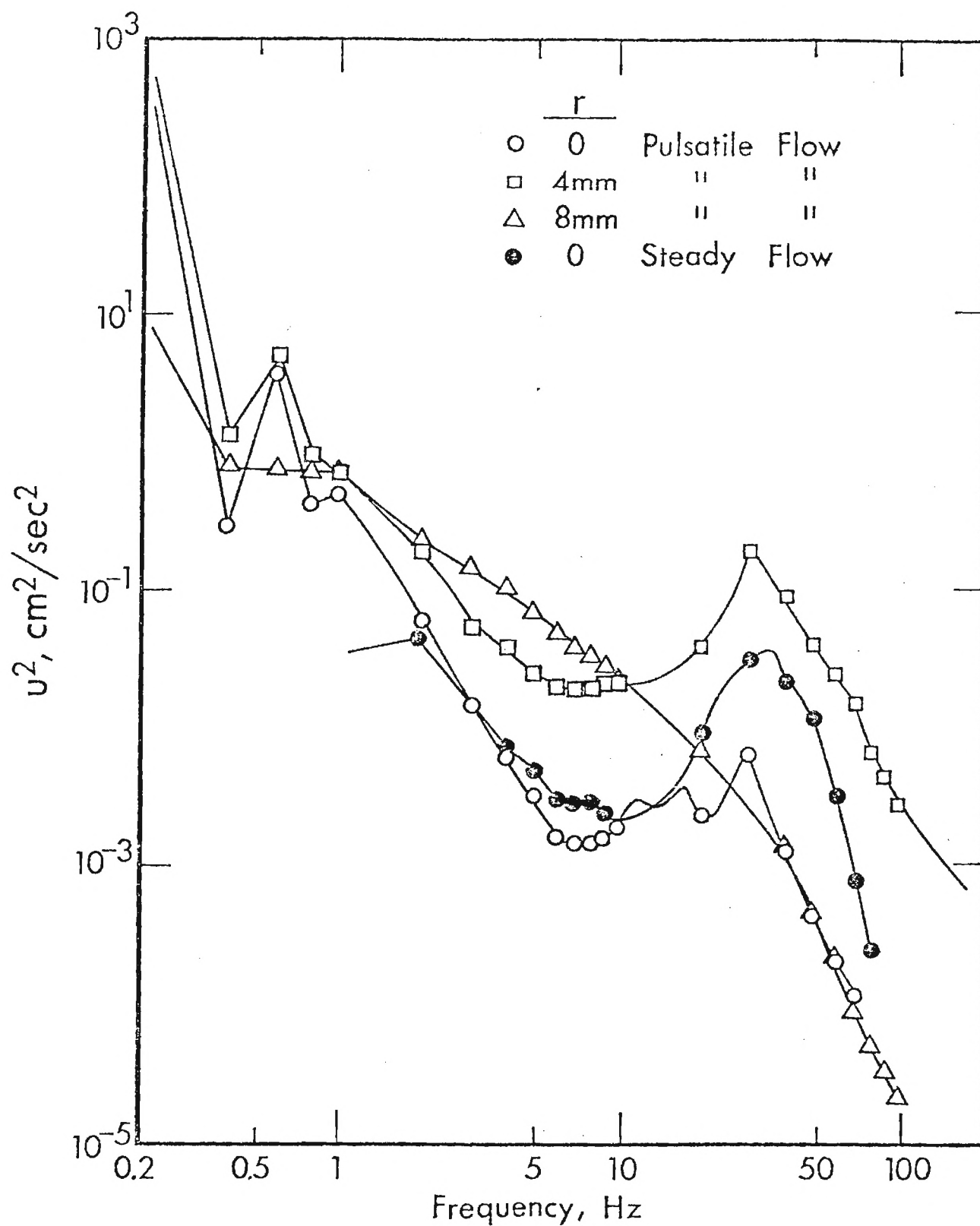


Figure 43. Energy spectra measured at $X/D = 0.5$ distal to the 75% sharp-edged stenosis showing a comparison with the vortex shedding spectra from steady flow data.

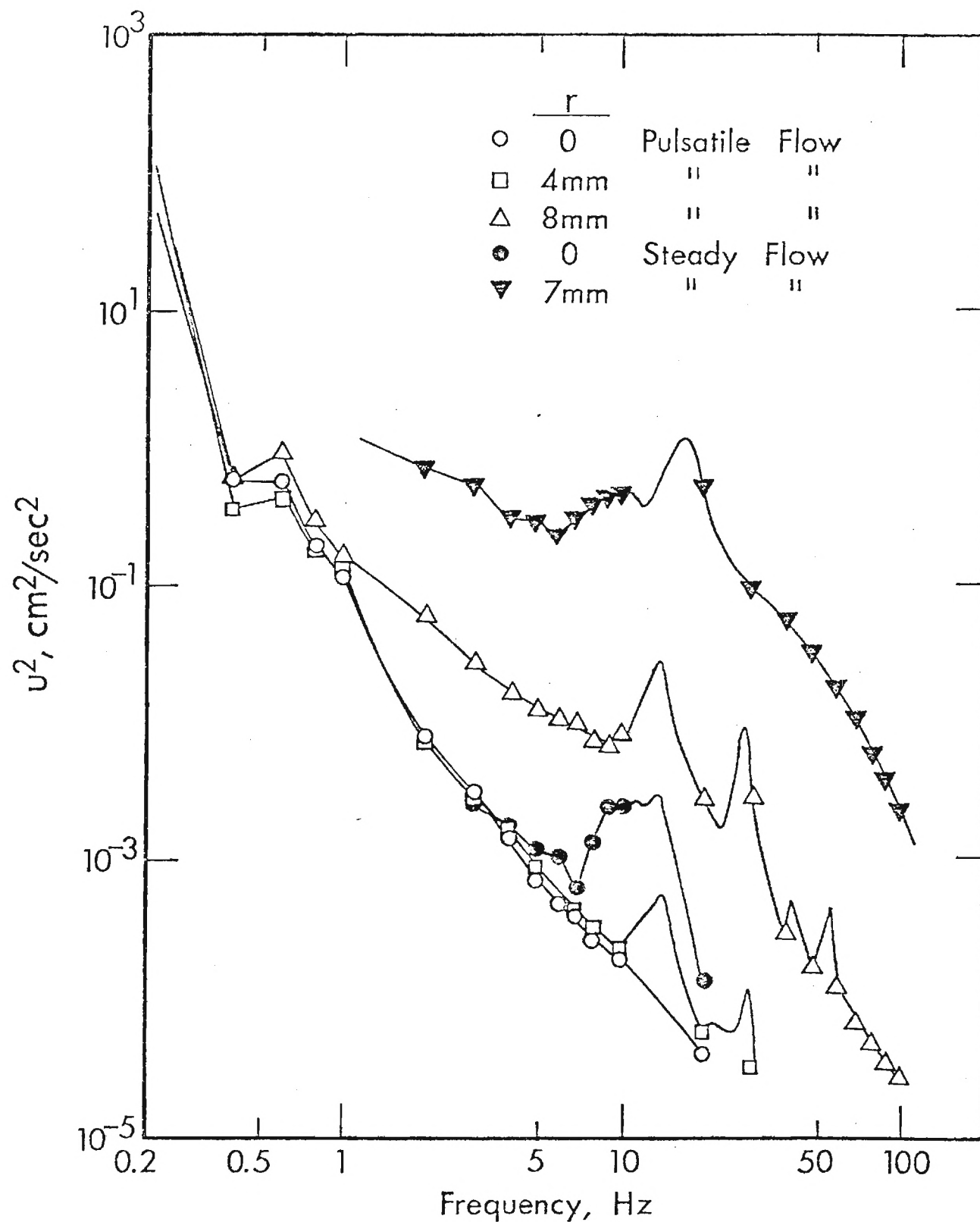


Figure 44. Energy spectra measured at $X/D = 0.5$ distal to the 50% sharp-edged stenosis showing a comparison with the vortex shedding from steady flow data.

In this region, the energy spectra obtained with different degrees of constriction correlate by using a Strouhal number fd/U_{op} and a non-dimensional energy, u^2/U_{op}^2 where U_{op} = peak velocity in the constriction minimum area. This correlation is shown in Figure 45 for the sinusoidal waveform. The unstenosed spectra would not be expected to correlate since the flow is essentially laminar. It was also found that the spectra produced by different degrees of occlusion would correlate even farther downstream if an effective jet diameter, D' , and a local mean peak velocity, U_{LP} , were used for nondimensionalization. D' is calculated by using the measured U_{LP} in a one dimensional continuity relationship:

$$D' = D \left(\frac{U_P}{U_{LP}} \right)^{1/2}$$

where U_P is the unstenosed peak centerline velocity. This nondimensionalization aids in accounting for the change in centerline velocity and turbulence intensity at locations where interactions with the tube wall become important. This "local" correlation is illustrated in Figure 46.

4. Discussion

The present study has illustrated the highly complex nature of poststenotic flow fields, even for the simplified in vitro models employed, in a transitional flow regime. Despite the complexity, however, certain definite trends have emerged which contribute to an understanding of flow through subtotal vascular stenoses.

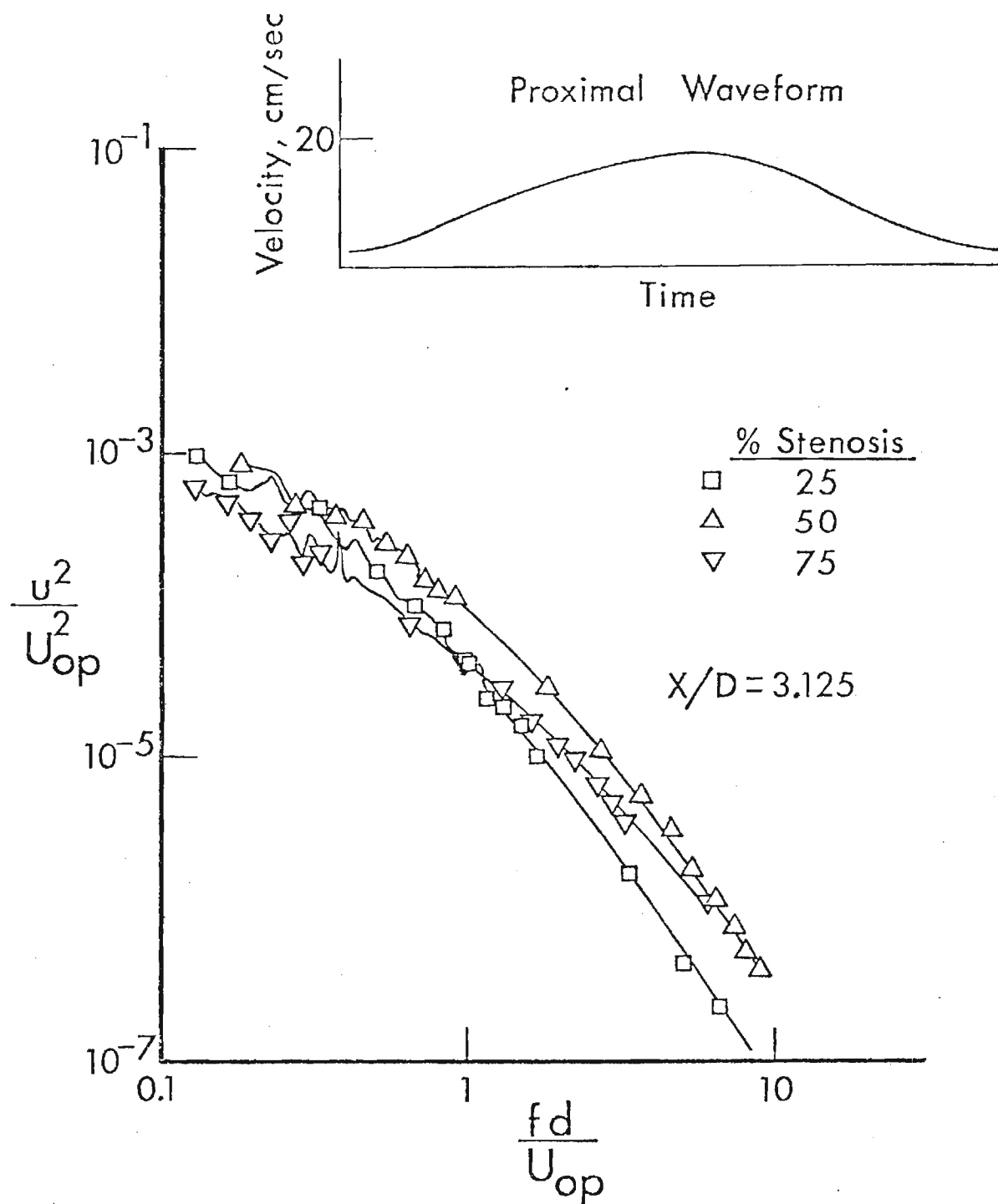


Figure 45. Correlation of the centerline energy spectra obtained with different sharp-edged stenoses by nondimensionalizing the energy and frequency with the stenosis conditions.

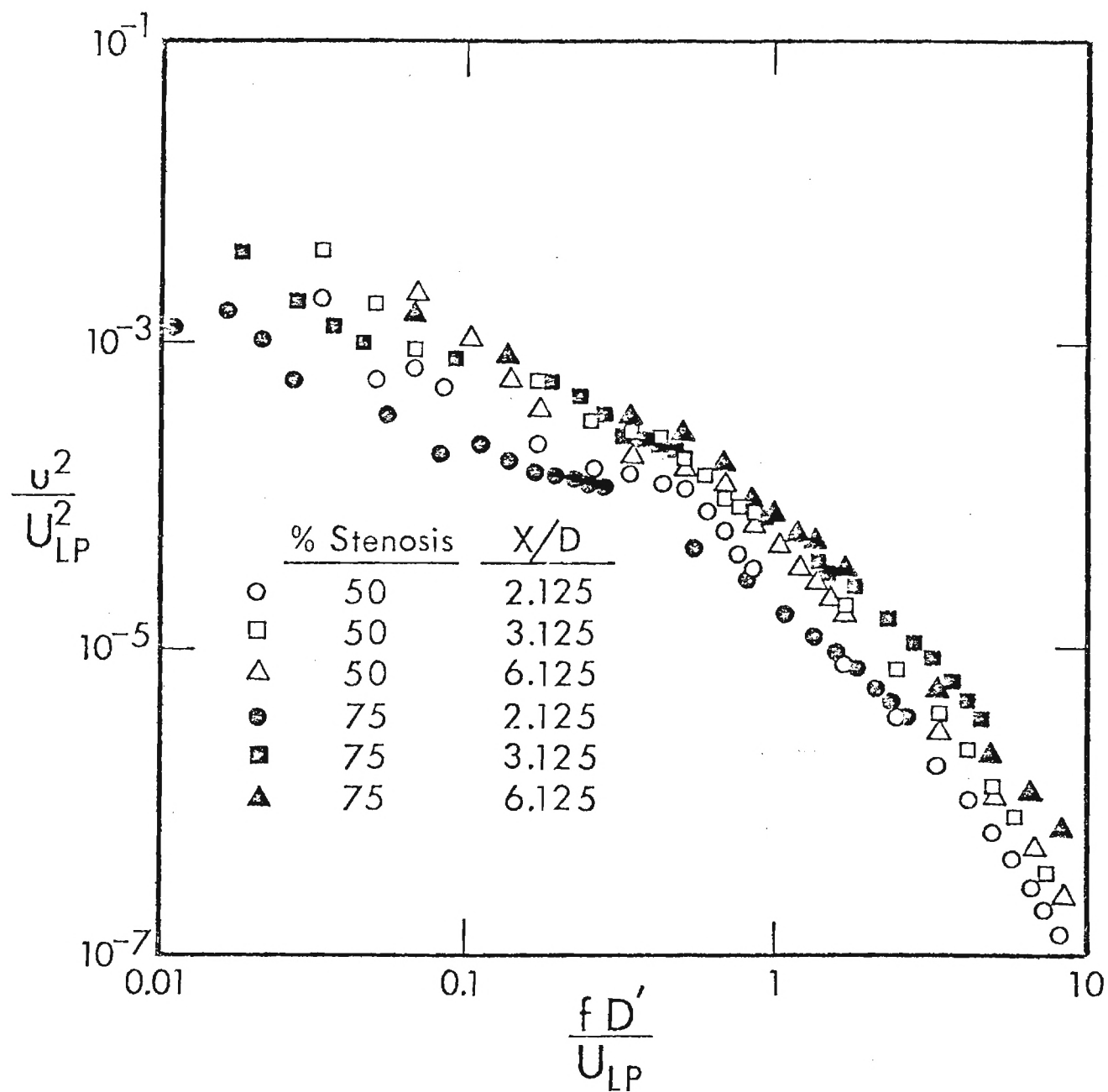


Figure 46. Correlation of the centerline energy by nondimensionalizing the energy and frequency with "local" conditions.

a. Stenosis geometry

The results of these experiments indicate that the more abrupt sharp-edged stenosis created a more intense flow disturbance at a given Reynolds number than the smoothly contoured stenosis. All data exhibited the trend that the greater the degree of blockage, the greater the disorder created in the distal field. This trend is in agreement with the results reported by Kim and Corcoran⁵⁸ who used stenoses with a rectangular cross-section, or multicornered stenosis geometry. Their results, however, did not indicate the presence of vortex shedding immediately distal to the stenosis. A multicornered configuration, as used by Kim and Corcoran, or irregularly shaped stenosis geometry, which may be encountered in pathological conditions, may tend to prevent the formation of an orderly structure in the flow disturbance, such as vortex shedding.

b. Distal wall interactions

In regions very near the plane of constriction of the severe stenosis (75%), the stenotic, or confined, jet behaves similarly to a free jet. Vortex shedding occurs at the same frequency and intensity for both cases and the disintegration of the large vortex eddies into a random distribution of smaller eddies occurs at about the same location. However, for milder stenoses where the wall is closer to the shear layer, the wall clearly modifies the development of flow instabilities. At low Reynolds numbers, the wall retards the development of vortex shedding; whereas, at high Reynolds numbers the wall reduces the amount of energy which is transferred to the vortex ring structure and increases the rate at which the energy is transferred into a random distribution of eddy sizes.

c. Steady versus pulsatile flow

For steady flow the visualization studies and measurements indicate that, if the stenosis is smoothly contoured, a degree of occlusion of about 50% is required to cause substantial flow disturbances at the Reynolds numbers studied. However, for a pulsatile flow, disturbances were created with mild 25% stenoses during the deceleration phase of a cycle. Thus, the effect of pulsatility was to destabilize the flow, and this was clearly evident in the energy spectra results.

d. Similarity parameters

Due to the extremely complex nature of the flow field any correlation of energy spectra will of necessity be valid only over a limited range of conditions and in limited regions of space. If the Reynolds numbers are relatively large, if the degree of occlusion is moderate to severe, if one avoids making measurements in zones of recirculation, and if one stays in the vicinity of reattachment, then the energy spectra are characteristically turbulent and can be correlated by similarity parameters. If these restrictions are not imposed, then correlation is virtually impossible in the transitional Reynolds number regime which was covered by the study.

e. Implications to stenotic disease

The present results illustrate certain trends which can realistically be expected to occur in the poststenotic field of a subtotal vascular stenosis. The experiments not only confirm previous in vivo observations that substantial flow disorder may occur for mild stenoses,

but they allow visualization of the instability mechanism active in pulsatile flow which creates the disorder. The limitations of employing spectral correlations to estimate the degree of stenosis have been outlined, and it would appear very unlikely that such correlations will be of value in estimating the size of localized atherosclerotic plaques at an early stage of development. On the other hand, the data suggest that detection of flow disorder could be a potentially useful indicator of the existence of mild stenoses provided, of course, that this detection could be achieved noninvasively. Further, the flow field studies give clues as to likely regions for searching out disorder in any diagnostic scheme.

C. Pulsatile Flow Studies - In Vivo

The work being reported here is derived from in vivo measurements of the velocity fields created by subtotal, externally placed vascular stenoses imposed upon the descending thoracic aortas of mongrel canines. The characterization of these fields in terms of velocity waveforms and their associated energy spectra should contribute to the description of hemodynamics in occlusive vascular disease and delineate possibilities for earlier and more quantitative diagnosis of localized vessel constrictions.

1. Methods

a. Instrumentation

Volume flow rate. The instantaneous volume flow rate was measured with a Carolina Medical Electronics electromagnetic flow meter. A cuff-type probe was situated several centimeters distal to the region where

the velocity is studied.

Velocity. The local instantaneous velocity was obtained using a DISA model 55D01 Anemometer and 55D10 Linearizer. Hot film probes mounted on the conical tip of a one mm hypodermic needle or a two mm diameter catheter are employed. These probes were manufactured by DISA Electronics. Since the calibration curves, and hence the linearization of the velocity versus voltage output, change with different fluids, it is necessary to calibrate each probe in the blood of the animal under investigation.

The right angle, hypodermic needle probe was stationed within the vessel in the following manner. It was aligned axially, facing proximally, by retracting against the vessel wall where it can be palpated. It was then rotated until judged to be parallel to the longitudinal axis of the aorta. This technique is satisfactory since a conical-tip probe is not sensitive to small errors in alignment, as has been verified repeatedly during in vitro experiments. The probe was positioned radially by traversing it across the vessel lumen using a micrometer. The velocity drops to zero when the probe presses into the vessel walls. These positions may be noted on the micrometer and the midline thus determined. This degree of control is not possible with the catheter probe, and measurements taken with this device are subject to errors in positioning, particularly in the radial direction.

It is important to designate the inherent limitations of hot film anemometry. One handicap is obviously that the presence of the sensor and its mounting structure may disturb the flow being measured. This is a difficulty in any experimental study. In the present work this problem is alleviated by using probes which are small in diameter (one mm to two

mm probe body) in comparison with the internal dimensions of the blood vessel (12 to 16 mm diameter). A second limitation of the hot film probe is its inability to sense direction of flow. Accordingly, the conical tipped instrument must be used in regions where the total velocity component of the flow is essentially aligned with the axis of the shank upon which the sensor is mounted. Furthermore, probes mounted on the tips of needles or catheters cannot accurately measure reverse flow.

Another difficulty in utilizing these probes in blood flow is the fact that the velocities to be measured range from zero to approximately 100 cm/sec. Precise linearization of the calibration curve over such a span is difficult. In the procedures employed in the present study the linearization was accurate to within ± 3 cm/sec. However, at low velocities this variation, although small, represents a substantial percentage error. This, coupled with the fact that reversal may occur in the aorta during parts of the cardiac cycle, means that inaccuracies may be present during the low velocity phase of the measured waveform. This point will be discussed further in the section describing the data analysis.

Finally, if the flow is essentially uni-directional and the probe is aligned properly, little error can be expected in describing the major velocity component. However, if fluctuating velocities occur in a turbulent flow, the signal detected by the hot film element is actually a composite of the fluctuating components which cannot be resolved with a single sensor.

Despite these limitations of hot film probes, they are extremely valuable in blood flow studies. During much of the cardiac cycle the flow in arteries is forward and, in the straight segments of these

vessels, is primarily axially oriented. The response of these probes up to frequencies reported here (1000 Hertz) is good under these conditions. We have compared measured energy spectra obtained for turbulent pipe flows in our laboratory with data from other investigators⁵⁹ and the spectral shapes are in good agreement. Furthermore, we have compared results obtained by these hot film probes with a laser velocimeter (DISA Model Mark II) measurement of energy spectra in a turbulent water flow. The curves agree out to a point where Doppler ambiguity occurs for the laser system (approximately 200 Hertz for the particular optical configuration employed). Thus, we believe that velocity and spectral data obtained with hot film probes provide valuable knowledge in blood flow studies.

ECG. As an aid in maintaining reasonably normal and constant status in the animal, the ECG was monitored and recorded on tape. This information also furnishes reference points in the cardiac cycle which are useful in describing events in the measurement of other parameters such as the velocity waveforms.

Viscosity. The blood viscosity is measured from samples drawn from the right femoral artery at selected times during the experiment. A Wells-Brookfield Microviscometer (cone-in-plate) is employed and the non-Newtonian apparent viscosity was determined at 37.5° C over a shear rate range from 11.5 to 230 sec⁻¹. A plot of apparent viscosity versus shear rate was extrapolated, if required, to give an estimate of the high shear rate asymptotic value of viscosity coefficient, η_{∞} , which is used in the calculation of Reynolds number.

b. Surgical Procedures

The laboratory animals used were mongrel canines, weighing from 18 to 25 kilograms. The subject was initially anesthetized using 10-20 cc of sodium surital (2.5%) intravenously via a forepaw superficial vein. This was followed immediately by 0.4 mgs of atropine sulphate (1 cc) and later, 150 mgs of sodium pentobarbital (usually 3 cc containing 50 mgs per cc). The animal was maintained in a satisfactory anesthetized state by administering 200 mgs of sodium pentobarbital per hour.

The descending aorta was exposed for a distance of approximately fifteen centimeters. An electromagnetic flow meter was placed about the vessel at the most distal accessible position, but above the diaphragm. The hot film probe was then inserted into the aorta and stationed in the mid-line.

Several precisely measured notched plastic strips were placed at predetermined locations about the aorta for the extra-vascular occlusions. These strips were then individually attached to a specially fabricated device for applying varying degrees of occlusion using a micrometer adjustment. This device gives a measurement of external occlusion diameter. The internal diameter is computed by increasing the constriction until flow is totally obstructed, noting the resultant external diameter, and then assuming that the vessel wall is deformed isovolumetrically at each occlusion stage. This method was checked for the zero occlusion case by comparing with the internal diameter ascertained from traversing the hot film probe across the lumen as described earlier. Such comparisons were consistently within one millimeter.

The strips employed as constricting bands were three millimeters in width. The resulting stenosis length is then in the range of four to seven millimeters as the occlusion passes from mild to severe.

At the conclusion of the experiment the animals were sacrificed with an injection of potassium chloride introduced through the jugular vein.

c. Data Reduction

The intra-aortic pressure, blood volume flow rate, anemometer signal, linearized output (velocity), ECG, and pressure indicator of the respiratory cycle are recorded on an Ampex Model 1300 fourteen channel FM tape recorder for subsequent analysis.

Mean volume flow rate. The recorded instantaneous volume flow rate signals are integrated to obtain mean values.

Velocity waveform analysis. There are several important methods of analysis for the velocity waveform. Two important examples are:

- (a) Time ensemble averaging of velocity waveforms
- (b) Determination of various energy spectra

Each of these is discussed briefly.

(a) Time ensemble averaging. This is accomplished by digitizing the velocity waveform results, always beginning the digitization at a specific point in the cardiac cycle, and forming a linear average over many heart beats which have the same duration. The onset of the QRS complex of the recorded ECG signal is used as a reference to insure correct triggering at the same point in each cycle. This activates a variable delay circuit which is set to give a one microsecond voltage pulse at any desired time subsequent to the ECG trigger. This pulse is used to

initiate the analog-to-digital conversion in the Hewlett-Packard Model 5451A Fourier Analyzer. Typically, 200 analog signals of one second duration are analyzed to form a time ensemble average, each signal being represented by 512 digital points. For the heart rates of the animals under study, each complete velocity waveform is represented by over 200 discrete points. Using the velocity waveform itself as the triggering signal rather than the ECG is not sufficiently accurate due to variations in velocity waveform from cycle to cycle, particularly once turbulence develops in a poststenotic flow.

(b) Energy spectra. The energy spectrum of a velocity signal is a measure of the kinetic energy (square of the velocity) contained within a frequency bandwidth, Δf . A steady, laminar flow would have energy contained only at zero frequency, whereas the presence of turbulence would distribute energy into higher frequencies. There are several approaches to studying the energy spectra, each offering certain information which complements that obtained with the others.

(i) Analysis of total waveforms. In this method the entire velocity waveform is analyzed. For the data reported here the frequency bandwidth is one Hertz; and fifty samples, each comprised of 1024 digitized data points, of the velocity signal were employed. The time duration for each analog sample obtained from the tape was one second. The maximum frequency shown in the figures to be presented is 512 Hertz. Higher frequencies in the signal being analyzed were filtered out to prevent aliasing.

(ii) Analysis of segments of waveforms. Energy spectra may be obtained for specific segments of the velocity waveform by using the ECG triggering method described above and by sampling data for a desired time

interval. As the sampling time is decreased, the resolution of the frequency bandwidth becomes wider since the bandwidth Δf is inversely proportional to the sampling time T . For the time-resolved data reported here the sampling time is 0.1 sec and Δf is 10 Hertz. The maximum frequency studied was 1280, and 50 samples were taken to form the energy spectra.

(iii) Analysis of velocity disturbance. It is possible to obtain a disturbance velocity $u'(t)$ by subtracting the ensemble average from a given velocity waveform. This process may also be accomplished for segments of the cycle.

(iv) Analysis of time ensemble average. Another method of examining the energy spectra is to perform a frequency analysis of the time ensemble average itself. This type of analysis may prove useful in searching for vortex shedding frequencies.

The spectral analyses which were completed under the NSF grant covered by this report were concentrated on methods (i) and (ii). Since award of the follow-on grant ENG 76-23876, considerable attention has been given to the analysis of disturbance velocities and to the problem of nonstationarity of these disturbances. Work is continuing in this direction and results will be reported in the Final Report for the follow-on study.

For the present report we present results obtained by analyzing the energy spectra of the total velocity $u(t)$, rather than the disturbance velocity $u'(t)$; and we consider the development of these spectra with time in the cardiac cycle.

2. Results

A series of animal experiments has been performed in which velocity waveforms were recorded at various locations distal to partial occlusions in the descending thoracic aorta. The important similarity parameters for a confined pulsatile flow are the frequency parameter, $\alpha = R\sqrt{\omega/\nu}$ (R - radius, ω - fundamental heart frequency in radians/sec, and ν - kinematic viscosity), and the Reynolds number, $Re = 2UR/\nu$ (U - velocity). The ranges spanned by these experiments are $9 < \alpha < 16$ and $1800 < Re < 2300$, where the Reynolds number is based on peak velocity as measured by the hot film probe. Table 3 presents a summary of the various parameters for Experiment 102974 in which a hypodermic needle hot film probe was employed. Table 4 shows similar data for Experiment 52075 which utilized a catheter-mounted hot film probe. Since the focus of the research was on disorder occurring in poststenotic flows and since substantial disorder was encountered for many stenotic conditions, no attempt was made to alter flow conditions by the use of drugs which affect cardiac output and heart rate. Subsequent studies at other Reynolds numbers would certainly be appropriate.

In the data presentation, it was decided to give representative results from the series of experiments. All experiments produced the same trends, supporting the postulate that the reported observations are not artifacts.

The occurrence of disturbances in the velocity waveforms recorded distally to the imposed stenoses was readily apparent. This is illustrated by the curves in Fig. 47 which were taken from experiment 102974. For these data the hot film probe was located 2 cm distal to the con-

TABLE 3. . Data for Experiment 102974

Percent Occlusion (Reduction in Area)	Constriction Diameter (cm)	Peak Local Velocity ($U_p \sim \text{cm/sec}$)	Mean Volume Flow Rate ($Q \sim \text{ml/sec}$)	Peak Reynolds Number ($\text{Rey}_p = \rho U_p D / \eta_\infty$)	Mean Reynolds Number ($\text{Rey}_m = 4 \rho Q / (\pi \eta_\infty D)$)
0	1.3	42	27	1870	960
20	1.1	41	-	1825	-
40	1.0	40	26	1780	910
57	.8	49	28	2180	1010
73	.7	48	28	2140	1010
87	.5	48	28	2140	1010

Frequency Parameter: $\alpha = 13.7$ ($\omega = 15 \text{ rad/sec}$, $\eta_\infty = .03 \text{ poise}$)

Hot film probe location: 5 cm distal to minimum area of constriction

TABLE 4. Data for Experiment 52075

Percent Occlusion	Constriction Diameter (cm)	Peak Local		Peak Local		Peak Local	
		Velocity	Peak Reynolds	Velocity	Peak Reynolds	Velocity	Peak Reynolds
		Probe Pos. 1 (cm/sec)	Number	Probe Pos. 2 (cm/sec)	Number	Probe Pos. 3 (cm/sec)	Number
0	1.6	48	2500	52	2800	50	2700
25	1.4	72	3800	46	2400	45	2400
36	1.3	69	3700	45	2400	47	2500
50	1.2	85	4500	49	2600	56	3000
69	.9	65	3500	60	3200	48	2500
77	.8	45	2400	60	3200	47	2500
83	.7	47	2500	70	3700	52	2800

Frequency Parameter: $\alpha = 15.8$ ($\omega = 11.7$ rad/sec, $\eta_{\infty} = 0.032$ poise)

Probe position 1: 3 cm distal to stenosis

Probe position 2: 5 cm distal to stenosis

Probe position 3: 7 cm distal to stenosis

striction. Figure 47a shows the measured velocity at the centerline of the unoccluded aorta. The shape of the waveform is typical of those found in the descending thoracic aorta in numerous experiments inasmuch as the curves are relatively smooth, well-defined, and repeatable, although occasional irregularities can be observed near the maximum velocity, during the deceleration phase of systole, and during diastole in some cases. Due to problems in measuring reverse flow discussed earlier, the irregularities observed near zero velocity in the waveforms of Figure 47a could be attributable to artifacts produced by the physical presence of the probe even though the electromagnetic flowmeter indicated that the mean flow was always forward. This point will again be considered in the discussion of the energy spectra.

Figure 47b illustrates the velocity waveform for a relatively slight degree of occlusion (20 percent). Although the flow could scarcely be described as turbulent, comparison with curve (a) of that figure clearly indicates the appearance of higher frequency disturbances near the maximum velocity and during the deceleration phase. This is also evident in the energy spectra, as will be seen subsequently. This result was found to be typical of all the experiments, provided the measurement was taken near the constriction; that is, when the degree of occlusion approached 20 percent, notable disturbances in the high velocity region of the waveform were detected, particularly during deceleration.

As the degree of stenosis is increased, the flow becomes more obviously disturbed as illustrated in Figures 47c-f. For a 40 percent reduction in area the flow is markedly disordered during deceleration although the basic pulsatile nature is clearly evident. However, for

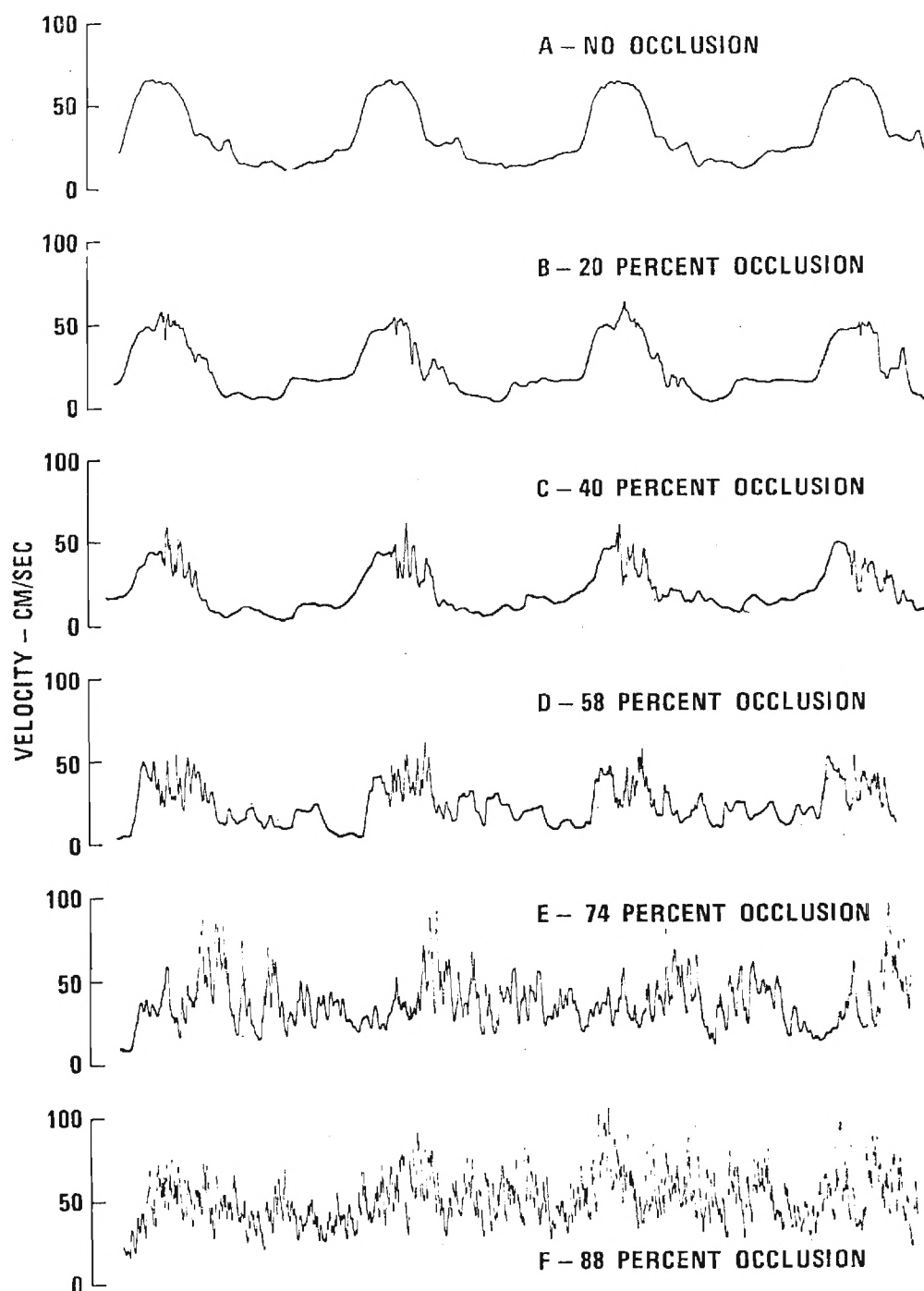


Figure 47. Velocity recorded at centerline of canine aorta for experiment 102974. The hot film sensor was located 2 centimeters distal to the minimum area of constriction.

severe degrees of occlusion the pulsating aspect diminishes so that the distal flow resembles a quasi-steady, turbulent jet.

a. Time ensemble average waveforms

The velocity measurements of experiment 102974 were used to form time varying mean velocity waveforms using methods previously described. These results are given in Figure 48 for 40 and 58 percent stenoses and may be compared with the corresponding individual waveform results of Figure 47. The average waveforms possess a very striking feature. Although the individual waveforms contain disturbances which appear random, their averages exhibit distinct double or multiple-peak patterns. This feature appeared in all other experiments, also. The similarity of these to waveforms we have observed in vitro using flow visualization are suggestive of vortex shedding. Additional evidence for this interpretation is the fact that the multiple-peaked patterns do not appear at all axial stations, but rather disappear, as would occur upon vortex breakup, as the anemometer probe is moved downstream. However, interactions of the flow with the distensible vessel cannot be discounted. These may take the form of resonance of the wall⁶⁰ or of wave reflections associated with the changing cross-sectional area presented by the stenoses. Therefore, until further analysis of the waveforms, their energy spectra, and comparisons with in vitro studies have been completed, we present these as an observed -- and potentially descriptive -- but unexplained, phenomenon.

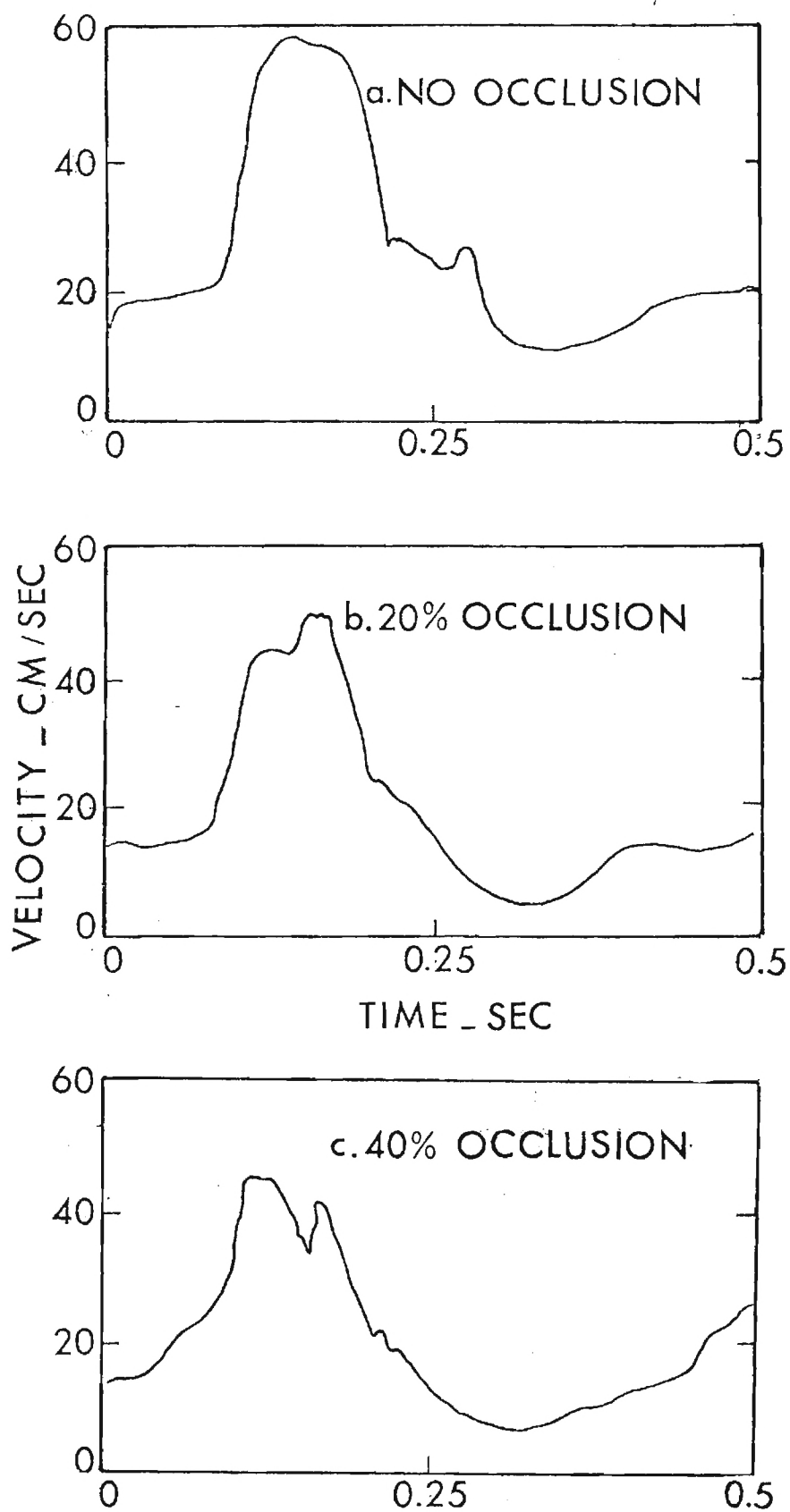


Figure 48. Time Varying Ensemble Average Waveforms for the Data of Figure 47.

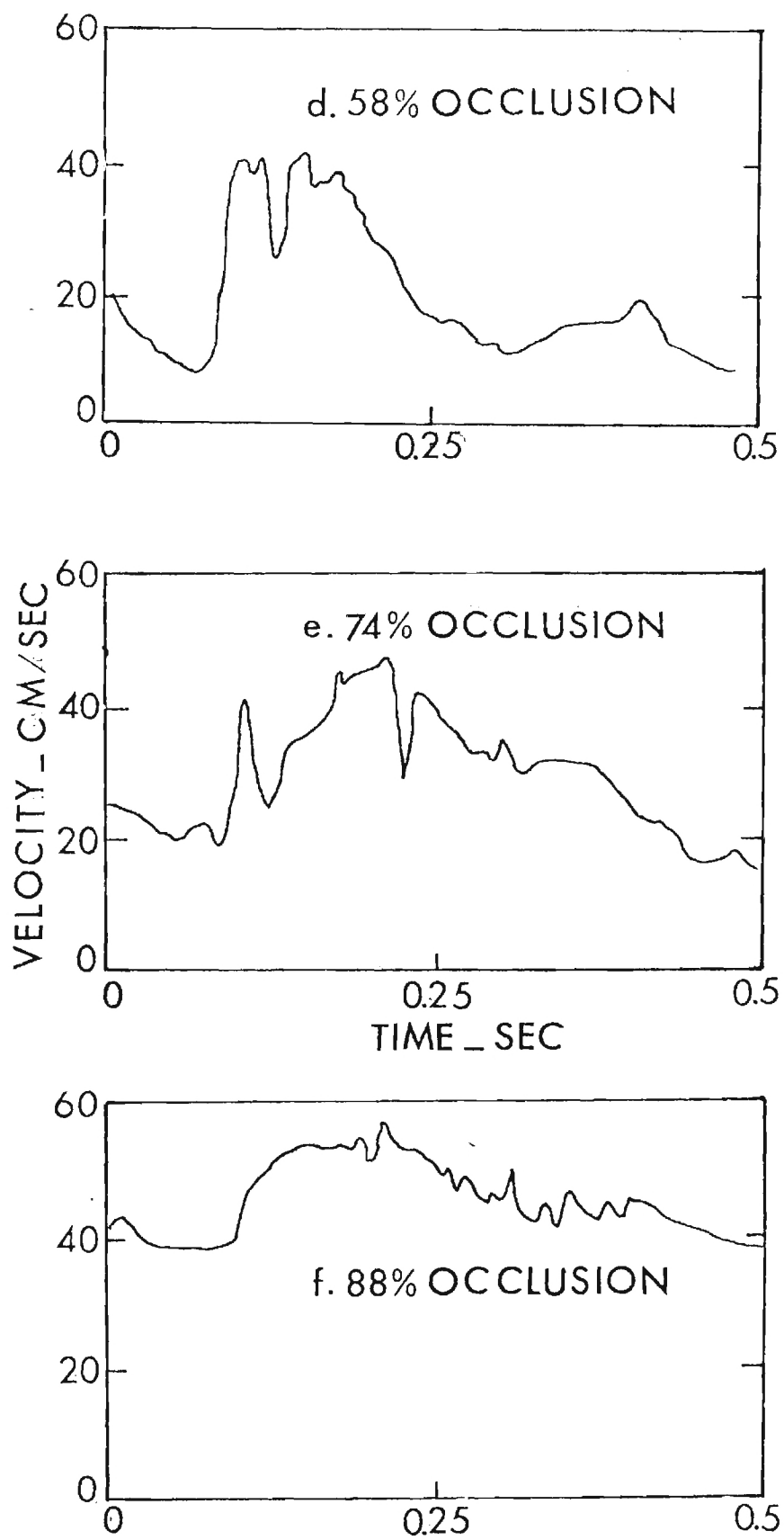


Figure 48 (continued)

b. Energy spectra

In the present study we have performed spectral analysis of the entire velocity waveform for several reasons. First, it is this entity which affects interaction of flow with the vessel wall. Second, the analysis of the total waveform yields information on harmonics of the fundamental heart-rate frequency which could be potentially interesting. Furthermore, since frequency bandwidth varies inversely with the sampling time, resolution of the data is sacrificed by resorting to shorter time intervals. Finally, once the stenosis is almost complete, the pulsatile nature of the flow is greatly subdued so that the spectra tend to become independent of the position in the cardiac cycle. We shall return to this point shortly.

Examples of energy spectra are illustrated in Figure 49. These correspond directly to the velocity waveforms shown in Figures 47a-f. The plots are in log-log coordinates with the ordinate being $10 \log (u^2/U_{\text{ref}}^2)$ where u^2 is the square of the instantaneous velocity and U_{ref} is a reference velocity which arbitrarily was taken to be 100cm/sec for the data here. This represents the energy contained within a frequency bandwidth Δf , which is one Hertz for the data presented. The abscissa is the frequency coordinate. If a periodic wave is predominantly (but not exclusively) at one fundamental frequency, then the energy spectrum would have a maximum peak at this fundamental and less prominent peaks at the various harmonics. The height of the spectral curve would decay rather rapidly with increasing frequency. Such appears to be the situation for the velocity waveform (Figure 47a) and the corresponding

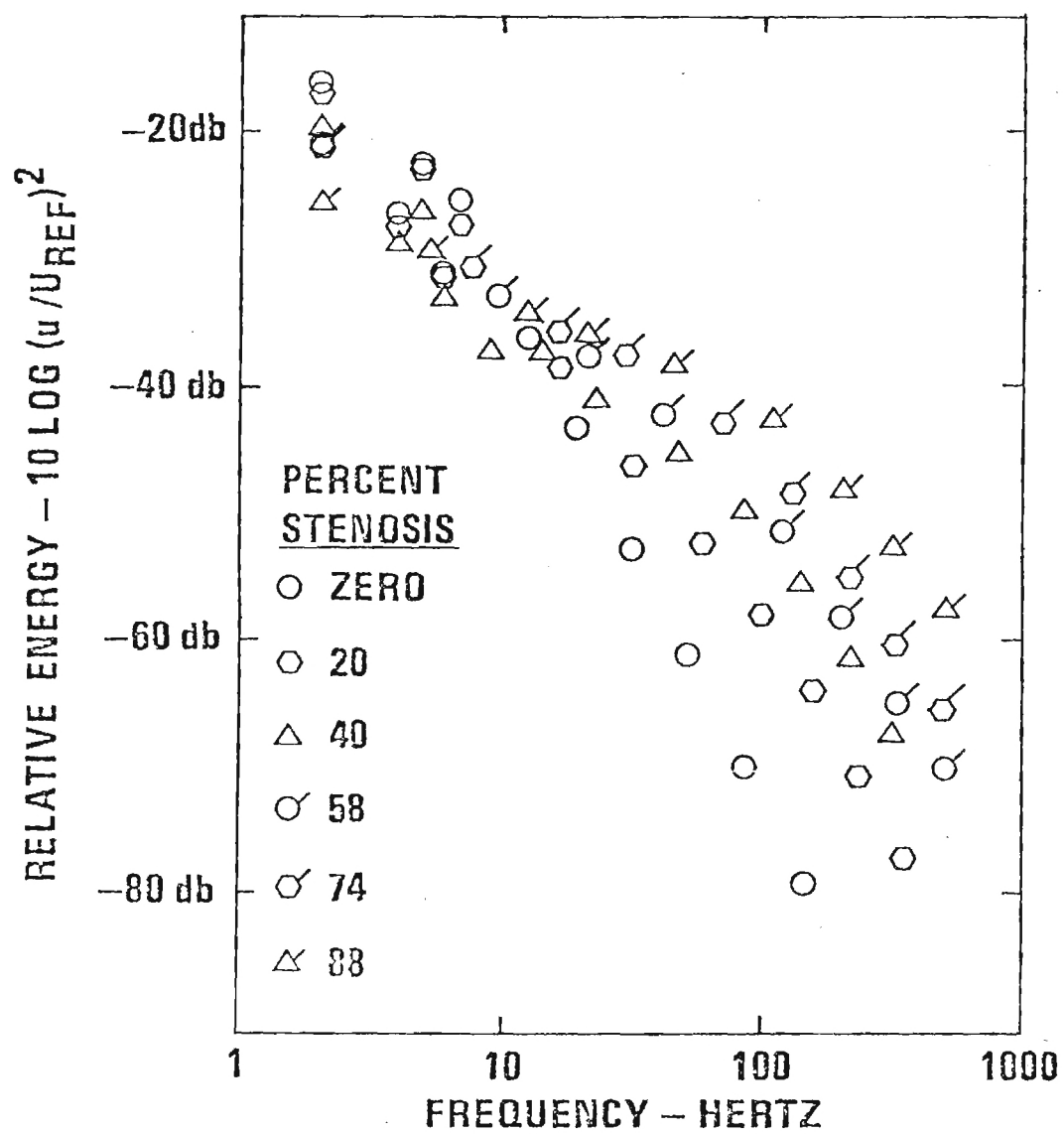


Figure 49. Energy spectra for the velocity waveforms shown in Figure 47

energy spectrum (Figure 49) for the case of no occlusion in the aorta. It would be presumptuous to state that this flow is totally "laminar" since a close inspection of the waveform trace indicates some irregular behavior in each cycle which is not strictly repeatable for every heart-beat. However, the velocity for this particular case is "predominantly" laminar; and the associated energy spectrum is composed primarily of frequencies which should be attributed to the decomposition of a curve which is almost periodic, rather than to turbulent velocity fluctuations.

Several characteristics of the spectra are apparent. The maximum energy is contained at the frequency corresponding to the fundamental heart rate. Thus, the highest peak in each of the spectral plots occurs at 2 Hertz, which is the discrete frequency in the digitized spectra that is nearest the heart rate. Further peaks in the spectra occur near harmonics of this value.

If the data for no occlusion are compared with the remaining curves in Figure 49, it may be seen that as the degree of occlusion is increased, the energy content in the higher frequencies is elevated. For severe stenoses the sharp, low frequency peaks which are characteristic of pulsatile flow are virtually absent, indicating that the flow immediately distal to the constriction approaches a quasi-steady, turbulent state.

We now consider the problem of uncertainty of the hot film anemometer results near zero velocity which was mentioned earlier. As was pointed out, one cannot be sure that the low velocity segment of the waveform which occurs during diastole is accurately representative of the actual velocity since the probe cannot distinguish reverse flow. Using the ECG trigger previously described we can eliminate this uncertain segment from

consideration and have performed spectral analysis over that part of the waveform beginning with the onset of systole and terminating when the velocity fell, following the systolic peak, to a value below approximately 10 cm/sec in the unoccluded case. This time interval was then maintained for analysis of the cases with occlusion present. When this procedure was applied, it was found that for zero occlusion there is a small contribution of the low velocity region over a wide frequency range. For the forty percent occlusion, on the other hand, the spectra are scarcely distinguishable from each other. This holds true for all higher degrees of occlusion.

The energy spectra indicate that the degree of disorder in the flow decays as one proceeds distally. Figure 50 illustrates this for one of the experiments, 52075, for 50 percent stenosis. The spectrum for no occlusion is shown for reference. From the fluid dynamics viewpoint the decay is rather rapid. This is likely caused by a combination of mechanisms, among them viscous dissipation of eddies, convection of the disturbance from confinement in a jet-like core to the entire vessel lumen, and absorption of energy by the aortic wall. Further experiments to make measurements at additional radial stations of varying distance from the centerline and at several axial locations will be helpful in determining which effect is dominant.

As discussed earlier the consideration of a time history of the energy spectra is of great interest. If one examines the velocity waveforms for cases of zero to moderate stenoses, it is seen that the acceleration phase of systole has virtually no observable high frequency content while that portion of the curves corresponding to peak velocity and the

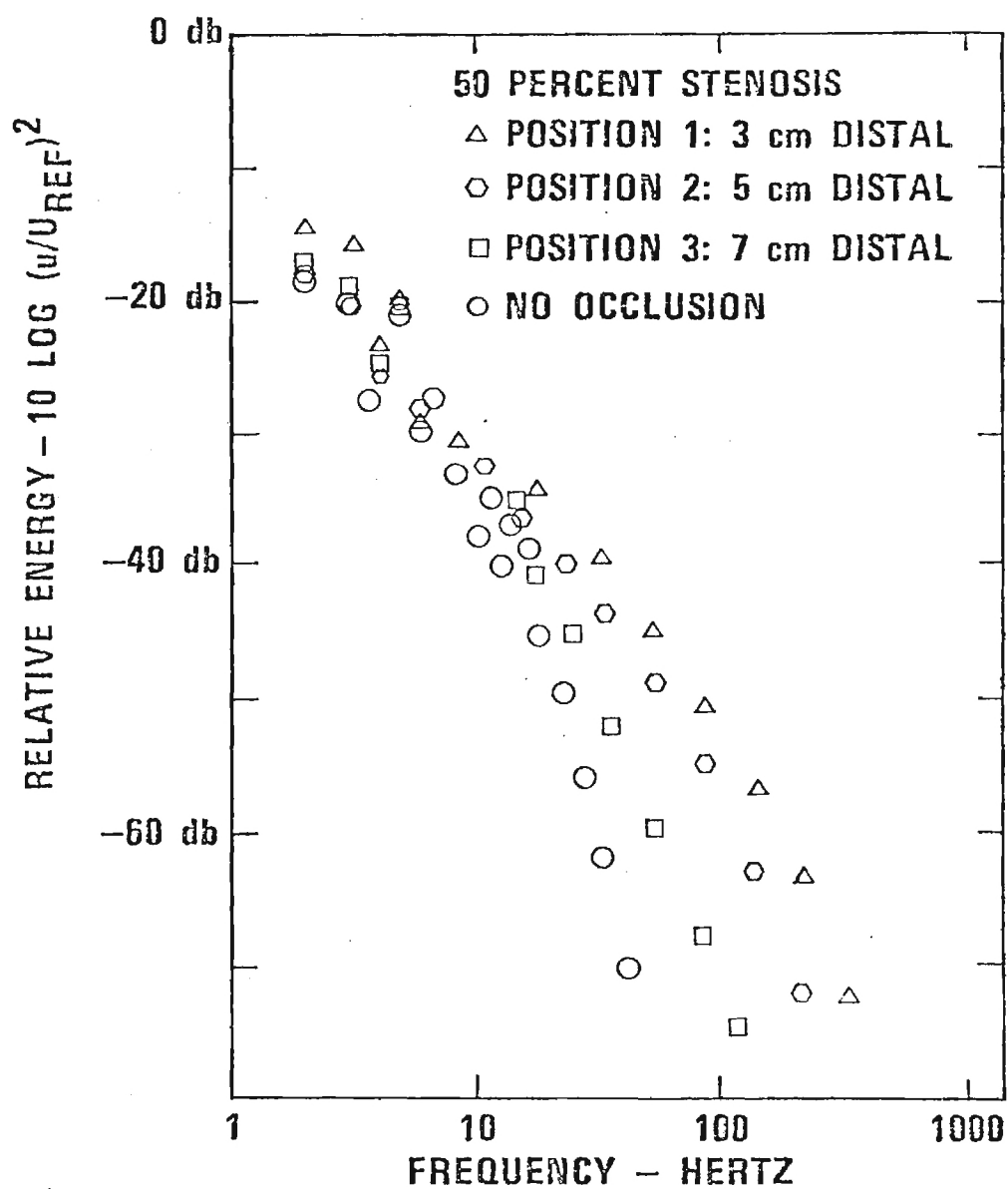


Figure 50. Axial decay of flow disorder, Experiment 52075

deceleration phase has higher frequency disturbances present. This is to be expected since an accelerating flow is inherently more stable than a decelerating one. Thus, we have selected for display here examples of energy spectra from these two phases of the flow. The specific segments examined are shown in Figure 51 for the no occlusion waveform. The acceleration phase is taken to begin prior to the onset of systole, and data are analyzed for 0.1 second. The end of this period occurs slightly prior to the peak velocity. The deceleration phase is taken to begin at the termination of the acceleration phase, and data are analyzed for 0.1 second. The same time intervals using the ECG trigger are maintained for each degree of occlusion. Because of the shortened time for analysis, the frequency bandwidth resolution is ten Hertz. Figure 52 gives the computed energy spectra for several degrees of occlusion for experiment 102975. For the case of no occlusion, differences in the spectra for acceleration and deceleration are not large. The corresponding spectra for 20 percent stenosis are also shown. The disorder during the deceleration phase is dramatically greater than that during acceleration. As the degree of occlusion increases and disturbances begin to occur throughout the waveform, the differences between acceleration and deceleration spectra become less. This is illustrated by the two remaining curves, for 88 percent occlusion, in Figure 52. It can be seen that the degree of disorder is very similar for both phases. This is, of course, entirely consistent with the results one would anticipate by examining the velocity waveforms themselves. Instabilities begin first in the immediate neighborhood of peak systolic velocity, usually just after the peak occurs. As the degree of stenosis increases, these

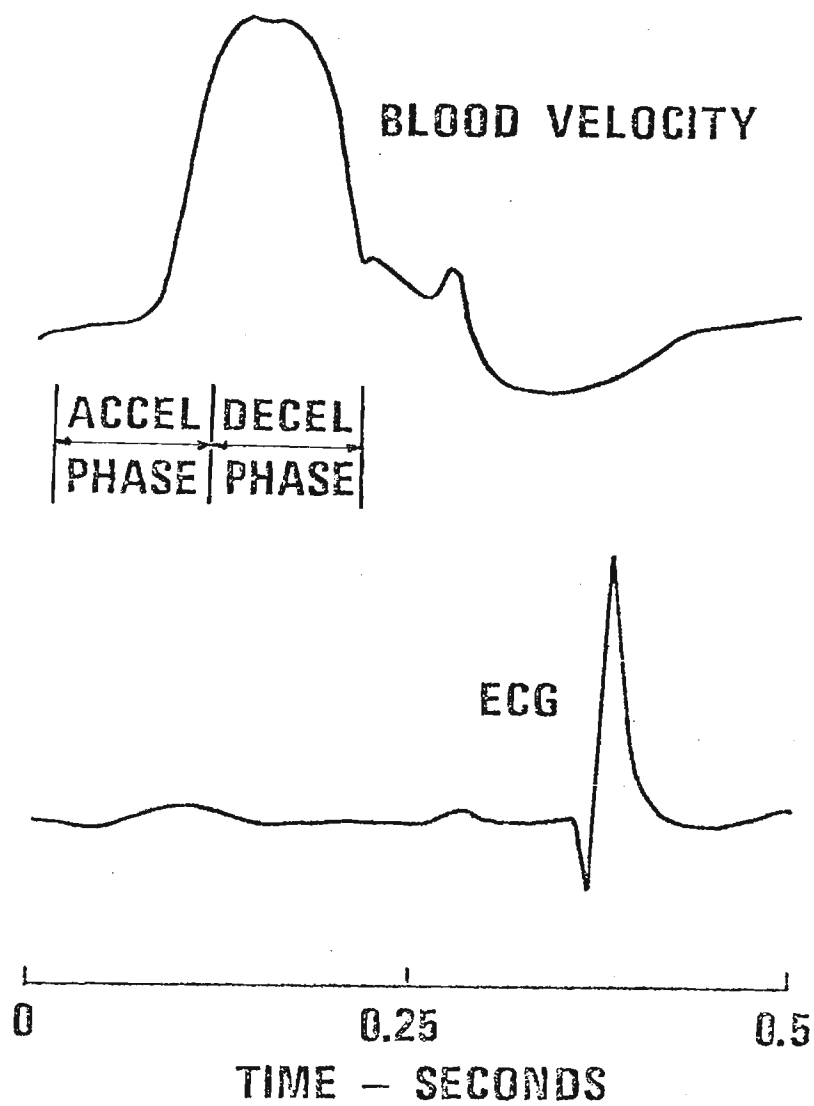


Figure 51. Segments of waveform selected for comparison of acceleration and deceleration phases of systole.

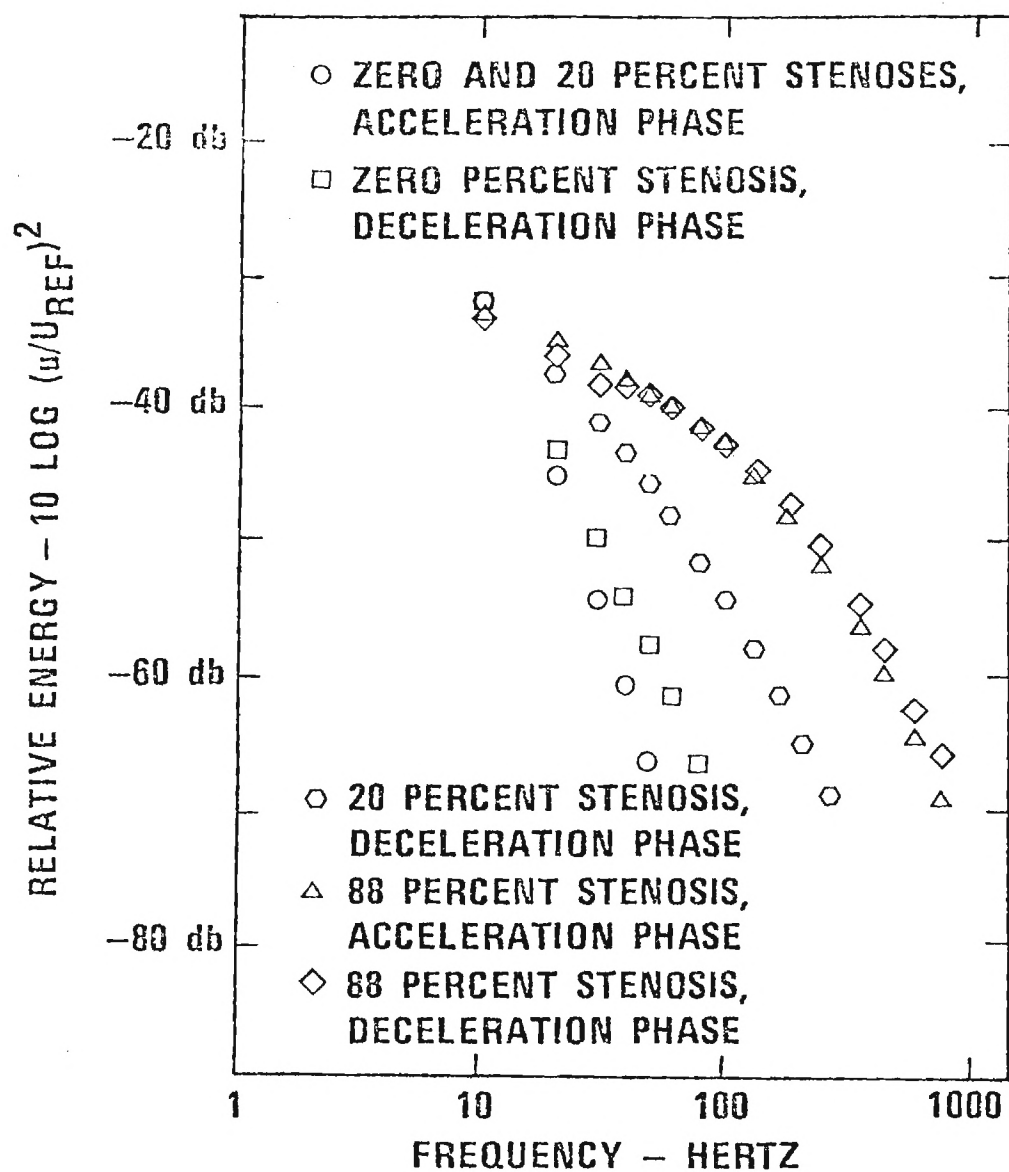


Figure 52. Spectra for acceleration and deceleration phases of systole. Data derived from Experiment 102974, Figure 47.

disturbances extend over a greater portion of the deceleration phase until, finally, virtually the entire waveform is turbulent and quasi-steady.

We have examined the possibility of expressing the energy spectra in terms of similarity parameters. In general, one would not expect to correlate spectral curves for zero occlusion with those for severe stenoses since the former typically possess little or no disorder while the latter are intensely turbulent. However, once the degree of vessel constriction is sufficient to create substantial flow disturbances, the existence of similarity in the energy spectra might prove useful. A frequency similarity parameter often employed in flow experiments is the Strouhal number, S (frequency \times characteristic length/characteristic velocity). Several different combinations for reference length and velocity were employed in an attempt to correlate the energy spectra by a Strouhal number. Although at present we view this problem as incompletely resolved, there does appear to be definite, but limited, region distal to the stenosis for which the spectral data are reasonably correlated by introducing a semi-local Strouhal number, fd/U_ℓ , where d is the constriction diameter and U_ℓ is the peak value of the velocity measured by the hot film probe at this distal location. This is illustrated by Figure 53 which shows the similarity plots of data taken from experiment 11474 in which the right angle probe was stationed 4 cm distal to the stenosis state. The energy axis has been nondimensionalized by U_ℓ^2 in these curves. The spectrum for zero occlusion is distinctly separated from the occlusion measurements, as would be expected. The remaining spectral curves all lie quite closely together, indicating good similarity.

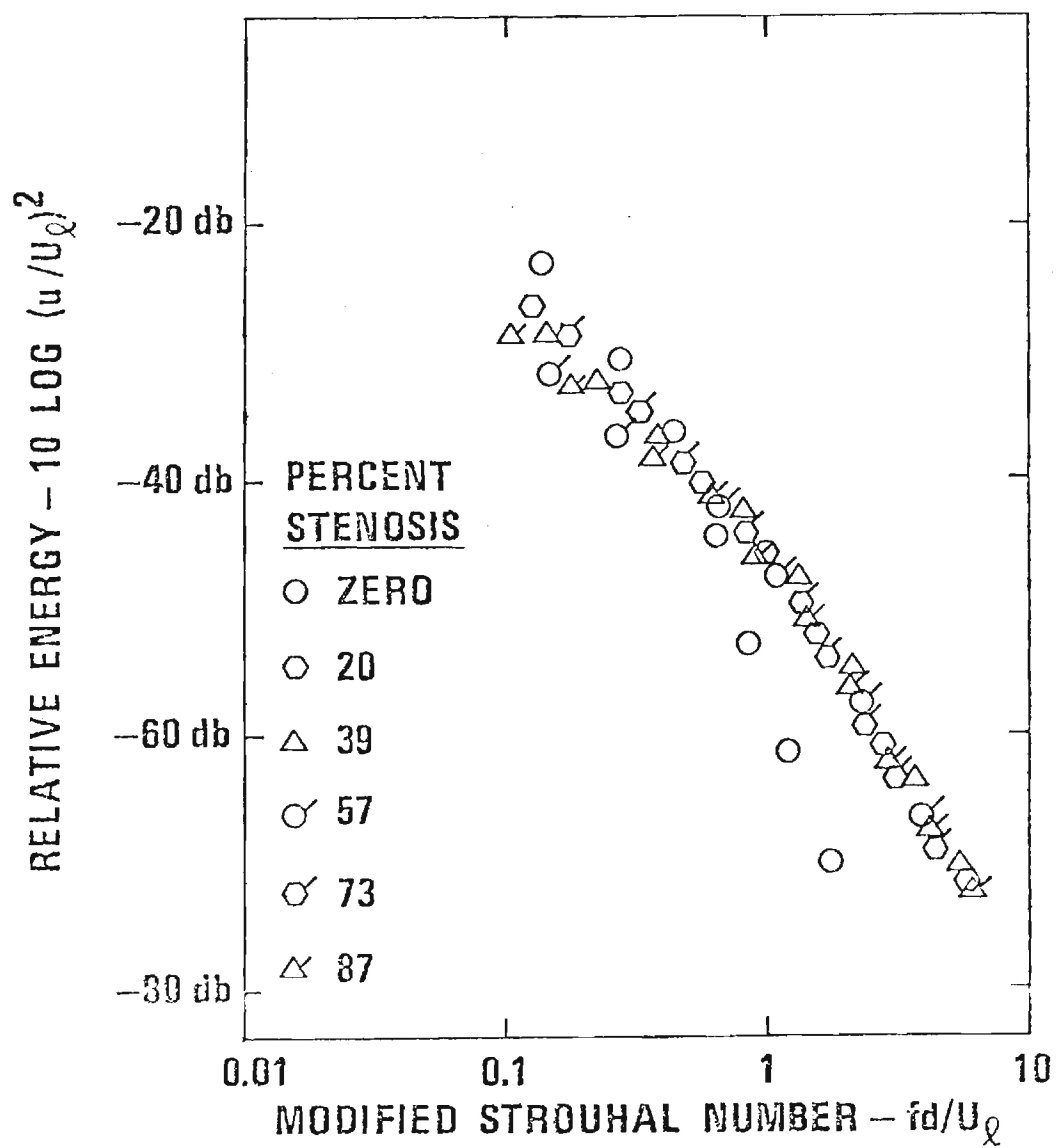


Figure 53. Energy spectra using similarity coordinates.
Data are from Experiment 11474.

This result was found in other experiments, also. It is emphasized, however, that the suggested parameters appear valid only within a limited distal region whose boundaries are as yet ill-defined. If the measurement site is quite close to the constriction, the spectral curves do not show good correlation, possibly because the large scale eddies created have not had sufficient time to decompose before intercepting the probe.

3. Discussion

The research reported herein has examined poststenotic flow fields in the canine descending aorta with emphasis on describing the disordered flow characteristics which occur. It has been demonstrated that clearly discernible alterations in the velocity waveform and corresponding energy spectra are found for mild degrees of stenosis and that very turbulent fields which are quasi-steady in nature are encountered for severe stenoses. Spectral analysis of the entire velocity waveform suggest the existence of a modified Strouhal number correlation over the near-field region distal to axisymmetric obstructions. Measurements over selected parts of the cardiac cycle indicate that the acceleration phase of systole is the most stable region of the waveform and is the last segment to encounter substantial disturbances as the degree of stenosis is increased. On the other hand, the deceleration phase immediately subsequent to the peak systolic velocity is the most unstable segment, and it is here that instabilities are first observed. The axial decay of disturbances has also been described and found to be rather rapid. This would indicate that disorder produced by a mild stenosis, by vessel

branching, or by bifurcation would likely be dissipated quickly as the flow proceeds distally. Presumably, this would likewise be true for disturbances created by actual or artificial cardiac valves.

Although the present study has not examined directly the questions of intimal injury, poststenotic dilation, or atherogenesis, the measurements of the fluid environment distal to vascular stenoses can be hypothesized as having some relationship to these problems. Fry²¹ has indicated that disordered flow patterns may have an effect on endothelial cell orientation and possibly on the transport of lipoproteins into the vessel wall. Our in vitro studies of pulsatile flow through modelled stenoses indicate that the region immediately distal to the constriction is filled with violently swirling flow. If the observations reported in Ref. 21 are eventually proven to be related to atherosclerosis, it may be possible that the flow field created by an early lesion could contribute to local enhancement of the disease.

Roach¹¹ has reported that the frequencies of vibration which lead to poststenotic dilation in arteries range from 25 to 400 Hertz. The turbulent energy spectra described in this study indicate substantial energy content through this range, provided the stenosis is moderately large.

The importance of early detection of occlusive vascular disease leads us to optimistically speculate that the velocity waveforms and corresponding energy spectra may provide valuable clues to the extent of disease development before clinical symptoms become apparent. Any eventual application of fluid dynamic measurements as a diagnostic tool for detecting occlusive vascular disease in its initial stages of development

would have to rely on noninvasive techniques. Clearly, the hot film anemometer would not be suitable. However, as refinements are made in Doppler ultrasound devices it may eventually be possible to detect and quantify blood flow disorder in a noninvasive, atraumatic fashion.

V. TURBULENCE MEASUREMENTS WITH DOPPLER ULTRASOUND

Our studies employing the hot film anemometer have led to contributions of a fundamental nature in the understanding of poststenotic flows. Further, they have indicated that the use of disordered flow analysis is a potentially useful early method of detection for localized vascular disease. However, this measurement technique has certain inherent limitations. Calibration for blood flow studies is tedious and difficult. Hot film probes cannot sense accurately reverse flow in a vessel, nor in regions of separation and recirculation due to problems in probe alignment. Furthermore, they require invasion of the artery which precludes their use as an early detection device for patients. Therefore, we have actively pursued the development of noninvasive instrumentation to complement the hot film anemometer.

During the past year we have worked with F. D. McLeod of the Radiological Health Laboratories, Colorado State University, on a pulsed ultrasonic Doppler system. A basic shortcoming of pulsed Doppler devices in detecting velocities is the severe lack of frequency response in determining velocity fluctuations. To our knowledge, there have been no reported reliable measurements of turbulence structure. Recently, in our laboratory, we have implemented a phase lock loop method of processing the Doppler signal from a pulsed ultrasonic system which gives promise of obtaining accurate recordings of turbulence. The first attempts at evaluating this advanced system were to investigate turbulent pipe flow with a steady flow rate. The system was composed of centrifugal pumps, which provided influx to a 2 inch I.D. plexiglas tube. Hot film anemometer, laser Doppler anemometer (LFA), and pulsed

ultrasonic Doppler measurements were obtained 40 diameters downstream of the tube inlet at Reynolds numbers of approximately 12,000 and 23,000. Figure 54 gives the measured energy spectra at $Re \cong 23,000$ for the three instrumentation systems. The agreement is quite good, although with our present optics, the Doppler ambiguity for the LDA limits frequency response of that system to about 200 Hz. The hot film and pulsed Doppler measurements agree out to 500 Hz which was the upper limit studied in this particular analysis. The spectral curves were obtained by digitizing 1024 sample points per second and averaging the spectral computations for 50 seconds.

Although we believe this represents significant progress in pulsed Doppler development, there is still much to accomplish. As yet, we have not attempted a pulsatile flow study, and there are aspects of the statistics of the scattering volume and signal processing which need refinement. Furthermore, we have begun analysis of a totally digital processing method of the Doppler signal which may complement the phase lock technique which we are presently using.

In addition to the development of the pulsed Doppler to measure turbulence quantitatively, we intend to employ this device in future in vivo studies. It offers a noninvasive technique which opens avenues of exploration and biomedical research not heretofore available in our laboratory.

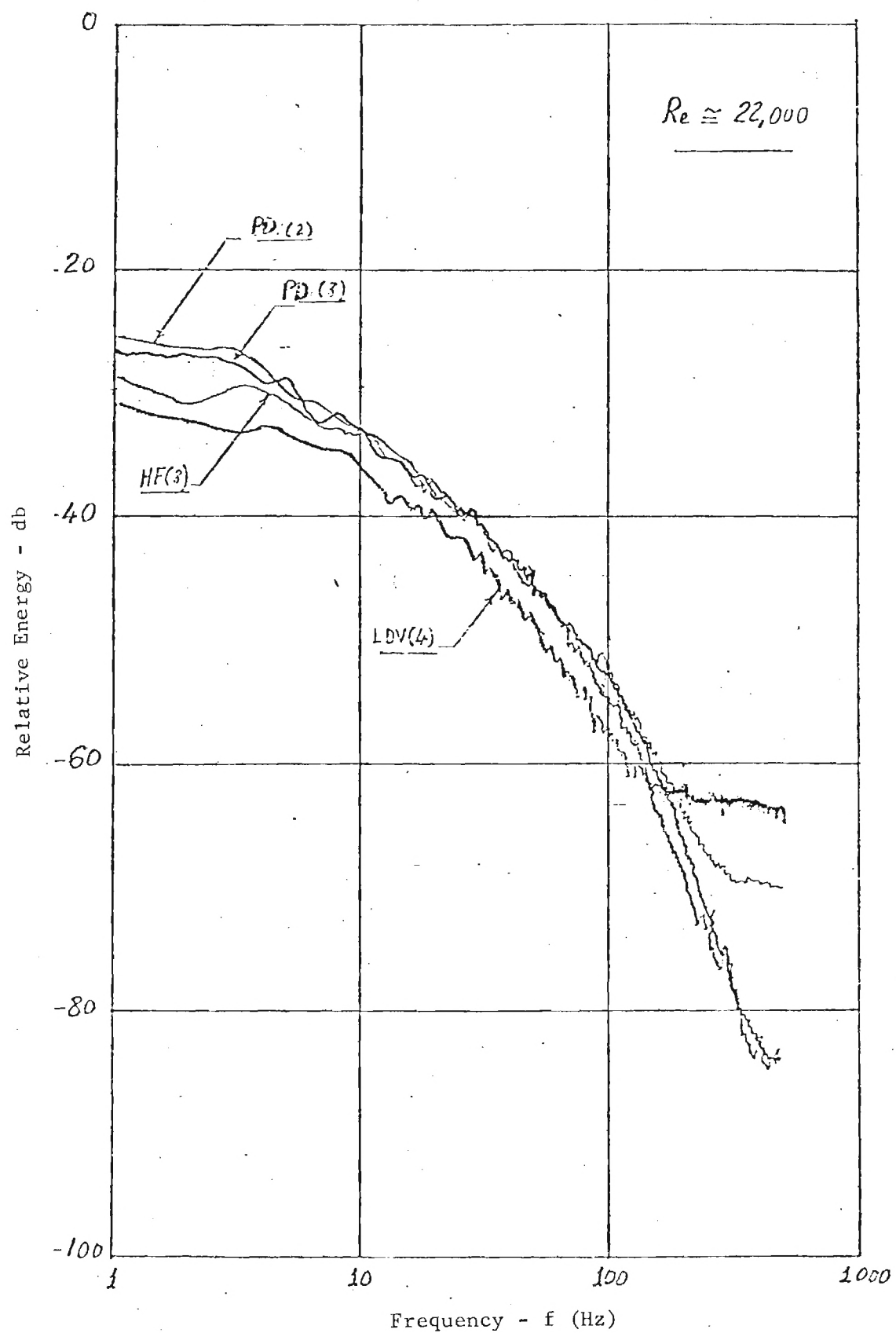


Figure 54. Comparison of power spectra measured by the hot film, LDV and PD for $Re = 22,000$.

VI. DISCUSSION AND DIRECTIONS FOR FUTURE RESEARCH

Extensive theoretical and experimental investigations into flows through subtotal stenoses have been completed under NSF Grant ENG74-21986. This report has presented some of the findings obtained during these studies. Additional details are available in References 10, 42, and 51. It is perhaps appropriate to summarize the results briefly at this point.

1. Computer programs were developed for finite difference solutions to the steady Navier-Stokes equations for laminar flow and the $k-\epsilon$ model equations for turbulent flow through contoured constrictions in rigid tubes. These provide theoretical models for stenotic flow fields over a wide range of Reynolds numbers.
2. Our calculations demonstrate that damagingly high wall shear stresses can occur at the site of maximum constriction. These high stresses could lead to the dislodgement of ulcerous material from an atherosclerotic plaque, causing emboli which obstruct distal vessels.
3. Experiments indicate that mild stenoses create marked disorder in distal velocity waveforms for both in vivo and in vitro environments. For example, flow visualization studies in pulsatile flow (frequency parameter = 15, peak upstream Reynolds number = 2540) indicate the formation of a large vortex-like swirl near the distal wall of a constriction, occurring during the initial acceleration portion of each velocity pulse. This vortex breaks away from

the wall during the deceleration phase of the cycle and migrates to the center region of the tube, breaking up as it travels. Thus, even for a 25 percent stenosis, significant turbulent disturbances are seen for a pulsatile flow, whereas the corresponding steady flow case exhibited no turbulence. In vivo measurements consistently showed distinct flow disorder for 20-25 percent stenoses.

4. Discrete vortex shedding was observed for 50, 75, and 90 percent stenoses over a wide range of Reynolds numbers studied in vitro for steady flow.
5. Sharp-edge occlusions produced flow instabilities at lower Reynolds numbers in steady flow than did the contoured occlusions. Also, more intense velocity fluctuations were produced by the sharp-edged constrictions.
6. The maximum turbulence energy at the centerline occurred between two and three unoccluded diameters for all occlusions in pulsatile flow.
7. For mild stenoses in vivo the decay of flow disorder is sufficiently rapid that there is no carryover of disturbances from one cycle to the next; but for moderate to severe obstructions, flow disorder persists throughout the cycle.
8. Time ensemble average waveforms in vivo show "split systolic peaks" for moderate stenoses and may offer an early detection technique for moderate arterial obstruction. The mechanism creating these peaks was not isolated.

9. Comparison of energy spectra for acceleration vs. deceleration phases of the velocity waveform is a sensitive method for detecting mild stenoses.
10. Correlation of energy spectra by similarity parameters exists over a limited region distal to stenoses for the in vivo experiments.
11. The pulsed Doppler with phaselock loop capture of the audio signal has been shown to give good high frequency response (up to 500 Hz) in a turbulent pipe flow at a Reynolds number of 23,000. This offers potential for noninvasive measurements of flow disorder if the technique can be applied to pulsatile flows at lower Reynolds numbers.

Although we believe that much has been accomplished by this research, it is clear that several important problems remain. One of these is the separation of biological disorder from flow disturbances. The physiologically normal flow in the region of a bifurcation, the prevalent geometry for development of atherosclerotic plaque, may contain a degree of disorder due to the highly three-dimensional nature of the flow field. This must be established before stenosis-induced flow disorder can be recognized at an early stage of disease development.

A second problem is that of nonstationarity of the disorder for mild to moderate stenoses. The disturbance velocity $u'(t)$ is found to be a nonstationary random variable; and thus the usual concepts of energy spectra, correlation functions, and rms disturbances must be modified. A rigorous treatment of this problem has not been put forth,

but our present research efforts are progressing in this area.

The separate and synergistic effects of the flow and the compliant vessel wall have not been isolated. Within the scope of our studies we did not examine whether the split systolic peaks in the time varying ensemble average waveforms were due to vessel elasticity or to a flow phenomenon such as vortex shedding. Likewise, the effects of the flow environment on the vessel wall were not studied.

Finally, the eventual application of characterizing flow disorder for diagnostic purposes in vascular disease will not be possible unless noninvasive methods of making the required measurements are developed. For this reason and from the standpoint of attempting to achieve basic advances in Doppler ultrasound, we have recently devoted considerable effort in studies which are directed at using a pulsed ultrasonic Doppler technique to measure turbulent velocities.

REFERENCES

1. Robert F. Rushmer; Cardiovascular Dynamics, 3rd Edition, W. B. Saunders Co., Philadelphia, 1970.
2. R. M. Nerem, W. A. Seed, and N. B. Wood; "An Experimental Study of the Velocity Distribution and Transition to Turbulence in the Aorta," Journal of Fluid Mechanics, Vol. 52, Part I, pp. 137-160, 1972.
3. J. A. Rumberger, Jr., D. R. Gross, G. L. Geiger, R. L. Hamlin, and R. M. Nerem; "In Vivo Hot-Film Anemometer Measurements of Arterial Flow," paper presented at 26th Annual Conference on Engineering in Medicine and Biology, Minneapolis, Minn., 1973.
4. R. M. Nerem and W. A. Seed; "An In Vivo Study of Aortic Flow Disturbances," Cardiovascular Research, Vol. 6, pp. 1-14, 1972.
5. G. G. Ferguson and M. R. Roach; "Flow Conditions at Bifurcations as Determined in Glass Models, with Reference to the Focal Distribution of Vascular Lesions," in Cardiovascular Fluid Dynamics, Vol. 2, edited by D. Bergel, Academic Press, London, 1972.
6. M. M. Kartchner and L. P. McRae; "Auscultation for Carotid Bruits in Cerebrovascular Insufficiency," Journal of the American Medical Association, Vol. 210, No. 3, October 20, 1969.
7. R. S. Lees and C. F. Dewey, Jr.; "Phonoangiography: A New Non-invasive Diagnostic Method for Studying Arterial Disease," Proceedings of the National Academy of Sciences, Vol. 67, No. 2, pp. 935-942, October, 1970.
8. A. H. Sacks, E. G. Tickner, and I. A. Macdonald; "Criteria for the Onset of Vascular Murmurs," Circulation Research, Vol. XXIX, September, 1971.
9. D. P. Giddens, R. F. Mabon, R. A. Cassanova, R. K. Menon, and J. Chandler; "The Velocity Field Distal to Partial Occlusions in Arteries," paper presented at 10th Anniversary Meeting of the Society of Engineering Science, North Carolina State University, Raleigh, N. C., November 1973.
10. D. P. Giddens, R. F. Mabon, and R. A. Cassanova; "Measurements of Disordered Flows Distal to Subtotal Vascular Stenoses in the Thoracic Aortas of Dogs," Circulation Research, Vol. 39, No. 1, pp. 112-119, 1976.

11. M. R. Roach; "Poststenotic Dilatation in Arteries," in Cardiovascular Fluid Dynamics, Vol. 2, edited by D. Bergel, Academic Press, London, 1972.
12. R. J. Tobin, I. D. Chang, and S. P. Koutsoyannis; "Wall Pressure and Displacement Measurements in a Simulation of Cardiovascular Murmur Generation," SUDAAR Report No. 484, Stanford University, 1976.
13. J. J. Fredberg; "Turbulent Pseudosound Production in Atherosclerotic Arteries," Ph.D. Thesis, Massachusetts Institute of Technology, 1973.
14. G. W. Duncan, J. O. Gruber, C. F. Dewey, G. S. Myers, and R. S. Lees; "Evaluation of Carotid Stenosis by Phonoangiography," New England Journal of Medicine, Vol. 293, No. 22, pp. 1124-1128, 1975.
15. D. L. Fry; "Acute Vascular Endothelial Changes Associated with Increased Blood Velocity Gradients," Circulation Research, Vol. 22, p. 165, 1968.
16. D. L. Fry; "Certain Histological and Chemical Responses of the Vascular Interface to Acutely Induced Mechanical Stress in the Aorta of the Dog," Circulation Research, Vol. 24, p. 93, 1969.
17. D. L. Fry; "Certain Chemorheologic Considerations Regarding the Blood Vascular Interface, with Particular Reference to Coronary Artery Disease," Circulation, Vols. 30 and 40, Supplement 4, p. 38, 1969.
18. J. T. Flaherty, V. J. Ferrans, J. E. Pierce, T. E. Carew, and D. L. Fry; "Localizing Factors in Experimental Atherosclerosis," in Atherosclerosis and Coronary Heart Disease, Chapter 6, Ed. by W. Likoff, et al, Grune and Stratton, New York, 1972.
19. J. T. Flaherty, J. E. Pierce, V. J. Ferrans, D. J. Patel, W. K. Tucker, and D. L. Fry; "Endothelial Nuclear Patterns in the Canine Arterial Tree with Particular Reference to Hemodynamic Events," Circulation Research, Vol. 30, p. 23, 1972.
20. D. L. Fry; "Localizing Factors in Artherosclerosis," in Atherosclerosis and Coronary Heart Disease, Chapter 7, Ed. by W. Likoff, et al, Grune and Stratton, New York, 1972.
21. D. L. Fry; "Responses of the Arterial Wall to Certain Physical Factors," in Atherogenesis: Initiating Factors, A Ciba Foundation Symposium 12 (New Series), pp. 93-125, Elsevier. Excerpta Medica. North - Holland, Amsterdam, 1973.

22. C. W. M. Adams; "Tissue Changes and Lipid Entry in Developing Atheroma," in Atherogenesis: Initiating Factors, A Ciba Foundation Symposium 12 (New Series), pp. 93-125, Elsevier. Excerpta Medica. North Holland, Amsterdam, 1973.
23. C. W. M. Adams, S. Virag, R. S. Morgan, and C. C. Orton; "Dissociation of [3H] - cholesterol and 125I-labelled Plasma Protein Influx in Normal and Atheromatous Rabbit Aorta," Journal of Atherosclerosis Research, Vol. 8, pp. 679-696, 1968.
24. C. W. M. Adams, "Lipids, Lipoproteins, and Atherosclerotic Lesions," Proceedings of the Royal Society of Medicine, Vol. 64, pp. 902-905, 1971.
25. C. G. Caro and R. M. Nerem; "Transport of ^{14}C -4-cholesterol Between Serum and Wall in Perfused Dog Common Carotid Artery," Circulation Research, Vol. 32, pp. 187-205, 1973.
26. C. G. Caro; "Transport of Material Between Blood and Wall in Arteries," in Atherogenesis: Initiating Factors, A Ciba Foundation Symposium 12 (New Series), pp. 127-164, Elsevier. Excerpta Medica. North-Holland, Amsterdam, 1973.
27. R. M. Nerem, J. S. Polsley, D. L. Robinson, and W. E. Carey; "Shear Dependent Transport of Albumin Between Blood and the Arterial Wall," paper presented at 26th Annual Conference on Engineering in Medicine and Biology, Minneapolis, Minnesota, 1973.
28. S. C. Ling and H. B. Atabek; "A Nonlinear Analysis of Pulsatile Flow in Arteries," Journal of Fluid Mechanics, Vol. 55, p. 493, 1972.
29. H. B. Atabek and S. C. Ling; "Pulsatile Flow in Distensible and Tapered Arteries," paper presented at 26th Annual Conference on Engineering in Medicine and Biology, Minneapolis, Minn., 1973.
30. J. S. Lee and Y. C. Fung; "Flow in Locally Constricted Tubes at Low Reynolds Numbers," Journal of Applied Mechanics, Vol. 37, p. 9, 1970.
31. T. A. Kozman and J. H. Forrester, "Pulsatile Flow in a Modeled Stenosis," paper presented at 26th Annual Conference on Engineering in Medicine and Biology, Minneapolis, Minn., 1973.

32. T. K. Hung; "Blood Flow Past a Stenotic Aortic Valve; A Computer Simulation," paper presented at 23rd Annual Conference on Engineering in Medicine and Biology, Washington, D. C., 1970.
33. B. E. Morgan and D. F. Young; "An Integral Method for the Analysis of Flow in Arterial Stenoses," Bulletin of Mathematical Biology, Vol. 36, pp. 39-53, 1974.
34. P. Imbert, R. Pelissier, et B. Roux; "Etude Theorique de L'e'coulement d'un Fluide Visqueux dans un Retre'cissement," C. R. Acad. Sc., Paris, t. 384, 1977, Series B, 73-76.
35. M. D. Deshpande, D. P. Giddens, and R. F. Mabon; "Steady Flow Through Modelled Vascular Stenoses," Journal of Biomechanics, Vol. 9, pp. 165-174, 1976.
36. R. K. Menon; "A Study of Ducted Jets Including the Effect of Dilute Polymer Solution," Ph.D. Thesis, Georgia Institute of Technology, 1976.
37. D. B. Spalding; "A Two-Equation Model of Turbulence," VDI-Forsch.-Heft 549, p. 5-16, 1971.
38. B. E. Launder and D. B. Spalding; "Turbulence Models and Their Application to the Prediction of Internal Flows," Heat and Fluid Flow, Vol. 2, No. 1, 1972.
39. H. E. Pawel; "Spectral Analysis of Turbulence in Simulated Arterial Flow," paper presented at 27th ACEMB Meeting, Philadelphia, 1974. Also, Ph.D. Thesis, Rutgers University, 1974.
40. K. H. Parker; "Instability in Arterial Blood Flow," Chapt. 16 in Cardiovascular Flow Dynamics and Measurements, ed. by N.H.C. Hwang and N. A. Normann, University Park Press, Baltimore, 1977.
41. A. K. M. F. Hussain; "Mechanics of Pulsatile Flows of Relevance to the Cardiovascular System," Chapt. 15 in Cardiovascular Flow Dynamics and Measurements, ed. by N.H.C. Hwang and N.A. Normann, University Park Press, Baltimore, 1977.
42. M. D. Deshpande; "Steady Laminar and Turbulent Flow Through Vascular Stenosis Models," Ph.D. Thesis, Georgia Institute of Technology, 1977.
43. A. D. Gosman, W. M. Pun, A. K. Runchal, D. B. Spalding, and M. Wolfshtein; Heat and Mass Transfer in Recirculating Flows, Academic Press, London, 1969.

44. D. F. Young and F. Y. Tsai; "Flow Characteristics in Models of Arterial Stenoses - I. Steady Flow," Journal of Biomechanics, Vol. 6, pp. 395-410, 1973.
45. Mellor, G. L. and Herring, H. J. (1973) A Survey of the Mean Turbulent Field Closure Models. A.I.A.A. Journal 11, pp. 590-599.
46. Harlow, F. H. and Nakayama, P. I. (1967) Turbulence Transport Equations. Physics Fluids 10, pp. 2323-2332.
47. Launder, B. E. and Spalding, D. B. (1972). Mathematical Models of Turbulence. Academic Press, New York.
48. Runchal, A. K. and Spalding, D. B. (1972). Steady Turbulent Flow and Heat Transfer Downstream of a Sudden Enlargement in a Pipe of Circular Cross-section. Warme-und Stoffubertragung 5, pp. 31-38.
49. Launder, B. E. (1975) Progress in the Modelling of Turbulent Transport. Supplementary Notes of Course "Turbulent Recirculating Flows -- Prediction and Measurement," held at the Pennsylvania State University.
50. Carnhan, B., Luther, H. A. and Wilkes, J. O. (1969) Applied Numerical Methods. John Wiley and Sons, Inc., New York.
51. R. A. Cassanova; "An Experimental Investigation of Steady and Pulsatile Flow Through Partial Occlusions in a Rigid Tube," Ph.D. Thesis, Georgia Institute of Technology, 1975.
52. E. J. Roschke and L. H. Back; "The Influence of Upstream Conditions on Flow Reattachment Lengths Downstream of an Abrupt Circular Channel Expansion," Journal of Biomechanics, Vol. 9, pp. 481-483, 1976.
53. F. C. Johansen; "Flow Through Pipe Orifice at Low Reynolds Numbers," Proc. Roy. Soc., A136, pp. 231-243, 1929.
54. G. S. Beavers and T. A. Wilson; "Vortex Growth in Jets," J. Fluid Mech., Vol. 44, pp. 97-112, 1970.
55. H. L. Falsetti, K. M. Kiser, G. P. Francis, and E. R. Belmore; "Sequential Velocity Development in the Ascending and Descending Aorta of the Dog," Circulation Research, Vol. 21, pp. 328-338, 1972.
56. A.K.F. Hussain and W. C. Reynolds; "The Mechanics of an Organized Wave in Turbulent Shear Flow," J. Fluid Mech., Vol. 41, pp. 241-259, 1970.
57. M. B. Priestly; "Evolutionary Spectra and Non-stationary Processes," J. Roy. Statis. Soc., Vol. B27, pp. 204-237, 1965.

58. B. M. Kim and W. H. Corcoran; "Experimental Measurements on Turbulence Spectra Distal to Stenoses", J. Biomechanics, Vol. 7, pp. 335-342, 1974.
59. J. M. Rodrigues, G. K. Patterson, and J. L. Zakin; "Effects of Probe Geometry on Turbulence Measurements in Liquid using Hot-Film Anemometry," J. Hydronautics, Vol. 4, pp. 16-21, 1970.
60. K. J. Hutchinson; "Effect of Variation of Transmural Pressure on the Frequency Response of Isolated Segments of Canine Carotid Arteries," Circulation Research, Vol. 35, pp. 742-751, 1974.